UNIVERSITY OF OKLAHOMA

GRADUATE COLLEGE

ENZYME SYSTEMS INVOLVED IN INTERSPECIES HYDROGEN AND FORMATE TRANSFER BETWEEN SYNTROPHIC FATTY AND AROMATIC ACID DEGRADERS AND *METHANOSPIRILLUM HUNGATEI*

A DISSERTATION

SUBMITTED TO THE GRADUATE FACULTY

in partial fulfillment of the requirements for the

Degree of

DOCTOR OF PHILOSOPHY

By

BRYAN REGIS CRABLE
Norman, Oklahoma
2013

ENZYME SYSTEMS INVOLVED IN INTERSPECIES HYDROGEN AND FORMATE TRANSFER BETWEEN SYNTROPHIC FATTY AND AROMATIC ACID DEGRADERS AND *METHANOSPIRILLUM HUNGATEI*

A DISSERTATION APPROVED FOR THE
DEPARTMENT OF MICROBIOLOGY AND PLANT BIOLOGY

BY

_____
Dr. Michael J. McInerney, Chair

_____
Dr. Joseph M. Suflita

_____
Dr. Ralph S. Tanner

_____
Dr. Elizabeth A. Karr

_____
Dr. Michael R. Markham

I dedicate this work to my parents, Larry and Kathy Crable. Thank you for all your support and all that you have done for me. I also dedicate this work to my sister, Laura Crable. Thank you for your support and encouragement.

Acknowledgements

First, I need to acknowledge the intellectual and academic support of my committee chair, Dr. Michael McInerney. I also need to acknowledge two outstanding colleagues from Dr. McInerney's group – both Neil Wofford and Dr. Jessica Sieber provided valuable technical support, training and intellectual input over the last several years. Additionally, my colleagues Dr. Housna Mouttaki, Kimberly James, Huynh Le and Dr. Johannes Kung have helped immensely with my research.

Outside of Dr. McInerney's group, I have received valuable advice and counseling from the members of my committee, Dr. Joseph Suflita, Dr. Ralph Tanner and Dr. Elizabeth Karr. Dr. Phil Klebba served as my external committee member until 2012 and provided valuable input into this research. I also thank Dr. Michael Markham, my current external committee member, for his valuable input and agreeing to join my committee so late in my program. I have also received valuable support from great colleagues here at the University of Oklahoma; among these are Dr. Chris Lyles and his wife, Laura, Chris Marks and Dr. Victoria Parisi.

My colleagues at the University of California – Los Angeles, Dr. Robert Gunsalus, Dr. Lars Rohlin, Dr. Rachel Loo and Dr. Loo's doctoral student Hong Nguyen have been instrumental in proteomic analysis. At Oak Ridge National Laboratory, Dr. Gregory Hurst was essential for completing the proteomic analysis of *M. hungatei*. Also, a special thank-you is due to Dr. Lisa Alvarez-Cohen and her student Xinwei Mao at the University of California – Berkley for their collaborative efforts on *S. wolfei*.

I need to also thank Dr. Alfons Stams and Dr. Caroline Plugge of the University of Wageningen, the Netherlands, for allowing me to work in their group for a year. This experience was a high-point of my doctoral work, and several colleagues from Wageningen and beyond need to be thanked. Ruud Heshoff, Peer Timmers, Michael Visser and Marjet Oosterkamp all provided valuable intellectual input during my time at Wageningen. Shawn Scarlett, Dennis Rütze, Jeroen Roskam and Jeanette Smits all provided valuable assistance in navigating the complexities (and oddities) of Dutch society for a year. I thank all of them for a year of *gezelligheid*.

Dr. Danielle Johnston, Dr. Bruce Bethke and Dr. John Stolz are all colleagues from past institutions who have continued to provide support and encouragement throughout my doctoral work. Also, I thank friends and relatives (too many to name) for all the support and encouragement over the last six years.

Last, and most importantly, I need to thank my family – it's been a long six years away from home. My parents, Larry and Kathy Crable, and sister, Laura Crable, have provided endless love, support and encouragement. I also need to acknowledge my cousin and fellow budding scientist, Jillian D'Amico – watching your intellectual growth has given me a valuable source of encouragement to keep moving forward.

Table of Contents

List of Tables

List of Figures

Preface

The main goal of this research was to investigate the mechanisms of reverse electron transfer in two organisms capable of syntrophy, *S. wolfei* and *S. aciditrophicus*. In 2007, the process of reverse electron transfer was poorly understood. In this work, I help expand our understanding of possible mechanisms of reverse electron transfer in organisms capable of syntrophy. Here, I use proteomic and enzymological approaches and couple these with mRNA expression analyses done in collaboration with investigators here, at the University of Oklahoma, and elsewhere; the University of California – Berkley and the University of California – Los Angeles.

Chapter 2 is an investigation into the membrane complexes formed by *S. wolfei* during growth on butyrate. Here, I used blue-native polyacrylamide gel electrophoresis (BN-PAGE) to separate membrane protein complexes. I prepared tryptic digests and peptide identification was carried out by our collaborators at the University of California – Los Angeles, Dr. Robert Gunsalus, Dr. Rachel Loo and Dr. Loo's doctoral student, Hong Nguyen. Additionally, I tested for hydrogen dependent reduction of tetrazolium red in membrane fractions separated by blue-native PAGE. Tryptic digestion and peptide mass fingerprint analysis for this complex was performed by the University of Oklahoma Health Sciences Center Proteomics Core Facility.

Expression analysis conducted with *S. wolfei* grown in pure culture or in methanogenic coculture with *Methanospirillum hungatei* were done in collaboration with Dr. Jessica Sieber and expression analysis conducted on *S. wolfei* cells grown with *Dehalococcoides* were done in collaboration with Xinwei Mao, a doctoral student at the University of California – Berkley under the direction of Dr. Lisa Alvarez-Cohen. The

importance of this contribution should not be understated since, in our methanogenic cocultures, hydrogen or formate can be used as the interspecies electron carrier while *Dehalococcoides* is not known to use formate as an electron source

Also in Chapter 2 are some of my contributions to the *S. wolfei* whole cell proteome. Whole cell proteomics analysis was performed by our collaborator at Oak Ridge National Laboratory, Dr. Gregory Hurst. This project was done in collaboration with Dr. Sieber. As part of the collaboration, much of this work has been detailed elsewhere (Sieber 2011). My primary contribution to this project was downstream data analysis. Between 2010 and present, I normalized, analyzed and manually curated a database of over 17,000 data points and identified the presence/absence of several key enzymes including membrane bound hydrogenases, formate dehydrogenases, butyryl-CoA dehydrogenases, heterodisulfide reductases and several enzymes associated with beta-oxidation. The findings presented here represent a portion of my contributions, but are those which are of direct importance to my findings regarding membrane complexes in *S. wolfei*.

Chapter 3 is a study into the membrane complexes formed by *S. aciditrophicus* during syntrophic growth. *S. aciditrophicus* is able to utilize benzoate or cyclohexane carboxylate when grown in coculture with the hydrogen/formate scavenging methanogen, *M. hungatei*. I performed blue-native PAGE and prepared tryptic digests of identified membrane complexes. My colleagues at the University of California – Los Angeles, Dr. Loo and Hong Nguyen, analyzed the proteins present in these complexes using peptide mass fingerprint analysis. Further, I tested intact membrane suspensions for the ability to catalyze an Rnf-like activity as well as hydrogenase, formate

dehydrogenase and NADH:quinone oxidoreductase activity. I partially purified fractions testing positive for Rnf-like activity and performed blue-native PAGE and SDS-PAGE analysis. Tryptic digestion and peptide identification for these experiments was performed by the University of Oklahoma Health Sciences Center Proteomics Core Facility.

Chapter 4 is an analysis of the genome sequence of *Methanospirillum hungatei* strain JF1. *M. hungatei* is a hydrogenotrophic methanogen which is capable of methanogenesis with electrons derived from hydrogen or formate. Genome sequencing was conducted by the Joint Genome Institute at Pacific Northwest National laboratory and whole-cell proteomic analysis was conducted by Dr. Gregory Hurst at Oak Ridge National Laboratory. Pure cultures for whole-cell proteomic analysis were grown by the group of Dr. Robert Gunsalus at the University of California – Los Angeles and cocultures for whole-cell proteomic analysis were grown by my University of Oklahoma Colleagues, Dr. Jessica Sieber and Huynh Le. My contributions included genome annotation, downstream data analysis and metabolic reconstruction. This includes normalizing, analyzing and manually curating a database of over 12,000 data points for proteomics analysis.

Abstract

The oxidation of either the fatty acid butyrate or the aromatic acid benzoate is essential for the efficient degradation of complex organic material to methane because they are central intermediates. The oxidation of butyrate to acetate and hydrogen is energy requiring under physiological conditions. Likewise, the oxidation of benzoate to acetate, carbon dioxide and hydrogen is energy requiring under physiological conditions. However, when hydrogen or formate are maintained at very low levels by a partner organism, through metabolic cooperation known as syntrophy, the oxidation of both butyrate and benzoate becomes energetically favorable. An essential feature of both the syntrophic oxidation of butyrate and benzoate is the need to produce hydrogen (E' = -260 mV at 1 Pa hydrogen) or formate (E' = -290 mV at 1 µM formate) from butyryl-CoA (butyrate oxidation by *S. wolfei*) or from glutaryl-CoA (benzoate oxidation by *S. aciditrophicus*). Ion gradients, and consequently membrane bound protein complexes, are known to be important for butyrate oxidation by *S. wolfei* and benzoate oxidation by bacteria related to *S. aciditrophicus* – *Syntrophus gentianae* and *Syntrophus buswellii*. The main goal of this research was to investigate the mechanisms of reverse electron transfer in *S. wolfei* and *S. aciditrophicus*. I used proteomic and enzymological approaches and coupled these approaches with mRNA expression analyses.

Here, I showed that an FeS oxidoreductase, the gene of which is linked on the chromosome to genes coding for electron transferring flavoprotein subunits, and components of a cytochrome *b* –linked hydrogenase (*hydIIABC* gene product) are codetected in a complex unique to syntrophic growth on butyrate. Expression analyses

of the genes coding for the electron transferring flavoprotein subunits, FeS oxidoreductase and *hydIIABC* gene product argue for the importance of these systems for syntrophic growth on butyrate.

In *S. aciditrophicus*, I showed that peptides derived from an Rnf-like complex were detected in membrane complexes from *S. aciditrophicus* cells. I used the low potential acceptors, benzyl viologen ($E^{0'}$ = -360 mV) and methyl viologen ($E^{0'}$ = -460 mV) to test for the ability of *S. aciditrophicus* cells to catalyze an Rnf-like activity - reduction of the viologen dyes with NADH ($E^{0'}$ = -320 mV). I showed that membrane fractions of *S. wolfei* catalyze the reduction of both benzyl and methyl viologen with electrons derived from NADH and that specific activity for this direction is higher than for the more thermodynamically favorable oxidation of benzyl or methyl viologen with concomitant reduction of NAD^+. Moreover, I showed that the Rnf-like activity is highest in cells grown syntrophically. I used size exclusion chromatography to partially purify the Rnf-like activity and I showed that peptides derived from an Rnf-like complex are present in these fractions.

Finally, I investigated the genome of *Methanospirillum hungatei* strain JF1 and used whole cell shotgun proteomics to interrogate the response of *M. hungatei* to growth in syntrophic partnership with *S. wolfei*. *M. hungatei* is a hydrogenotrophic methanogen which is capable of utilizing formate or hydrogen for methane production. *M. hungatei* is a partner organism for several syntrophic systems and members of the genus *Methanospirillum* have been found in many environments where syntrophy is important. Proteomic analysis showed that *M. hungatei* uses both hydrogenases and formate dehydrogenases and increases the relative abundance of the core methanogenic

machinery during syntrophic growth relative to pure culture growth on hydrogen and formate. The relative abundance of peptides associated with energy production and cofactor synthesis increased while those involved in translation decreased in syntrophically grown cells compared to axenically-grown cells. The above data are consistent with a strategy to maximize energy production efficiency and curtail biosynthesis during syntrophic growth.

Chapter 1: Summary

Methane has been recognized as an important fuel source for over 200 years. Current research and development support from countries including Japan, the United States, Sweden and Germany to develop the next generation of vehicles and power plants fueled by biologically produced methane serves to underscore the important role of biological methane production (Ahman 2010; Deublein and Steinhauser 2008). Biologically, methane production is a complex process that requires cooperation between at least three trophic guilds. In short, complex organic molecules are fermented to acetate, hydrogen, formate and a variety of organic acids (lactate, propionate, and butyrate) and ethanol. Acetogenic bacteria convert these compounds to the methanogenic substrates hydrogen, formate and acetate.

Efficient degradation of fatty acid, aromatic acid and alcohol intermediates requires removal of hydrogen and formate by methanogens in a process known as interspecies electron transfer (Sieber *et al.* 2013). The relationship between the secondary fermenters and the methanogens is known as syntrophy and is characterized by the ability of the consortium to degrade a substrate that neither organism alone can degrade. An essential feature of this system is that oxidation of the principle substrate (e.g. butyrate or benzoate) by the fermenting syntrophic bacterium is not thermodynamically favorable (Table 1), but only becomes energetically favorable when hydrogen- and/or formate-using methanogens or sulfate-reducers are present to keep concentrations of hydrogen and formate very low (Table 1).

Table 1: Thermodynamics of butyrate, benzoate and propionate oxidation. $\Delta G^{0'}$ = Gibb's free energy change at one atmosphere with one molar concentration of products and reactants at pH 7. The change in free energy of butyrate, benzoate or propionate presents a thermodynamic barrier under physiological conditions. With the introduction of an electron scavenging organism, in this example a hydrogenotrophic methanogen, degradation becomes results in a release of free energy. References: [1] (Jackson and McInerney 2002), [2] (Scholten and Conrad 2000) and [3] (de Bok *et al.* 2004).

Syntrophic degradation without electron transfer	**$\Delta G^{0'}$ (kJ/reaction)**
butyrate + 2 $H_2O \rightarrow$ 2 acetate + H^+ + 2 H_2	+48.3 [1]
benzoate + 7 $H_2O \rightarrow$ 3 acetate + HCO_3^- + 3 H^+ + 3 H_2	+70.6 [1]
propionate + 2 $H_2O \rightarrow$ acetate + CO_2 + 3 H_2	+68.4 [2]
Syntrophic degradation with electron transfer	
2 butyrate$^-$ + HCO_3^- + $H_2O \rightarrow$ 4 acetate$^-$ + H^+ + CH_4	-39.4 [1]
4 benzoate$^-$ + 19 $H_2O \rightarrow$ 12 acetate$^-$ + HCO_3^- + 9 H^+ + 3 CH_4	-124.4 [1]
propionate + $H_2O \rightarrow$ 1.75 CH_4 + 1.25 HCO_3^- + H^+	-56.4 [3]

Syntrophic butyrate oxidation by *Syntrophomonas wolfei* is a well-known example (McInerney *et al.* 1979; Muller *et al.* 2009; Schmidt *et al.* 2013; Sieber *et al.* 2010; Wallrabenstein and Schink 1994; Wofford *et al.* 1986) as it was the first stable fatty acid oxidizing co-culture isolated. In methanogenic cultures containing *S. wolfei*, two moles of butyrate are oxidized to four mols of acetate and one mole of methane. This reaction has a free energy release of 39.4 kJ ($\Delta G^{0'}$ = -39.4 kJ/mol) per reaction at physiological conditions (1 atm with 1 M concentration of products and reactants at pH 7). In the absence of interspecies electron transfer, the oxidation of 1 mol butyrate to 2 mols acetate and hydrogen requires an input of 48.3 kJ per ($\Delta G^{0'}$ = + 48 kJ per reaction) (Table 1). A central challenge for *S. wolfei* during butyrate oxidation is the production of hydrogen with electrons derived from butyryl-CoA (McInerney *et al.* 2008). Butyryl-CoA has a midpoint redox potential under physiological conditions of about -10 mV (Sato *et al.* 1999) and the midpoint potential of electrons needs to be shifted to a midpoint potential of about -260 mV for production of hydrogen (at 1 Pa hydrogen) or -290 mV for the reduction of carbon dioxide to formate (at 1 µM formate).

Benzoate oxidation by *Syntrophus aciditrophicus* occurs under similar thermodynamic constraints. The oxidation of benzoate by *S. aciditrophicus* in partnership with a methanogen results in the production of twelve moles acetate and three moles of methane. This reaction releases 124.4 kJ per reaction. Without a methanogenic partner, the oxidation of one mole benzoate to three moles acetate and hydrogen would require the input of 70.6 kJ per reaction (Table 1) (Jackson and McInerney 2002). *S. aciditrophicus* faces a challenge similar to that of *S. wolfei* –

notably electrons derived from glutaryl-CoA ($E^{0'}$= -10 mV) (Sato *et al.* 1999) must be used for the production of hydrogen or formate (Sieber *et al.* 2013).

The production of hydrogen or formate with electrons derived from acyl-CoA intermediates is a central question for our understanding of syntrophic metabolism. In both butyrate oxidation (Schink 1997; Wallrabenstein and Schink 1994) and benzoate oxidation (Schink 1997; Schöcke and Schink 1997), reverse electron transfer is needed to overcome a change in midpoint redox potential of approximately 250 mV (for hydrogen production) or 280 mV (for formate production). The importance of chemiosmotic energy has been demonstrated for butyrate oxidation in *S. wolfei* (Wallrabenstein and Schink 1994) and benzoate oxidation by members of the genus *Syntrophus* (Schöcke and Schink 1997; Wallrabenstein and Schink 1994). Additionally, electron confurcation, a process where the energy yielding oxidation of a low potential donor provides energy for the oxidation of a high potential donor, is thought to play a role (McInerney *et al.* 2008). A central issue, however, with an electron confurcating strategy is that these strategies require reduced ferredoxin as a low potential donor and it is not clear from where this would be derived (Buckel and Thauer 2013).

The release of the genomes of *S. aciditrophicus* (McInerney *et al.* 2007) and *S. wolfei* (Sieber *et al.* 2010) led to candidate mechanisms for reverse electron transfer. Both *S. aciditrophicus* and *S. wolfei* were found to code for confurcating hydrogenases though, again, the physiological source of reduced ferredoxin is not yet established (McInerney *et al.* 2007; Sieber *et al.* 2010). *S. aciditrophicus* was found to contain genes coding for an Rnf-like complex which couples the oxidation of ferredoxin to the formation of a sodium ion gradient and could, in principle, operate in reverse to supply

reduced ferredoxin for electron confurcation (McInerney *et al.* 2007). Genes encoding an Rnf-like complex, however, were not detected in the genome of *S. wolfei* (Sieber *et al.* 2010).

Both *S. aciditrophicus* and *S. wolfei* were found to contain a gene coding for an FeS oxidoreductase adjacent to genes coding for electron transferring flavoprotein subunits (Sieber *et al.* 2012). Additionally, genes coding for a Fix complex, which catalyzes ferredoxin dependent reduction of menaquinone with electrons derived from acyl-CoA intermediates, were found on the *S. wolfei* chromosome (Sieber *et al.* 2010). It was proposed, then, that oxidation of acyl-CoA intermediates to enoyl-CoA products could be driven by a reverse quinone loop (Sieber *et al.* 2010).

M. hungatei is a well-established partner organism for syntrophic associations and members of the genus *Methanospirillum* are widely found in ecosystems where syntrophic associations are important. Under methanogenic conditions, hydrogenotrophic methanogens such as *M. hungatei* rely on syntrophic partners to produce hydrogen or formate for methanogenesis (Thauer *et al.* 2008). *M. hungatei* belongs to the Methanomicrobiales order. Members of the Methanomicrobiales order lack cytochromes (Thauer *et al.* 2008) and an ability to grow on low hydrogen partial pressures is well established (Walker *et al.* 2012). Sixty-two genes were found to be unique to the Methanomicrobiales, suggesting they form a class of methanogens separate from the "Class I" methanogens and separate from the Class III methanogens, Methanosarcinales (Anderson *et al.* 2009).

The main goal of this research was to investigate the mechanisms of reverse electron transfer in two organisms capable of syntrophy, *S. wolfei* and *S. aciditrophicus*.

As discussed, the importance of ion gradients has been demonstrated for both butyrate oxidation in *S. wolfei* and for benzoate oxidation in two members of the genus *Syntrophus* (Schink 1997; Schöcke and Schink 1997; Wallrabenstein and Schink 1994). In these studies, hydrogen production from butyryl-CoA (for *S. wolfei*) or benzoyl-CoA (*Syntrophus gentianae* or *Syntrophus buswellii*) by inverted membrane vesicles was inhibited by carbonylcyanide chlorophenylhydrazone, a protonophore, as well as the ATP synthase inhibitor dicyclohexylcarbodiimide. Therefore, I hypothesized that membrane protein complexes are involved in reverse electron transfer in both *S. wolfei* and *S. aciditrophicus*. More specifically, for *S. aciditrophicus*, I hypothesized that an Rnf-like complex catalyzes reverse electron transfer and is an important source of reduced ferredoxin which can ultimately be used for glutaryl-CoA oxidation by confurcating acyl-CoA dehydrogenases, or for hydrogen/formate production by a ferredoxin dependent hydrogenase or formate dehydrogenase.

I identified a number of membrane complexes formed in *S. wolfei* during growth in pure culture on crotonate, in coculture with *M. hungatei* on crotonate and in coculture with *M. hungatei* on butyrate. One membrane complex was unique to syntrophic growth on butyrate, and components of an ETF-linked FeS oxidoreductase and a cytochrome *b* linked hydrogenase (*hydIIABC* gene product) were detected. I also observed the ability of this complex to reduce tetrazolium red, a tetrazolium salt which forms a red precipitate in its reduced form. Expression analyses for the genes coding the ETF subunits (Swol_0696-7), the FeS oxidoreductase (Swol_0698) and the *hydIIABC* (Swol_1925-27) gene product revealed the importance of these proteins for syntrophic growth on butyrate with both *M. hungatei* and *Dehalococcoides* sp., an

organism which is not known to use formate (Maymó-Gatell *et al.* 1997). Taken together, these data suggest that electrons derived from the oxidation of butyryl-CoA are delivered to the membrane bound cytochrome *b* -linked hydrogenase (*hydIIABC* gene product) via the FeS oxidoreductase. I propose two possible pathways for the production of hydrogen with electrons derived from butyryl-CoA oxidation. In the first, the FeS oxidoreductase physically associates with the *hydIIABC* gene product. In the second proposed mechanism, electrons are delivered via the menaquinone pool, with the FeS oxidoreductase serving as an electron transferring flavoprotein:menaquinone oxidoreductase.

The genome of *S. aciditrophicus* contains genes predicted to encode an Rnf-like complex. This complex is thought to be essential for reverse electron transfer during benzoate oxidation. A total of thirty-two membrane complexes were identified from membrane fractions of *S. aciditrophicus* and three of these were unique to cells from both benzoate and cyclohexane carboxylate grown cultures. I did detect peptides derived from Rnf-like subunits, though these were not specific to syntrophically grown cells. To test for the ability of *S. aciditrophicus* membrane vesicles to catalyze an Rnf-like activity, I assayed for the reduction of the low potential acceptors benzyl viologen ($E^{0'}$ = -360 mV) or methyl viologen ($E^{0'}$ = -460 mV) with electrons derived from NADH. Membrane fractions were able to reduce benzyl viologen and methyl viologen with electrons derived from NADH. Notably, fractions obtained from cells grown syntrophically had higher specific activities. Curiously, my assays demonstrated that this ability was retained in the presence of the detergent, dodecyl maltoside, though only at about 40% of what was observed in fractions without detergent. I partially

purified fractions demonstrating this Rnf-like activity using size exclusion chromatography and Rnf-like subunits were detected in these fractions using peptide mass fingerprint analysis. Taken together, these data argue that *S. aciditrophicus* uses an Rnf-like complex to catalyze reverse electron transport and that, relative to syntrophic physiology, this activity is probably an important source of reduced ferredoxin for acyl-CoA oxidation by acyl-CoA dehydrogenase, and/or for production of hydrogen or formate by ferredoxin-linked hydrogenase or formate dehydrogenase.

As expected, the full suite of enzymes necessary for hydrogenotrophic methanogenesis was detected in the genome of *M. hungatei*. Gene clusters predicted to code for five different formate dehydrogenase enzymes, three membrane-bound hydrogenases and a soluble hydrogenase predicted to be factor 420 reducing were detected. A catalytic subunit for a factor 420 non-reducing hydrogenase was not detected. I did find complete biosynthetic pathways for all amino acids except histidine. My analyses of data from the whole-cell proteome of *M. hungatei* demonstrated that *M. hungatei* expressed both hydrogenases and formate dehydrogenases and also showed an increase in the core methanogenic machinery during growth in crotonate-oxidizing and syntrophic butyrate-oxidizing cocultures. I also noted that the relative abundance of energy production and cofactor synthesis associated peptides increased while those involved in translation decreased in cells grown in coculture relative to those grown axenically on hydrogen and carbon dioxide. Overall, these data are consistent with a strategy to maximize energy production efficiency and curtail biosynthesis under hydrogen limitation.

Chapter 2: Membrane complexes formed by *Syntrophomonas wolfei* during axenic and syntrophic growth

Abstract

Reverse electron transport is necessary for coupling the syntrophic oxidation of butyrate ($E^{0'}$ = -10 mV) to the production of hydrogen (E' = -260 mV at 1 Pa H_2 and pH 7) and/or formate (E' = -290 mV at 1 µM formate and pH 7) during syntrophic metabolism of butyrate. The enzyme systems involved in this phenomenon are not known. Here, I investigated the composition of the membrane proteome of replicate *Syntrophomonas wolfei* cultures grown either fermentatively on crotonate or in syntrophic coculture on crotonate and butyrate with the methanogen, *Methanospirillum hungatei* JF1. *S. wolfei* membrane complexes were electrophoretically separated using blue-native polyacrylamide gel electrophoresis (BN-PAGE). Observable bands were excised, digested with trypsin, and peptides were sequenced using liquid chromatography tandem mass spectrometry (LC-MS/MS). Peptides were identified using the MASCOT server. I observed a total of 12 bands, four of which were unique to syntrophic growth on butyrate. One band (Bt6), with an apparent molecular weight of ~160 kDa, was found only in membranes of butyrate-grown *S. wolfei* cells. Peptide mass fingerprint analysis revealed that this band was composed of peptides encoded by gene clusters annotated as an FeS oxidoreductase, electron transfer flavoprotein (*etfAB*), and a cytochrome-*b* linked hydrogenase (*hydIIABC* gene product). Separated membrane complexes were tested for their ability to reduce tetrazolium red with hydrogen as electron donor. A complex corresponding to Bt6 tested positive for this activity, and peptide mass fingerprint analysis showed that peptides encoded by *hydIIABC* were present in this complex. Whole cell, shotgun proteomic analysis showed that peptides coded for by *hydIIAB* were about six-fold more abundant when *S. wolfei* grew in

coculture on butyrate or on crotonate relative to *S. wolfei* grown in pure culture on crotonate. I was unable to detect peptides derived from cytochrome *b* from whole cell shotgun proteomic analysis. No difference was observed in the relative abundance of peptides derived from the Etf subunits or peptides derived from the FeS oxidoreductase among the three growth conditions. Transcriptomic analyses by quantitative RT-PCR revealed that the expression of *hydIIABC* and the gene encoding the FeS oxidoreductase (Swol_0698) were upregulated during syntrophic growth on butyrate with *M. hungatei* or *Dehalococcoides* sp. The presence of a sodium dependent ATP synthase subunit in band Bt6 may suggest that a chemiosmotic gradient drives the production of hydrogen with electrons derived from butyryl-CoA. Based on the cooccurrence of the FeS oxidoreductase with ETFα/β, I propose that the Swol_0698 gene product is the membrane input module for electrons derived from oxidation of acyl-CoA intermediates in *S. wolfei*. The upregulation of Swol_0698 and *hydIIABC* when *S. wolfei* was grown in coculture on butyrate argues strongly for the importance of these genes in syntrophic butyrate metabolism. The FeS oxidoreductase (Swol_0698 gene product), *etfAB* gene products, and *hydIIABC* gene products may form one membrane complex that uses chemiosmotic energy to shift the redox level of electrons derived from butyryl-CoA oxidation to the redox level of hydrogen. Alternatively, the *etfAB* gene products and FeS oxidoreductase may form one complex while *hydIIABC* gene products may form a separate complex with electron transfer between the complexes mediated by menaquinone.

Introduction

Fatty acid oxidation by syntrophic bacteria is essential for biological methane production (McInerney *et al.* 1979; McInerney *et al.* 1981). Butyrate degradation by *Syntrophomonas wolfei*, a member of the *Syntrophobacterales* order of the Deltaproteobacteria, serves as the model system for investigating and understanding this important topic (McInerney *et al.* 1981; Muller *et al.* 2009; Muller *et al.* 2010; Schmidt *et al.* 2013; Sieber *et al.* 2010; Wallrabenstein and Schink 1994) because it was the first stable fatty acid oxidizing coculture isolated. Butyrate oxidation is endergonic under standard conditions according to the following equation:

(eq. 1) butyrate $+ 2\ H_2O \rightarrow 2$ acetate $+ H^+ + 2\ H_2$ $\Delta G^{0'} = +48.3$ kJ/mol

However, butyrate oxidation becomes exergonic when the fatty acid oxidizer is partnered with a hydrogen- and/or formate-scavenging organism such as *Methanospirillum hungatei* (McInerney *et al.* 2009; McInerney *et al.* 2008; Stams and Plugge 2009). This process, known as syntrophy, is a thermodynamically based interaction whereby metabolic end products of fatty-acid fermentation such as hydrogen, formate and acetate are maintained at extremely low levels (e.g. less than 1 Pa hydrogen at pH 7 or less than 1 μM formate at pH 7) by hydrogen/formate-consuming organisms. This relationship allows for the thermodynamically favorable oxidation of butyrate by *S. wolfei* (McInerney *et al.* 2009; McInerney *et al.* 2008; Stams and Plugge 2009).

S. wolfei oxidizes butyrate to acetate, hydrogen and/or formate in syntrophic association with a hydrogen and/or formate using microorganism, such as *M. hungatei (McInerney et al. 1981)*. Electrons derived from the activated form of butyrate, butyryl-CoA, are at a high redox potential ($E^{o'}$ = -10 mV) (Sato *et al.* 1999) relative to the low redox potential of the electron accepting processes, proton reduction to hydrogen or carbon dioxide reduction to formate (McInerney *et al.* 2008). The latter two processes have redox potentials of E' = -260 mV and E = -290 mV at pH 7, respectively, when the concentrations of hydrogen and formate are low, 1 Pa and 1 μM, respectively (Sieber *et al.* 2012). The change in redox potential for hydrogen or formate production from the oxidation of butyryl-CoA is unfavorable (ΔE of -250 or -280 mV, respectively). This redox reaction can only occur if energy input occurs by a process called reverse electron transfer (Sieber *et al.* 2012). The major questions concerning syntrophic fatty acid metabolism are what mechanisms are used for reverse electron transfer and what protein complexes are involved in this important reaction.

One possible explanation is electron bifurcation (Buckel and Thauer 2013), where the energy released by an energetically favorable reaction is used to drive an unfavorable redox reaction. One of the first examples of electron bifurcation in anaerobic metabolism was the butyryl-CoA dehydrogenase complex found in *Clostridium kluyveri* (Li *et al.* 2008). *C. kluyveri* ferments ethanol and acetate to butyrate and small amounts of hydrogen. A soluble enzyme complex in *C. kluyveri* couples the energetically favorable reduction of crotonyl-CoA to butyryl-CoA by NADH with the unfavorable reduction of ferredoxin (Fd) by NADH according to the following equation:

(eq. 2) Crotonyl-CoA + Fd_{ox} + 2 NADH → Butyryl-CoA + Fd_{red} + 2NAD^+

Purification of the enzyme complex showed that it was FAD-dependent (Li *et al.* 2008). All three subunits of the complex contain FAD binding sites (Li *et al.* 2008). Once $FADH_2$ is formed, electron flow is split with one electron used for the exergonic reduction of crotonyl-CoA ($E^{0'}$= - 10 mV), which drives the endergonic reduction of ferredoxin ($E^{0'}$ = - 410 mV) by the other electron. The reversal of this reaction could accomplish reverse electron transport during syntrophic butyrate metabolism. Here, the electron flow from two different donors, butyryl-CoA and reduced ferredoxin, would combine, or confurcate, to reduce one electron acceptor, NAD^+. *S. wolfei* has a gene cluster containing electron transfer flavoprotein genes, *etfAB*, and a gene for an acyl-CoA dehydrogenase (*bcd*) (Swol_0266-268) (Sieber *et al.* 2010). It is possible that the three gene products form a soluble reverse electron transport complex analogous to that in *Clostridium kluyveri* (Herrmann *et al.* 2008; Li *et al.* 2008). Electron bifurcation has also been shown to drive hydrogen production from NADH by coupling this endergonic reaction with the exergonic reaction of hydrogen production from reduced ferredoxin (Schut and Adams 2009). The fully sequenced and annotated genome of *S. wolfei* contains genes predicted to code for confurcating hydrogenases and formate dehydrogenases (Sieber *et al.* 2010), which may play a role in the energetically unfavorable reaction of making hydrogen or formate from NADH.

Another possibility is to use a chemiosmotic gradient to drive reverse electron transfer. Inverted membrane vesicles of *S. wolfei* were shown to produce small amounts

of hydrogen *in vitro* in the presence of butyrate (Wallrabenstein and Schink 1994) and hydrogen production was shown to be inhibited with the addition of the protonophore carbonylcyanide m-chlorophenyl-hydrazone (Wallrabenstein and Schink 1994). The addition of the ATPase inhibitor N,N' dicyclohexylcarbodiimide resulted in near complete inhibition of hydrogen production with electrons derived from butyrate by inverted *S. wolfei* vesicles (Wallrabenstein and Schink 1994). This led the authors to conclude that a chemiosmotic gradient is maintained through ATP hydrolysis and that chemiosmotic energy allows for butyryl-CoA oxidation coupled to hydrogen production (Wallrabenstein and Schink 1994). Chemiosmotic energy has also been implicated in the syntrophic oxidation of benzoate by *Syntrophus gentianae* (Schöcke and Schink 1997) and *Syntrophus buswellii* (Wallrabenstein and Schink 1994) and during syntrophic glycolate oxidation (Friedrich and Schink 1993).

I, therefore, hypothesized that *S. wolfei* contains a membrane complex that uses chemiosmotic energy to couple the production of hydrogen with electrons derived from butyryl-CoA. To test this hypothesis, I used native gel electrophoresis to separate proteins from the membrane fractions of *S. wolfei* cells grown axenically on crotonate, in methanogenic coculture on crotonate and in syntrophic butyrate-oxidizing coculture on butyrate. I identified a membrane-bound complex of approximately 162 kDa (Bt 6) which appeared unique to the syntrophic growth condition (butyrate). Peptide mass fingerprint analysis revealed the presence of an FeS oxidoreductase (Swol_0698 gene product), electron transferring flavoprotein subunits (Swol_0696-7 or *etfAB* gene products) and subunits from a cytochrome *b* –linked hydrogenase (Swol_1925-7 or *hydIIABC* gene products). I tested native complexes for the ability to reduce

tetrazolium red with hydrogen as an electron donor and a complex analogous to Bt6 tested positive for this activity. Peptide mass fingerprint analysis revealed the presence of peptides derived from all three of the *hydIIABC* gene products. Proteomic and transcriptomic analyses in butyrate-oxidizing cocultures of *S. wolfei* and either *Methanospirillum hungatei* or *Dehalococcoides* sp. confirmed the importance of these proteins during hydrogen-transfer-dependent butyrate oxidation by *S. wolfei*.

Materials and Methods

Cell culture, growth and harvesting

Syntrophomonas wolfei subsp. *wolfei* strain Göttingen (ATCC# BAA-1933) in pure-culture and in coculture with *Methanospirillum hungatei* strain JF1 (ATCC# 27890) were obtained from our culture collection. For whole-cell proteomic analyses, *S. wolfei* was grown in pure culture in defined basal medium with an 80% N_2:20% CO_2 gas phase as described previously (Beaty *et al.* 1987) with 20 mM crotonate as substrate. *S. wolfei* and *M. hungatei* cocultures were grown in the above defined basal medium with either crotonate (20 mM) or butyrate (20 mM) as carbon sources. Cocultures were grown in 2-L sealed glass bottles with one liter of medium (Beaty *et al.* 1987). For all other experiments described herein, the organisms were grown in a basal medium described elsewhere (Tanner 2002) amended with 20 mM crotonate or 10 mM butyrate as carbon source. The basal medium (Tanner 2002) was composed of the following salts in final concentration: sodium chloride (0.8 mg/L), ammonium chloride (1 mg/L), potassium chloride (1 mg/L), potassium phosphate (0.1 mg/L) magnesium

sulfate heptahydrate (0.2 mg/L), calcium chloride dihydrate (0.04 mg/L). The basal medium was composed of the following vitamins in final concentration: pyridoxine hydrochloride (0.1 mg/L), thiamine hydrochloride (0.05 mg/L), riboflavin (0.05 mg/L), calcium pantothenate (0.05 mg/L), thioctic acid (0.05 mg/L), *para*-aminobenzoic acid (0.05 mg/L), nicotinic acid (0.05 mg/L), vitamin B_{12} (0.05 mg/L), mercaptoethanesulfonic acid (0.05 mg/L), biotin (0.02 mg/L), and folic acid (0.02 mg/L). The basal medium was composed of the following metals in final concentration: nitrilotriacetic acid (0.01 mg/L), manganese (II) sulfate monohydrate (0.005 mg/L), ammonium iron (II) sulfate hexahydrate (0.004 mg/L), cobalt (II) chloride hexahydrate (0.001 mg/L), zinc sulfate heptahydrate (0.001 mg/L), copper (II) chloride dihydrate ($1 \cdot 10^{-5}$ mg/L), nickel (II) chloride ($1 \cdot 10^{-5}$ mg/L), sodium molybdate dihydrate ($1 \cdot 10^{-5}$ mg/L), sodium selenite ($1 \cdot 10^{-5}$ mg/L) and sodium tungstate ($1 \cdot 10^{-5}$ mg/L).

One liter of sterile medium in a 2-L Schott bottle was inoculated with 200 ml of *S. wolfei* pure culture or coculture grown in the same medium. All cultures were transferred a minimum of three times as one-liter cultures prior to harvesting the cells for proteomic analysis. All cultures were incubated at 37^{o}C and growth was monitored via measuring the OD_{600} with time. Substrate utilization was monitored via high-pressure liquid chromatography (Sieber *et al.* 2010). The cultures were harvested when 50 to 70% of the substrate was used. Cells were harvested anaerobically in 1-L centrifuge vessels via centrifugation at 7,000 • *g* for 20 min at 4^{o}C. The cells were washed twice by centrifugation and resuspension of the pellet with anoxic 50 mM potassium phosphate buffer (pH of 7.2) as described above. Cell pellets were stored frozen in liquid nitrogen.

In all cases except that of whole cell proteomics, cells of *S. wolfei* grown in coculture were separated from *M. hungatei* by Percoll gradient centrifugation. Frozen cell pellets were thawed and suspended in a 5:4 ratio of standard isotonic Percoll to 50 mM potassium phosphate buffer (pH of 7.2), which was anaerobically prepared. Cell suspensions were transferred into sealed anaerobic disposable centrifuge tubes and centrifuged at 20,000 • *g*, for 40 min at 4^0C (Beaty *et al.* 1987; Sieber *et al.* 2013). Contamination of *S. wolfei* cells with *M. hungatei* cells was determined microscopically and fractions containing less than one *M. hungatei* cell per 100 *S. wolfei* cells were pooled. Pooled fractions were diluted 500-fold in 50 mM potassium phosphate buffer (pH 7.2) and centrifuged at 7,000 • *g* for 20 minutes to dilute out remaining Percoll. After separation, cells were used immediately.

Sample preparation for whole-cell proteomic analysis

Two cell pellets were obtained from replicate cultures of *S. wolfei* grown with 20 mM crotonate grown as described (see cell culture, growth and harvesting). Two cell pellets were obtained from replicate cocultures of *S. wolfei* plus *M. hungatei* strain JF1 grown with 20 mM crotonate as described (see cell culture, growth and harvesting). Finally, two cell pellets were obtained from replicate cocultures of *S. wolfei* plus *M. hungatei* strain JF1 grown with 20 mM crotonate as described (see cell culture, growth and harvesting). Cell pellets were not enriched by Percoll density gradient centrifugation. Cell pellets were shipped frozen on dry ice.

Each cell pellet was prepared separately for shotgun proteomics analysis by following a protocol optimized for the measurement of small bacterial samples

(Thompson *et al.* 2008). Cell pellets were lysed and proteins denatured by incubating each cell pellet overnight at 37°C in 250 to 400 ml of 6 M guanidine and 10 mM dithiothreitol (the larger volumes used for larger cell pellets). The lysates were cooled to ambient temperature, and diluted with 50 mM tris(hydroxymethyl)aminomethane (Tris) buffer with 10mM calcium chloride to decrease the guanidine concentration to ~ 1 M. Ten milligrams of trypsin (sequencing grade, Promega, Madison WI) were added to each lysate, followed by incubation at 37°C for five hours. An additional 10 mg trypsin was added, followed by a further overnight incubation at 37°C. Any remaining disulfide bonds were reduced by adding additional dithiothreitol to a final concentration of 10 mM and incubating for one hour at 37°C. Desalting was performed using reverse-phase solid-phase extraction cartridges (Sep-Pak Lite C18, Waters, Milford MA), with final elution using 0.1% formic acid in acetonitrile. Solvent transfer to aqueous 0.1% formic acid was performed by vacuum centrifugation, with final volume adjusted to 150 ml. Particulates and remaining cellular debris were removed by centrifugation through 0.45mm pore filters (Ultrafree-MC, Millipore, Billerica MA). The samples were then frozen at -80°C until used.

Whole cell proteomic analysis

Tryptic peptide mixtures were analyzed by two-dimensional liquid chromatography/tandem mass spectrometry (2D LC-MS-MS), using the MudPIT approach (Washburn *et al.* 2001; Wolters *et al.* 2001) implemented as previously described by our colleagues at Oak Ridge National Laboratory. Two LC-MS/MS analyses were performed on the tryptic digest from each cell pellet, which would result

in two technical replicates for each of two biological replicates per growth condition. Aliquots (50 ml) were loaded via a pressure cell (New Objective, Woburn MA) onto a "back" column fabricated from 150 mm internal diameter fused silica tubing (Polymicro Technologies, Phoenix AZ) packed with a ~4 cm-long bed of reverse-phase chromatographic phase (Jupiter C18, 3 mm particle size, Phenomenex, Torrance CA) upstream of a ~4 cm bed of strong cation exchange material (5 mm particle size SCX, Phenomenex).

After sample loading, the back column was attached via a filter union (Upchurch Scientific, Oak Harbor WA) to a "front" analytical column fabricated from a 100 mm internal diameter PicoTip Emitter (New Objective), packed with a ~14 cm bed of reverse-phase material (Jupiter C18, 3 mm particle size, Phenomenex). Two-dimensional liquid chromatography was performed via twelve step-gradients of increasing salt (ammonium acetate) concentration, with the eluted peptides from each strong cation exchange step subsequently resolved via a separate reverse-phase gradient (Ultimate HPLC, LCPackings/Dionex, Sunnyvale, CA). The liquid chromatography eluent was interfaced via a nanospray source (Proxeon, Odense, Denmark) with a linear-geometry quadrupole ion trap mass spectrometer (LTQ, ThermoFinnigan, San Jose, CA). Data acquisition was performed in data-dependent mode under the control of XCalibur software. Up to 5 tandem mass spectra were acquired from the most abundant parent ions in full-scan mass spectra; dynamic exclusion was enabled with a repeat count of one and duration of 60 seconds.

Whole cell proteomics data analysis

Whole-cell proteomics data analysis was performed by our colleagues at Oak Ridge National Laboratory. Peptide identifications were obtained from tandem mass spectra using Sequest software (version 27) (Eng *et al.* 1994), and protein identifications were compiled from peptide identifications using DTASelect (version 1.9) (Tabb *et al.* 2002). A multiple-species protein FASTA file was constructed from individual FASTA files for *S. wolfei* subsp. *wolfei* Göttingen, *M. hungatei* JF1, and *Syntrophus aciditrophicus* SB, all downloaded from the Department of Energy Joint Genome Institute website. The sequence-reversed analog of each protein sequence was appended to the FASTA file to allow estimation of the false discovery rate of peptide identification (Elias *et al.* 2007; Moore *et al.* 2002). Sequences of 36 common contaminant proteins were also appended to the FASTA file. Peptide identifications were retained for XCorr ≥1.8 (z=1), ≥2.5 (z=2), or ≥3.5 (z=3), with DeltaCN ≥0.08. Protein identifications required identification of two peptides. The false discovery rate for peptides was generally ≤1%. Estimates of protein abundance were calculated using normalized spectral abundance factors (Zybailov *et al.* 2006).

Blue-native polyacrylamide gel electrophoresis

Blue-native polyacrylamide gel electrophoresis was usually conducted aerobically. Gels destined for testing in-gel activity staining were run anaerobically (see below). Percoll enriched *S. wolfei* pellets (see cell culture, growth and harvesting) were obtained from pure cultures or separated from *M. hungatei* cells by Percoll separation and were resuspended in 4 ml of lysis buffer described elsewhere (Swamy *et al.* 2006), which contained 20 mM 2,2-Bis(hydroxymethyl)-2,2',2''-nitrilotriethanol

(Bis-tris), ε-aminocaproic acid (500 mM), NaCl (20 mM), ethylenediaminetetraacetic acid (EDTA)(10 mM) and glycerol (10% v/v). The pH of the lysis buffer was adjusted to within 0.2 pH units of pH 7.2 with one normal hydrochloric acid and then adjusted to pH 7.2 with 0.1 N hydrochloric acid. The cells were lysed by passage through a French pressure cell at an internal pressure of 138,000 kPA. After one pass, unbroken cells and cell debris were removed by centrifugation at 8,000 • *g* for two min at ambient temperature in sealed cryovial tubes. The resulting supernatant was decanted into disposable polyallomer centrifuge tubes and the soluble and insoluble fractions were separated by ultracentrifugation at 132,000 • *g*, 60 min, 4^0C. The supernatant was decanted and the insoluble pellet was washed by resuspending in 50 mM potassium phosphate (pH 7.2) and ultracentrifuged as above. The supernatant was decanted and the remaining pellet was resuspended in approximately 250 µl of anaerobically prepared lysis buffer containing 0.5% n-dodecyl-β-maltoside (DDM) to obtain the solubilized membrane fraction. Protein quantification was done using the Pierce BCA assay. Except for membrane fractions destined for activity staining (see below), small (25 µl) aliquots of the solubilized membrane fraction were stored frozen at -20^{o}C in sealed microcentrifuge tubes after protein quantification.

BN-PAGE analysis was conducted using the methods of Schägger and von Jagow (1991) and Swamy *et al.* (2006) with the following modifications. Gel mixtures contained 50 mM Bis-tris, 67 mM ε-aminocaproic acid (pH 7.2) and a final concentration of 4% or 16% acrylamide (37.5:1 acrylamide:bis-acrylamide). The sixteen percent acrylamide gel solution additionally contained 20% glycerol (v/v). Each gel solution was polymerized with the addition of 10% ammonium persulfate (APS) and

tetramethylethylenediamine (TEMED) in a 10:1 ratio (e.g. 54 µl APS to 5.4 µl TEMED) as described previously (Swamy *et al.* 2006). Immediately after the addition of APS and TEMED, a gradient gel was prepared using a mechanical gradient mixer (BioRad) and the gel was allowed to completely polymerize after pouring (~2 hours). Occasionally, unused gels were stored overnight at 4^{o}C wrapped in wet paper towels.

The cathode buffer (Swamy *et al.* 2006) was prepared as a 10X stock solution containing 15 mM Bis-tris, 50 mM tricine, and 0.02% Coomassie blue G250 (w/v). The anode buffer (Swamy *et al.* 2006) was prepared as a 10X stock solution containing 50 mM Bis-tris. Both buffers were adjusted to within 0.2 pH units of pH 7.0 with one normal hydrochloric acid and then adjusted to pH 7.0 with 0.1 N hydrochloric acid. Prepared buffers were stored at 4^{o}C. Buffers were diluted 1:10 with deionized nanopure water prior to use. The solubilized membrane fraction (ranging from 2 to 35 µg protein) was thawed and mixed with equal parts (v:v) of BN-PAGE sample buffer. BN-PAGE sample buffer was prepared by diluting 1 ml of cathode buffer, described above, with 7 ml of deionized nanopure water and 2 ml of electrophoresis grade glycerol (≥ 99%). Gels were run at a constant 130 V for several hours until the dye front migrated to within a few millimeters of the gel bottom. Gels were fixed and destained in a solution containing 50% methanol (v/v) and 7% acetic acid (v/v), washed twice in nanopure water and then stained with either Imperial stain (ThermoFisher), SilverStain (Pierce) or SyproRuby (Thermofisher) according to manufacturer's instructions.

Tryptic digest of BN-PAGE membrane complexes

Predominant protein bands and protein bands that were unique to a given growth condition were selected for proteomic analysis. Protein bands of interest were first manually excised, washed and digested with trypsin. Gel slices were washed first in a solution of 50 mM sodium bicarbonate and 50% acetonitrile and then in 100% acetonitrile. This step was performed three times. Disulfide bonds were reduced by incubation of the gel slice in 10 mM dithiothreitol at 60°C for 1 hr. Free sulfhydryl bonds were blocked by incubating the gel slice in 50 mM iodoacetamide at 45°C for 45 min in the dark, followed by washing three times in alternating solutions of 100 mM sodium bicarbonate and 100% acetonitrile. The slices were dried and then individually incubated in a 20 ng/µl solution of porcine trypsin (Promega, Madison, WI, USA) for 45 min at 4°C, followed by incubation at 37°C for 4 to 6 hr in the same solution. Afterwards, the solution with the digested protein was transferred into a fresh collection tube. The gel slice was then incubated for 10 min in a solution of 50% acetonitrile:1% trifluoroacetic acid. The solution was removed and combined with the previously collected digested protein solutions from that gel. Gel pieces were washed three times with 50% acetonitrile:1% trifluoroacetic acid. The solution containing the digested gel peptides was then spun to dryness using a rotary evaporator at 30^0C.

Peptide sequencing was accomplished by colleagues at University of California, Los Angeles, with a nano-liquid chromatography tandem mass spectrometer (nano LC-MS/MS) (QSTAR Pulsar XL, Applied Biosystems, Foster City, CA, USA) equipped with nanoelectrospray interface (Protana, Odense, Denmark) and LC Packings (Sunnyvale, CA, USA) nano-LC system. The nano-LC was equipped with a homemade precolumn (150 × 5 mm) and analytical column (75 × 150 mm) packed with Jupiter

Proteo C12 resin (particle size 4 mm, Phenomenex, Torrance, CA, USA). The dried digested peptides were resuspended in 1% formic acid solution. Six microliters of the sample solution was loaded to the precolumn for each LC-MS/MS run. The precolumn was washed with the loading solvent (0.1% formic acid) for 4 min before the sample was injected onto the LC column. The eluents used for the LC were 0.1% formic acid (solvent A) and 95% acetonitrile containing 0.1% formic acid. The flow rate was 200 nl/min, and the following gradient was used: 3% B to 35% B in 72 min, 35% B to 80% B in 18 min, followed by 80% B for 9 min. The column was then equilibrated with 3% B for 15 min prior to the next run. Electrospray ionization was performed using a 30 mm (internal diameter) nanobore stainless steel online emitter (Proxeon, Odense, Denmark) and a voltage set at 1900 V. Peptide sequences were searched against the NCBI genomes for *S. wolfei*, *S. aciditrophicus* and *M. hungatei* using MASCOT software versions 2.1.0 and 2.1.04 (Matrix Science, London, UK). Peptides were required to have a rank = 1 and a score >18.

In-gel activity staining.

Gels used for staining with tetrazolium red as the redox indicator were run using essentially the same BN-PAGE technique described above with the following modifications. All buffers except for the lysis buffer were prepared and boiled under 80% N_2: 80% CO_2 for five minutes to remove oxygen. Because the lysis buffer contained presumably heat labile components (e.g. ε-aminocaproate and EDTA), it was prepared in the anaerobic chamber using anoxic water which had been prepared by boiling under 80% N_2:20% CO_2 for five minutes. All manipulations were performed in

the anaerobic chamber, and all centrifuge steps occurred in sealed anaerobic centrifuge tubes.

To enhance resolution, activity staining was done using 4-16% precast NativePage gels obtained from Life Technologies. Gels were run in the anaerobic chamber using anaerobic anode and cathode buffer. To minimize oxygen interference with the activity assay, precast gels were run with just anode and cathode buffer for ten minutes before the protein suspension was loaded.

After electrophoresis, gels were cut into lanes and the lanes were carefully transferred into anaerobic glass tubes. The tubes were stoppered with butyl-rubber stoppers. The headspace of these tubes was changed to 80% N_2:20% CO_2 prior to the addition of reaction buffer. Ten milliliters of reaction buffer (1 mM triphenyl tetrazolium chloride in 50 mM potassium phosphate pH 7.2) were added to the sealed tubes containing gel slices. Activity staining began with the addition of formate to 1mM from a 100 mM stock solution prepared in 50 mM potassium phosphate (pH 7.2) or the addition of hydrogen to 138 kPa. Activity was monitored by the formation of a reddish-purple precipitate. A band testing positive for hydrogenase was manually excised and sent for peptide mass fingerprint analysis by the University of Oklahoma Health Sciences Center Proteomics Core Facility, Oklahoma City, OK.

RNA extraction and quantitative reverse transcriptase polymerase chain reaction (qRT-PCR).

Cell cultures destined for qRT-PCR analysis were harvested after 50% substrate loss which corresponded to the mid-log phase of growth. Triplicate cultures were

cooled in a dry ice-ethanol bath and taken into the anaerobic chamber. Cultures were dispensed into RNase ZAP treated centrifuge bottles (1 L) and centrifuged at 8,000 • *g* for 15 min. The cell pellet was resuspended in 1.5 ml of RNAlater and stored at -70^{o}C. Total RNA was obtained using an RNeasy mini kit. DNA was removed using an off-column DNA digestion and total RNA was concentrated using the RNeasy kit. RNA quality was determined by gel electrophoresis. Locus tag specific primers (Table 2) were designed using primer-BLAST and checked against the genome sequences of *M. hungatei* and *Dehalococcoides*. RNA was verified to be free of DNA contamination by PCR without reverse transcriptase. Desalted primers were made by Life Technologies. qRT-PCR was performed on biological triplicates with technical duplicates.

Table 2: Primers for quantitative RT-PCR analysis of *hydIIABC, etfAB,* Swol_0698*, fdhA-1, fdhA-2 and fdhA-4* in *S. wolfei*. Primers were designed using primer-BLAST and checked against genome sequences for *M. hungatei* and *Dehalococcoides* sp. [1] Sieber *et al.* 2013

Gene	Locus Tag	Primer sequence (5' → 3')
gyrB[1]	Swol_0006	TGAAGGACAGACCAAAACCA
		AATATAGCCTGGTAGGTGCG
hydIIA[1]	Swol_1925	TATGCGGAGGACAACTACCC
		CTGAGGATTTCATAGGCGGT
hydIIB	Swol_1926	GAAAGTGAAGGCATCACCAG
		GCTTCATGCACATAATGGGG
hydIIC	Swol_1927	CCAACGCCTCTCTAGTTCAT
		AGAAATACTGCAGGCACAGA
etfA	Swol_0697	TGTTGCCAACTTCACATACG
		TATGGTGCGGACAAGGTTTA
etfB	Swol_0696	AATAGTGGTTGTTGCTGCTG
		ACTTCGGTTACCTGAGTTCC
FeS	Swol_0698	ACCCTGGTAAGCCAGAACCT
oxidoreductase		TGGTCGTAGACCCCGTTGTG
fdhA1[1]	Swol_0786	CATAGAAGCCAACCGGGAAA
		CCCTTCTCTCGGTGTTGGTA
fdhA2[1]	Swol_0800	CAGCATCAGCAGCAAAAGAG
		CTTCCCACTTGTCACTACCA
fdhA4[1]	Swol_1825	CCAAGAACAACCCAGCAAAT
		GGGGTTTTAATGCCACTTCC

Results

Results from whole cell proteomic studies

Using whole cell shotgun proteomics, a total of 1,405 unique peptides were identified by peptide mass fingerprint analysis across all three culture conditions; *S. wolfei* in pure culture on crotonate, *S. wolfei* in coculture with *M. hungatei* on crotonate and *S. wolfei* in coculture with *M. hungatei* on butyrate. Alignment of peptide sequences with predicted amino acid sequences of *S. wolfei* genes was possible for 1,095 peptide sequences representing approximately 80% of the detected peptides. As detailed elsewhere (Sieber *et al.* 2010), 2,574 protein coding open reading frames (ORFs) have been identified in the genome of *S. wolfei*. Thus, the peptides detected by whole cell shot gun proteomic analysis accounts for approximately 45% of protein coding genes in the *S. wolfei* genome. Two-hundred and fifty peptide sequences aligned to predicted amino acid sequences for ORFs in the genome of *M. hungatei* and 57 peptide sequences matched predicted amino acid sequences for ORFs found in the genome of the syntrophic bacterium *Syntrophus aciditrophicus* strain SB. The full dataset is available elsewhere (Sieber 2011). *M. hungatei* proteins are likely from remnant cells that were not removed by Percoll separation. *S. aciditrophicus* proteins may be contaminants on glassware as this organism is also grown in Dr. McInerney's laboratory. Peptides from *M. hungatei* and *S. aciditrophicus* were removed from the dataset prior to calculation of normalized spectral abundance of the *S. wolfei* peptides.

A recent report suggested that interspecies formate transfer plays a more prominent role than interspecies hydrogen transfer when *S. wolfei* grows syntrophically on butyrate based on the presence of formate dehydrogenases in the cytoplasmic

proteome and formate dehydrogenase activity but not hydrogenase activity in membranes (Schmidt *et al.* 2013). We used whole cell shotgun proteomic analysis to determine the relative abundance of hydrogenases and formate dehydrogenases in the *S. wolfei* proteome grown axenically and syntrophically.

Multiple genes encoding hydrogenase and formate dehydrogenase enzymes were identified in the genome of *S. wolfei* (Sieber *et al.* 2010). Three hydrogenase-encoding regions were reported in the *S. wolfei* genome and all three hydrogenases are predicted to be [FeFe]-type hydrogenases (Sieber *et al.* 2010). Peptides were detected which correspond to subunits of each of these. Interestingly, subunits of the hydrogenase encoded by Swol_1925-26 (*hydIIAB* gene products) were detected at levels six-fold higher in abundance when *S. wolfei* was grown in coculture on butyrate or on crotonate relative to *S. wolfei* grown in pure culture on crotonate (Figure 1).

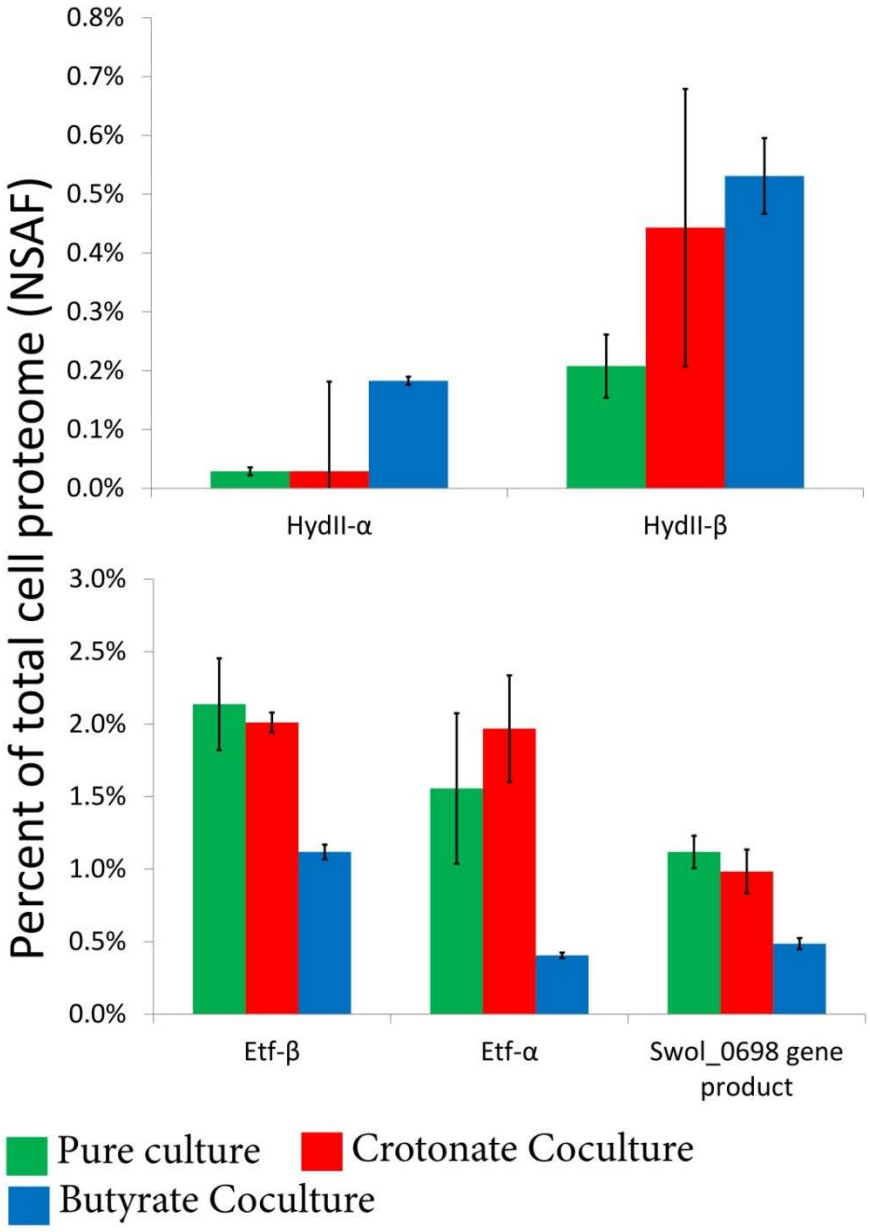

Figure 1: Detection of the predicted membrane-bound [FeFe]-hydrogenase (Swol_1925-26 gene products) in cultures of *S. wolfei* grown under different conditions. Tryptic digests of the whole-cell proteome were prepared from cells harvested after 50% substrate utilization. Peptides were sequenced via peptide mass fingerprinting via LC-MS/MS and peptides were identified using MASCOT. Values represent Normalized Spectral Abundance Factor (NSAF) • 100 to represent percent of peptide in the proteome. Peptides from both subunits of the cytochrome *b*-linked hydrogenase provided more signal intensity during growth in crotonate-oxidizing coculture or during syntrophic growth on butyrate. Error bars represent standard deviation of replicate cultures.

Swol_1925-26 are predicted to encode an externally oriented cytochrome *b* -linked membrane hydrogenase (Sieber *et al.* 2010). The cytochrome *b* subunit encoded by Swol_1927 (*hydIIC* gene product) is predicted to be an integral membrane protein. A total of five formate dehydrogenase-encoding regions were identified in the genome of *S. wolfei* (Sieber *et al.* 2010) though no obvious changes in normalized abundance values were detected for any of the formate dehydrogenases between different growth conditions (not shown). Based on these data, we conclude that interspecies hydrogen transfer is essential for syntrophic oxidation of butyrate.

Predicted membrane proteins from complexes identified in S. wolfei membrane enrichments.

Whole cell shot gun proteomic analysis showed that syntrophically grown cells of *S. wolfei* are enzymatically conditioned for hydrogen rather than formate production. I hypothesized that an integral membrane complex uses chemiosmotic energy to drive reverse electron transfer to produce hydrogen from high potential electrons derived from butyryl-CoA oxidation. To identify membrane-bound protein complexes potentially involved in reverse electron transfer, membrane proteins from *S. wolfei* cells grown in pure culture on crotonate and in coculture on crotonate (conditions that do not require reverse electron transfer) were compared to membrane proteins from *S. wolfei* cells grown syntrophically on butyrate (a condition that requires reverse electron transfer). Membrane proteins were solubilized with the detergent, n-dodecyl-β-d-maltoside (DDM), and electrophoretically separated using BN-PAGE.

I consistently observed twelve membrane complexes (Figure 2) across multiple biological and technical replicates. Several faint bands were occasionally observable and were largely dependent on the amount of protein loaded. Tryptic digests were prepared from bands observed from two experiments and sequenced by peptide mass fingerprint analysis (Figure 2). The main difference between these experiments was whether *S. wolfei* cells had been purified by Percoll separation prior to BN-PAGE. Except where indicated, all data refer to the experiment where cells were not first separated by Percoll density gradient ultracentrifugation.

A large 1,060 kDa complex (bands CPC1, CCC1 and Bt1) was detected under all three growth conditions (Figure 2). This band was primarily composed of proteins of unknown function encoded by genes Swol_0143 and Swol_0141 (Table 3). Both are

Table 3: Peptides detected from non-denaturing blue-native PAGE separation of solubilized *S. wolfei* membranes. Observed bands were excised, digested with trypsin and peptides sequenced by peptide mass fingerprint analysis. Unique peptides correspond to the number of unique peptides detected by peptide mass fingerprint analysis from the respective band. Peptides were identified by a MASCOT search using the NCBInr database. Scores represent the score returned by MASCOT. TMH = predicted transmembrane helices, MW_{app} apparent molecular weight for the indicated band, MW_p = molecular weight of the predicted amino acid sequence for the respective locus tag, pI = isoelectric point of the predicted amino acid sequence for the respective locus tag.

Band # (MW_{app})	Locus Tag	Annotation	Score	Unique Peptides	TMH	MW_p	pI
CPC1	Swol_0143	hypothetical protein Swol_0143	4385	150	Yes	142	4.3
(1060	Swol_0141	hypothetical protein Swol_0141	2181	83	Yes	76	5.3
kDa)	Swol_1348	3-deoxy-D-arabinoheptulosonate-7-phosphate synthase	1003	37	No	37	6.7
	Swol_2051	acetyl-CoA acetyltransferase / 3-ketoacyl-CoA thiolase	767	32	No	41	5.9
	Swol_1934	acetyl-CoA acetyltransferase	397	23	No	42	6.3
	Swol_2386	F0F1-type ATP synthase subunit b-like protein	263	11	Yes	19	5.1
	Swol_0809	3-deoxy-D-arabinoheptulosonate-7-phosphate synthase	254	16	No	30	7.4
	Swol_2167	SPFH domain, Band 7 family protein	142	5	No	32	8.4
	Swol_2382	Sodium-transporting two-sector ATPase	137	3	Yes	52	4.6
	Swol_2384	Sodium-transporting two-sector ATPase	132	5	Yes	55	4.9
	Swol_1863	SPFH domain, Band 7 family protein	126	6	No	34	4.9
	Swol_2335	translation elongation factor 1A (EF-1A/EF-Tu)	118	3	No	44	5.0
	Swol_0815	phenylacetate-CoA ligase	110	3	No	50	5.2
	Swol_0644	tryptophan synthase, beta chain	95	2	Yes	51	5.7

	Swol_1855	conserved hypothetical protein	69	2	No	58	4.6
	Swol_2387	ATP synthase F0, C subunit	68	4	No	7	6.6
	Swol_2321	LSU ribosomal protein L5P	58	5	No	20	9.9
	Swol_0410	(R)-2-hydroxyglutaryl-CoA dehydratase beta-subunit, putative	44	2	No	43	4.8
	Swol_0411	CoA enzyme activase	44	3	No	28	5.7
	Swol_0325	conserved hypothetical protein	41	5	No	36	5.3
	Swol_2030	3-hydroxyacyl-CoA dehydrogenase	41	2	No	30	7.3
	Swol_1577	chaperone DnaJ	38	2	No	42	8.3
	Swol_0278	putative esterase/lipase	29	8	No	29	7.3
	Swol_1195	indolepyruvate oxidoreductase subunit beta 2	26	2	No	22	9.3
CPC2	Swol_0143	hypothetical protein Swol_0143	887	29	Yes	142	4.3
(585	Swol_2384	Sodium-transporting two-sector ATPase	145	4	No	55	4.9
kDa)	Swol_1424	protein translocase subunit secF	115	3	Yes	32	9.2
	Swol_1425	protein-export membrane protein SecD	106	3	Yes	43	9.0
	Swol_0222	hypothetical protein Swol_0222	26	3	No	47	4.5
	Swol_2089	conserved hypothetical protein	86	2	Yes	38	8.7

CPC3	Swol_0133	hypothetical protein Swol_0133	13978	406	No	78	4.7
(310	Swol_2384	Sodium-transporting two-sector ATPase	580	22	No	55	4.9
kDa)	Swol_1871	glycosyl hydrolase-like protein	88	11	Yes	52	5.4
	Swol_0698	putative iron-sulfur-binding reductase	54	9	Yes	81	5.5
	Swol_1142	DNA helicase/exodeoxyribonuclease V, subunit B	30	8	No	131	5.7
	Swol_2382	Sodium-transporting two-sector ATPase	74	6	No	51	4.6
	Swol_0405	ABC-type sugar transport system periplasmic component-like protein	60	4	Yes	48	5.5
	Swol_0457	hypothetical protein Swol_0457	41	4	No	13	4.2
	Swol_0331	extracellular solute-binding protein, family 7	100	2	Yes	41	8.6
	Swol_2432	conserved hypothetical protein	71	2	Yes	30	5.5
	Swol_0490	chaperone protein DnaK	25	2	No	68	4.7
CCC1	Swol_0143	hypothetical protein Swol_0143	5082	182	Yes	142	4.3
(1060	Swol_0141	hypothetical protein Swol_0141	2664	91	Yes	76	5.3
kDa)	Swol_2386	F0F1-type ATP synthase subunit b-like protein	590	23	Yes	19	5.1
	Swol_1185	lemA protein	240	10	Yes	20	9.6
	Swol_2387	ATP synthase F0, C subunit	169	8	Yes	7	6.6
	Swol_0278	putative esterase/lipase	30	8	No	28	7.3

	Swol_2321	LSU ribosomal protein L5P	67	7	No	20	9.9
	Swol_0325	conserved hypothetical protein	31	7	No	36	5.3
	Swol_2563	YyaC	39	5	No	22	8.0
	Swol_2382	Sodium-transporting two-sector ATPase	115	3	No	51	4.6
	Swol_1161	protein of unknown function UPF0182	36	3	Yes	106	5.9
	Swol_1417	condensin subunit ScpB	22	3	No	19	4.9
	Swol_0133	hypothetical protein Swol_0133	88	2	No	78	4.7
	Swol_1855	conserved hypothetical protein	85	2	No	58	4.6
	Swol_0562	hypothetical protein Swol_0562	76	2	Yes	19	9.4
	Swol_2384	Sodium-transporting two-sector ATPase	62	2	No	55	4.9
CCC2 (585 kDa)	Swol_0143	hypothetical protein Swol_0143	2781	99	Yes	142	4.3
	Swol_1425	protein-export membrane protein SecD	290	11	Yes	43	9.0
	Swol_2384	Sodium-transporting two-sector ATPase	279	10	No	55	4.9
	Swol_0133	hypothetical protein Swol_0133	285	9	No	78	4.7
	Swol_1855	conserved hypothetical protein	333	8	No	58	4.6
	Swol_2432	conserved hypothetical protein	244	7	Yes	30	5.5
	Swol_1424	protein translocase subunit secF	197	6	Yes	32	9.2
	Swol_1925	Ferredoxin hydrogenase	197	5	No	42	4.9
	Swol_0278	putative esterase/lipase	28	5	No	28	7.3

	Swol_0413	conserved hypothetical lipoprotein	185	4	No	43	5.2
	Swol_0698	putative iron-sulfur-binding reductase	144	3	Yes	81	5.5
	Swol_2089	conserved hypothetical protein	112	3	Yes	38	8.7
	Swol_2387	ATP synthase F0, C subunit	91	3	Yes	7	6.6
	Swol_1911	conserved hypothetical protein	53	3	Yes	21	5.8
	Swol_2563	YyaC	26	3	No	22	8.0
	Swol_2556	branched chain amino acid ABC transporter (substrate-binding protein)	122	2	Yes	42	5.6
	Swol_0331	extracellular solute-binding protein, family 7	96	2	Yes	41	8.6
	Swol_1871	glycosyl hydrolase-like protein	26	2	Yes	52	5.4
CCC3 (310 kDa)	Swol_0133	hypothetical protein Swol_0133	10757	332	No	78	4.7
	Swol_0698	putative iron-sulfur-binding reductase	285	18	Yes	81	5.5
	Swol_1871	glycosyl hydrolase-like protein	78	11	Yes	52	5.4
	Swol_1730	exonuclease	26	11	No	142	5.4
	Swol_2384	Sodium-transporting two-sector ATPase	240	9	No	55	4.9
	Swol_0331	extracellular solute-binding protein, family 7	120	5	Yes	41	8.6
	Swol_0457	hypothetical protein Swol_0457	32	3	No	13	4.2
	Swol_2556	branched chain amino acid ABC transporter (substrate-binding protein)	118	2	Yes	42	5.6

	Swol_0490	chaperone protein DnaK	27	2	No	68	4.7
	Swol_2472	peptidase M23B	22	2	Yes	50	8.4
Bt1 (1060 kDa)	Swol_0143	hypothetical protein Swol_0143	4745	163	Yes	142	4.3
	Swol_0141	hypothetical protein Swol_0141	1810	64	Yes	76	5.3
	Swol_2386	F0F1-type ATP synthase subunit b-like protein	227	9	Yes	19	5.1
	Swol_0278	putative esterase/lipase	30	9	No	28	7.3
	Swol_2321	LSU ribosomal protein L5P	75	5	No	20	9.9
	Swol_0325	conserved hypothetical protein	32	5	No	36	5.3
	Swol_0133	hypothetical protein Swol_0133	158	3	No	78	4.7
	Swol_1855	conserved hypothetical protein	78	2	No	58	4.6
Bt2 (870 kDa)	Swol_2384	Sodium-transporting two-sector ATPase	237	8	No	55	4.9
	Swol_2386	F0F1-type ATP synthase subunit b-like protein	56	2	Yes	19	5.1
Bt3 (640 kDa)	Swol_2386	F0F1-type ATP synthase subunit b-like protein	316	13	Yes	19	5.1
	Swol_0927	putative methyl-accepting chemotaxis sensory transducer	126	2	Yes	62	4.5
	Swol_2384	Sodium-transporting two-sector ATPase	74	2	No	55	4.9

Bt4	Swol_0133	hypothetical protein Swol_0133	1050	45	No	78	4.7
(460	Swol_0091	Formate/nitrite family of transporters	623	11	Yes	31	8.4
kDa)	Swol_2384	Sodium-transporting two-sector ATPase	360	11	No	55	4.9
	Swol_1855	conserved hypothetical protein	188	8	No	58	4.6
	Swol_2382	Sodium-transporting two-sector ATPase	191	4	No	51	4.6
	Swol_1911	conserved hypothetical protein	79	4	Yes	21	5.8
Bt5	Swol_0133	hypothetical protein Swol_0133	14699	413	No	78	4.7
(310	Swol_1064	Inorganic diphosphatase	336	17	Yes	88	5.4
kDa)	Swol_1730	exonuclease	24	13	No	142	5.4
	Swol_1855	conserved hypothetical protein	303	12	No	58	4.6
	Swol_0698	putative iron-sulfur-binding reductase	49	10	Yes	81	5.5
	Swol_1871	glycosyl hydrolase-like protein	85	9	Yes	52	5.4
	Swol_1424	protein translocase subunit secF	278	8	Yes	32	9.2
	Swol_1925	Ferredoxin hydrogenase	284	7	No	42	4.9
	Swol_2384	Sodium-transporting two-sector ATPase	194	6	No	55	4.9
	Swol_1425	protein-export membrane protein SecD	182	5	Yes	43	9.0
	Swol_2089	conserved hypothetical protein	144	4	Yes	38	8.7
	Swol_2556	branched chain amino acid ABC transporter (substrate-binding protein)	169	3	Yes	42	5.6

	Swol_1934	acetyl-CoA acetyltransferase	59	3	No	41	6.3
	Swol_0331	extracellular solute-binding protein, family 7	92	2	Yes	41	8.6
	Swol_0457	hypothetical protein Swol_0457	31	2	No	13	4.2
Bt6	Swol_1925	Ferredoxin hydrogenase	1208	41	No	42	4.9
(165	Swol_1926	hypothetical protein Swol_1926	379	10	Yes	15	5.9
kDa)	Swol_0133	hypothetical protein Swol_0133	311	6	No	78	4.7
	Swol_2384	Sodium-transporting two-sector ATPase	197	5	No	55	4.9
	Swol_0696	electron transfer flavoprotein, beta subunit	151	2	No	26	4.8
	Swol_0698	putative iron-sulfur-binding reductase	106	2	Yes	81	5.5

predicted to contain transmembrane helices. Three conserved S-layer homology domains were detected in the predicted peptide sequence for Swol_0141 gene product (not shown). No conserved domains were detected in the predicted peptide sequence of Swol_0143 gene product (not shown). Several other peptides were detected in which the peptide sequence is predicted to contain at least one transmembrane helix. These were peptides from ATP synthase beta- (all conditions) and gamma-subunits (crotonate pure culture and coculture) (Table 3). An approximately 310 kDa complex (CPC3, CCC3 and Bt5) was also detected under all three growth conditions (Figure 2).

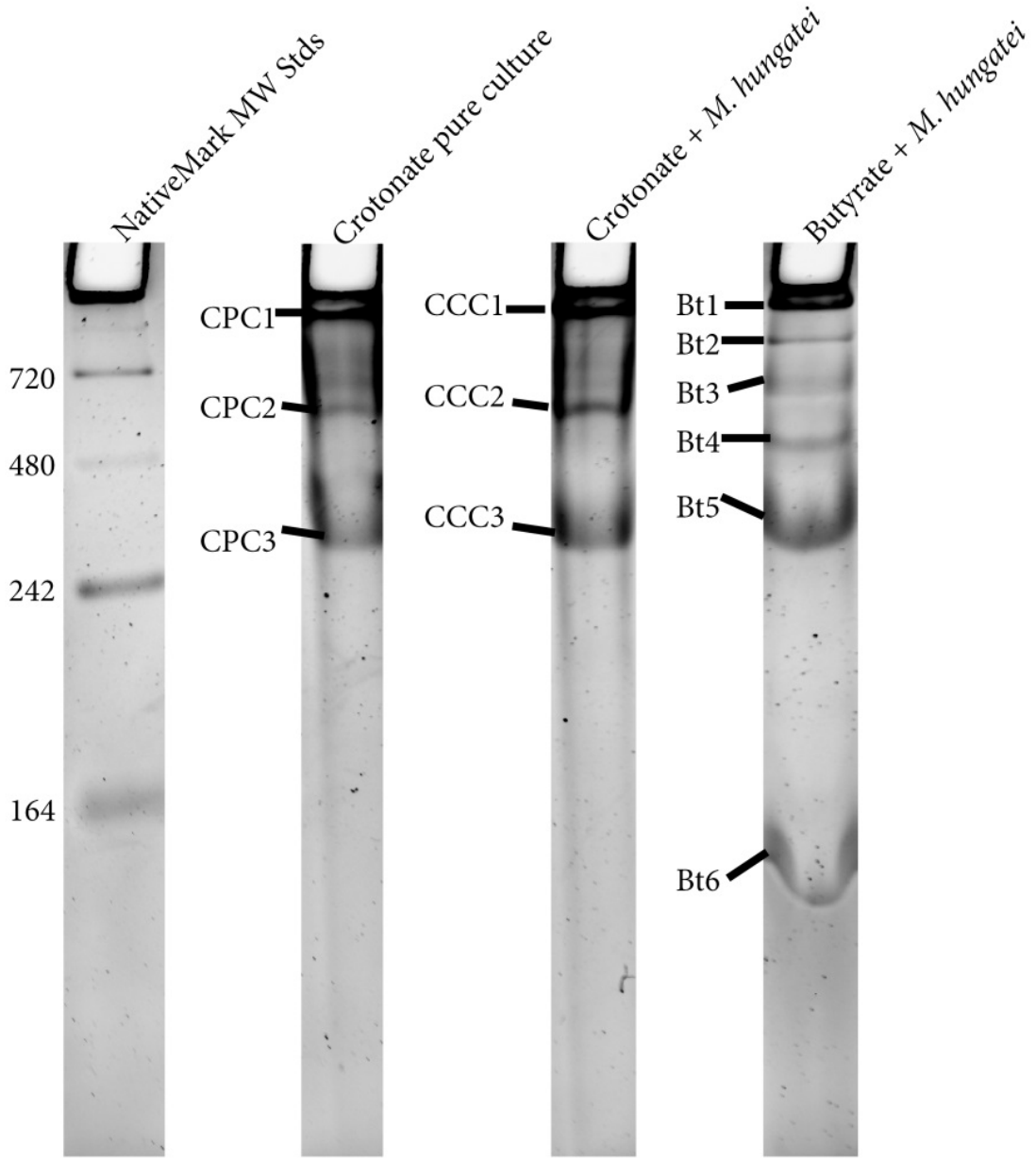

Figure 2: BN-PAGE separation of membrane enrichments derived from *S. wolfei*. Cells were harvested late log-phase, lysed via French pressure and membrane enrichments were prepared by ultracentrifugation. Membranes were solubilized with 0.5% dodecyl maltoside and separated on a 4-16% gradient polyacrylamide gel using BN-PAGE and stained using Sypro Ruby Red. A total of 12 complexes were detected. Bands were excised, digested with trypsin, sequenced using peptide mass fingerprint analysis and identified with MASCOT (see Table 3). Apparent molecular weights for each band are given in Table 3.

The dominant transmembrane helix-containing peptide detected from this band in membranes from cultures grown in pure culture was a glycosyl transferase protein while the dominant transmembrane helix-containing peptides detected from this band in membranes from cultures grown in coculture on crotonate and in coculture on butyrate were those derived from an FeS oxidoreductase (Swol_0698 gene product) (Table 3).

An approximately 585 kDa complex (CPC2, CCC2) was detected in membrane fractions derived from crotonate-grown, pure culture and coculture *S. wolfei* cells, but not from membranes of cells grown syntrophically on butyrate (Figure 2). The dominant peptides detected in these complexes were proteins of an unknown function corresponding to Swol_0143 and Swol_0141 gene products (Table 3).

Interestingly, four of the detected complexes (Bt2, Bt3, Bt4 and Bt6) appear unique to the syntrophic growth condition – growth in coculture on butyrate (Figure 2). Peptides derived from a gene coding for ATP synthase beta-subunit (Swol_2386 gene product) were detected in conjunction with a chemotaxis sensory protein (Swol_0927 gene product) in a band of approximately 640 kDa (Bt3) (Table 3). A smaller 460 kDa complex (Bt4) was composed of peptides derived from a formate/nitrite transport protein (Swol_0091 gene product) and a protein of unknown function, Swol_1911 gene product (Table 3). Peptides derived from *hydIIB* (Swol_1926) gene product and an electron transfer flavoprotein (Etf)-linked FeS oxidoreductase (Swol_0698 gene product) were detected in an approximately 165 kDa protein complex (Bt6) (Table 3). The FeS oxidoreductase was detected in several of the above bands (CPC3, CCC2, CCC3, Bt 5 and Bt 6). These results were confirmed with sequence analysis (not shown) of *S. wolfei-M.hungatei* cells grown in the same manner, but separately from,

those described above (see cell cultures, harvesting and separation) without Percoll separation.

Of note, peptides corresponding to the *hydIIA* (Swol_1925) gene product were detected in the 165 kDa band, which was unique to syntrophic growth on butyrate (Table 3). Likewise, the beta-subunit of Etf (Swol_0696 gene product) was detected in the 165 kDa complex (Bt6). Swol_0696 is part of a gene cluster containing the genes for the alpha subunit of Etf (Swol_0697) and for an FeS oxidoreductase (Swol_0698) (Table 3). Peptides derived from the *hydIIC* (Swol_1927) gene product, cytochrome *b*, were detected from an analogous band (not shown) from cells grown in the same manner, but separately from, those described above without Percoll separation. Therefore, I conclude that a unique complex forms between the *hydIIABC* gene products and the Etf-linked FeS oxidoreductase and is present in syntrophically grown cells.

Membrane fractions of S. wolfei contain hydrogenase and formate dehydrogenase activity.

The results from BN-PAGE suggested that *S. wolfei* makes a novel membrane complex when grown syntrophically on butyrate. Functional annotation of the polypeptides detected in the complex indicates that the complex serves as the membrane input component to receive electrons derived in the ß-oxidation of acyl-CoA intermediates and produce hydrogen. However, Schmidt et al (2013) found the Swol_0698 gene product, the FeS oxidoreductase, associated with formate dehydrogenase subunits and not subunits of hydrogenase enzymes. To determine

whether membranes of *S. wolfei* grown on butyrate contained hydrogenase or formate dehydrogenase activity, the solubilized membrane fractions of *S. wolfei* grown on butyrate were electrophoretically separated using BN-PAGE and lanes were incubated in the presence of tetrazolium red as the indicator with either hydrogen or formate as the electron donor. The formation of a red precipitate indicated that tetrazolium red was reduced by either hydrogen or formate as electron donor.

Precipitation was observed in one distinct membrane complex under a hydrogen atmosphere after overnight incubation showing that tetrazolium red was reduced in the presence of hydrogen (Figure 3). The region of hydrogenase activity in membranes

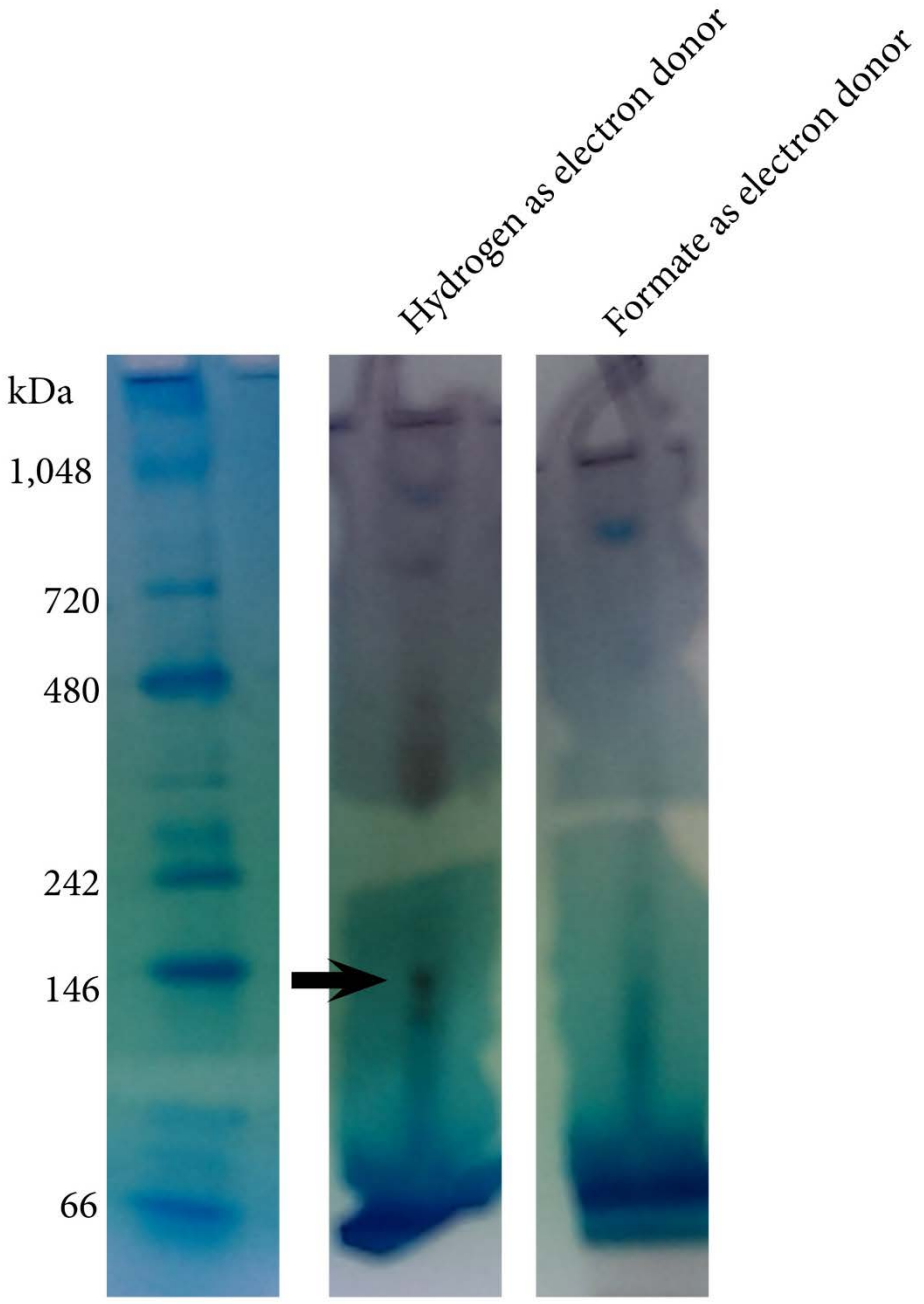

Figure 3: Hydrogenase and formate dehydrogenase zymograms. Membrane enrichments were solubilized in 0.5% dodecyl maltoside and electrophoretically separated in an anaerobic chamber. Gel slices were placed into sealed anaerobic cuvettes under N_2:CO_2 atmosphere or, where indicated, H_2 atmosphere. Reaction buffer containing 1 mM of the redox indicator tetrazolium red was added to the sealed cuvettes and the reaction buffer was amended to 1 mM formate for formate dehydrogenase activity. Hydrogenase activity was started with the addition of H_2 to 138 Pa. Activity was observed through formation of red precipitate. Arrow indicates band excised and analyzed by peptide mass fingerprint analysis. Results in Table 4

from butyrate coculture-grown cells coincides with the expected position of band Bt6, which contained the FeS oxidoreductase and hydrogenase subunits. The band was excised and peptides were identified by peptide mass fingerprint analysis. This analysis showed the presence of peptides encoded by all three genes of the *hydIIABC* gene cluster (Table 4).

Table 4: Peptides detected from membrane complex testing positive for hydrogenase activity in membrane fractions of *S. wolfei* grown on butyrate. Cells were grown and harvested as described and the reduction of tetrazolium red (1 mM) with hydrogen or formate as electron donor was monitored by the formation of a red precipitate. The band indicated in Figure 3 was excised and sent for peptide mass fingerprint analysis as described.

Locus Tag	Annotation	Unique Peptides	Score
Swol_1925	HydII (alpha)	11	1043
Swol_1926	HydII (beta)	6	586
Swol_2432	Unknown function	1	171
Swol_2382	ATP synthase (beta)	1	79
Swol_1927	Cytochrome *b*	1	61

Transcription of the genes encoding EtfAB, FeS oxidoreductase and the cytochrome b-linked hydrogenase

I detected a unique membrane complex in membranes of *S. wolfei* grown syntrophically on butyrate. This complex is predicted to contain several redox active proteins, which could provide a conduit for the production of hydrogen with electrons derived from oxidation of butyryl-CoA (see above). I hypothesized that these proteins are essential for syntrophic growth on butyrate. Together with Dr. Jessica Sieber, I used quantitative PCR to test the relative expression levels of *hydIIABC* (Swol_1925, Swol_1926 and Swol_1927), which encodes the cytochrome *b*-linked hydrogenase, *etfAB* (Swol_0696 and Swol_0697), which encodes electron transfer flavoprotein AB, and Swol_0698, which encodes the FeS oxidoreductase.

Levels of transcripts for *hydIIABC* were clearly elevated in *S. wolfei* cells grown syntrophically on butyrate compared to cells grown in pure culture on crotonate and in coculture on crotonate (Figure 4). The levels of expression of *hydIIABC* were at least

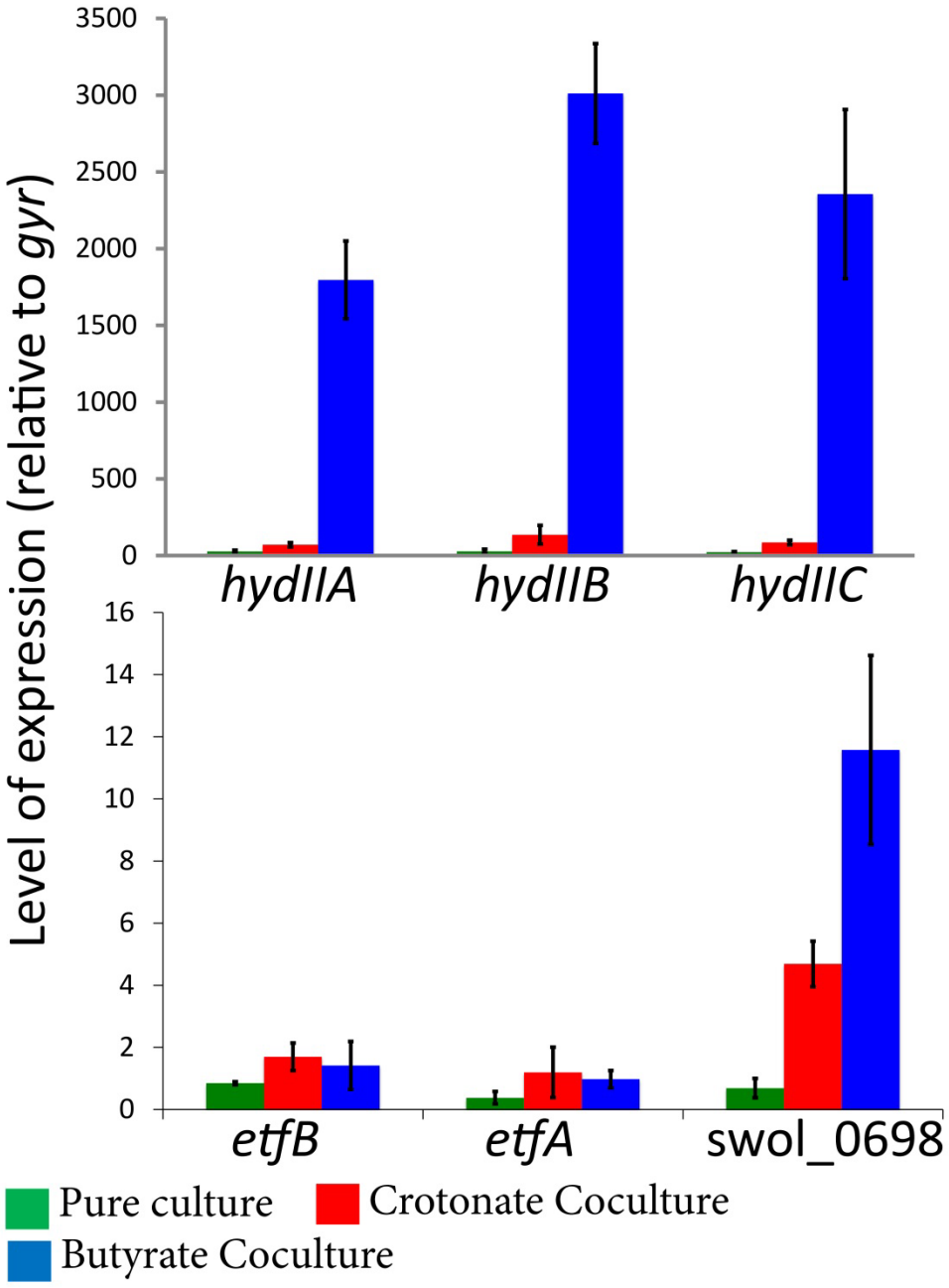

Figure 4: Relative expression of *hydIIABC* (Swol_1925-27), *etfAB* (Swol_0696-97) and Swol_0698 (FeS oxidoreductase) in *S. wolfei* grown with *M. hungatei*. Cells were grown as described and total RNA was extracted. Values represent the mean of three replicates with technical duplicates for each. Relative expression of *hydIIABC* subunits was at least 15-fold higher from cells grown in syntrophic butyrate-oxidizing cultures (blue) relative to growth in coculture on crotonate (red) and in pure culture on crotonate (green). Error bars represent standard deviation of replicate cultures.

two orders of magnitude higher from cells grown syntrophically on butyrate than their expression in crotonate-grown coculture cells, which shows that these genes are differentially expressed when *S. wolfei* grows syntrophically on butyrate. *etfAb* expression was similar under all three growth conditions (Figure 4). Levels of transcript for the FeS oxidoreductase were much higher (6- and 12-fold higher, respectively) during coculture growth on crotonate or butyrate compared to pure culture growth on crotonate (Figure 4), showing differential expression of the gene for FeS oxidoreductase when *S. wolfei* grows syntrophically. The marked differential expression of *hydIIABC* and Swol_0698 provides strong evidence for the importance of these genes in syntrophic metabolism of butyrate.

Genomic analysis of *S. wolfei* and *M. hungatei* shows that both organisms have hydrogenases and formate dehydrogenases, which indicates that either hydrogen or formate transfer could be used for interspecies electron exchange. In principle, the complex detected by BN-PAGE should be specific to hydrogen-dependent growth based on the predicted functions of the components of the complex. Butyrate oxidation by *S. wolfei* can be syntrophically coupled to tetrachloroethene reduction by *Dehalococcoides* sp., and *Dehalococcoides* sp. are not known to use formate as an electron donor (Maymó-Gatell *et al.* 1997). Therefore, in collaboration with Xinwei Mao and Dr. Lisa Alvarez-Cohen at the University of California, Berkeley, I tested the relative expression levels of *hydIIABC* (Swol_1925-27), *etfAB* (Swol_0696 and Swol_0697) and Swol_0698 in cocultures of *S. wolfei* and *Dehalococcoides* sp. that syntrophically oxidize butyrate coupled to tetrachloroethene reduction. We also tested

the relative expression levels of *fdhA-1* (Swol_0786), *fdhA-2* (Swol_0800) and *fdhA-4* (Swol_1825).

The expression of *hydIIA* and *hydIIB* were 15- to 20-fold higher in cells grown syntrophically on butyrate with *Dehalococcoides* relative to cells grown in coculture on crotonate or *S. wolfei* grown in pure culture on crotonate (Figure 5). The expression of *hydIIC* was approximately the same in crotonate-grown and butyrate-grown coculture cells and this level was at least three-fold higher in these two growth conditions compared to its expression in crotonate-grown pure culture cells. The expression of *etfA* and *etfB* were at least six-fold higher in cells grown syntrophically on butyrate relative to cells grown in coculture on crotonate or *S. wolfei* grown in pure culture on crotonate (Figure 5). Expression of Swol_0698 was approximately two-fold higher in cells grown syntrophically on butyrate relative to cells obtained from crotonate-grown pure culture and coculture (Figure 5). The relative expression of *fdhA* subunits relative to *gyr* was generally in the range of 0.6-1.2 units, though very low levels (less than 0.05 units) of *fdh-3* were detected from *S. wolfei* cells grown in coculture with *Dehalococcoides* on crotonate (Figure 5).

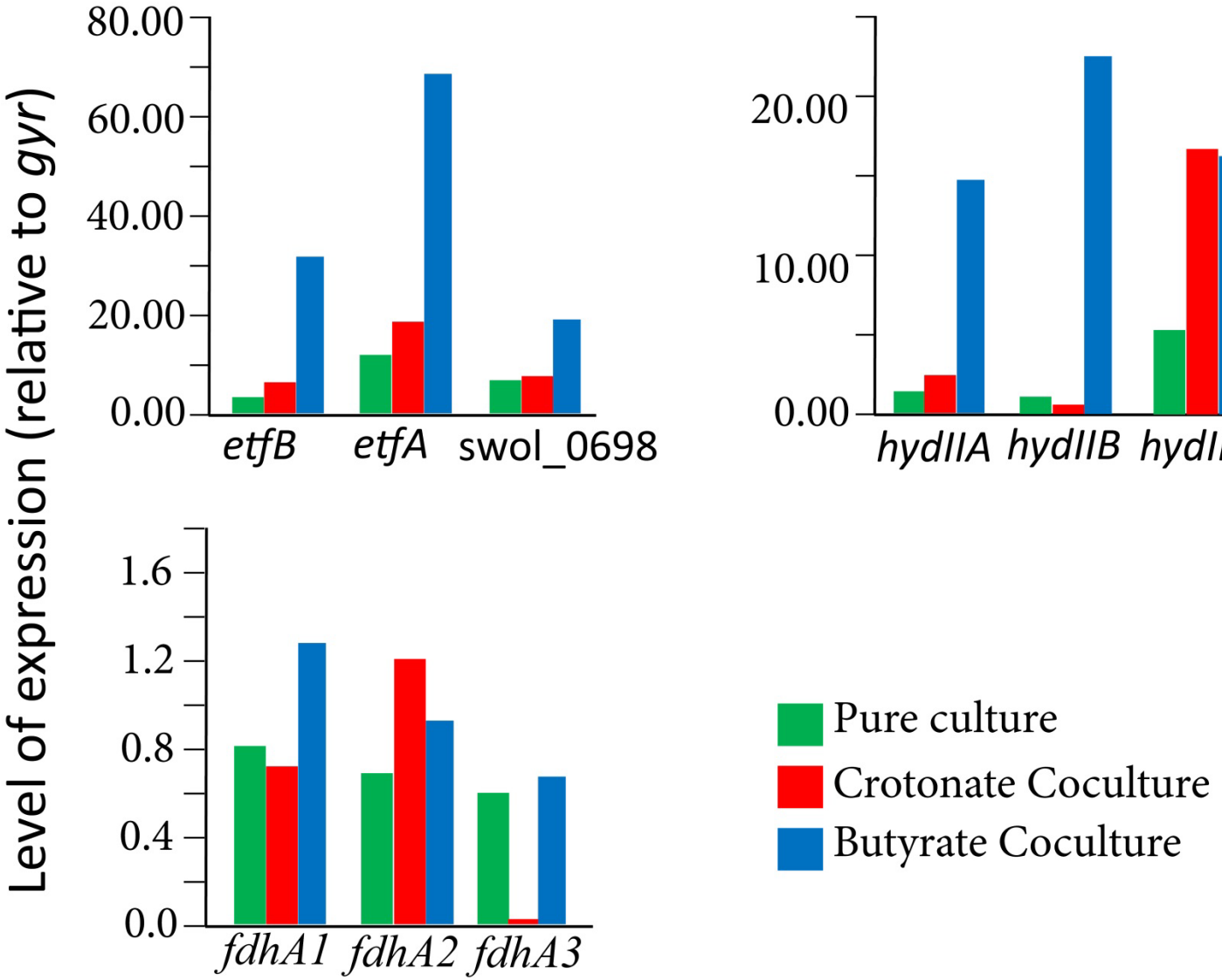
Level of expression (relative to gyr)
80.00
60.00
40.00
20.00
0.00
etfB
etfA
swol_0698
20.00
10.00
0.00
hydIIA
hydIIB
hydIIC
1.6
1.2
0.8
0.4
0.0
fdhA1
fdhA2
fdhA3
Pure culture
Crotonate Coculture
Butyrate Coculture

Figure 5: Relative expression of *hydIIABC* (Swol_1925-27), *etfAB* (Swol_0696-97) and Swol_0698 (FeS oxidoreductase) in *S. wolfei* grown with *Dehalococcoides* sp. Cells were grown as described and total RNA was extracted. Values represent the mean of three replicates with technical duplicates for each. Relative expression of *hydIIABC* subunits was at least 15-fold higher from cells grown in syntrophic butyrate-oxidizing cultures (blue) relative to growth in coculture on crotonate (red) and in pure culture on crotonate (green). Also tested were the relative expression of *fdhA1, fdhA2* and *fdhA4* (Swol_786, Swol_800 and Swol_1825, respectively).

Discussion

McInerney *et al.* (2007) hypothesized that, in *S. aciditrophicus*, an FeS oxidoreductase is the membrane input module for electrons derived from oxidation of acyl-CoA intermediates. Genomic evidence to support this hypothesis included the location of genes for electron transfer flavoprotein and an acyl-CoA dehydrogenase adjacent to genes predicted to code for alpha- and beta-subunits of electron transferring flavoproteins. The genome of *S. wolfei* contains a gene, Swol_0698, which is predicted to code for an analogous FeS oxidoreductase (Sieber 2010). Peptides of the Swol_0698 gene product were detected in band Bt6, which was unique to butyrate-grown *S. wolfei* cells. Band Bt6 also contained peptides of EtfAB (Swol_0696-97 gene products), which is the electron carrier associated with acyl-CoA dehydrogenases (Li *et al.* 2008). In addition, Müller *et al.* (2009) found peptides of the Swol_0698 gene product associated with butyryl-CoA dehydrogenases purified from *S. wolfei*. The above proteomic and biochemical results implicate the Swol_0698 gene product as the membrane input module for electrons derived from the oxidation of acyl-CoA intermediates in *S. wolfei*. Its homolog, Syn_02638, most likely has the same function in *S. aciditrophicus*.

The next question is what protein complexes are involved in hydrogen or formate production. In principle, *S. wolfei* can use either formate or hydrogen as an interspecies electron carrier as genomic analyses detected multiple formate dehydrogenase and hydrogenase genes and both activities have been detected in *S. wolfei* whole cells and cell extracts regardless of whether *S. wolfei* was grown axenically or syntrophically (Sieber *et al.* 2013). The recent study of Schmidt and colleagues (Schmidt *et al.* 2013) detected a dominant band in BN-PAGE in butyrate-

grown *S. wolfei* cells comprised of subunits of a membrane bound formate dehydrogenase. Activity staining confirmed that this complex had formate dehydrogenase activity. An NADH:acceptor oxidoreductase activity was partially purified from cell-free extracts of *S. wolfei* (Muller *et al.* 2009). Proteomic analysis of the NADH:acceptor oxidoreductase detected subunits of a NADH-linked formate dehydrogenase (Swol_0783, Swol_0785, and Swol_0786 gene products) and a NADH-linked hydrogenase (Swol_1017, Swol_1018, and Swol_1019) (Muller *et al.* 2009). Having hydrogenase and formate dehydrogenase subunits together with those for NADH oxidation would allow *S. wolfei* to produce either hydrogen or formate from NADH.

Sieber *et al*. (2010, 2012) suggested that the (Swol_1017, Swol_1018, and Swol_1019 gene products encode an electron bifurcating hydrogenase analogous to the enzyme recently described in *Thermotoga maritima* (Schut and Adams, 2009). The electron bifurcating hydrogenase functions by coupling the exergonic oxidation of reduced ferredoxin with the endergonic oxidation of NADH to produce hydrogen. Electrons derived from one NADH and one reduced ferredoxin are used to reduce four protons to two molecules of hydrogen according to (eq. 3) (Schut and Adams 2009):

(eq. 3) $NADH + Fd^{red} + 3\ H^{+} \rightarrow 2\ H_2 + NAD^{+} + 2\ Fd^{ox}$

Genes homologous to the electron-bifurcating hydrogenase have been identified in the genomes of other organisms capable of syntrophy such as *Pelotomaculum thermopropionicum* and *S. aciditrophicus* (Sieber *et al.* 2012; Sieber *et al.* 2010).

These comparative genomic analyses led Sieber and colleagues (2010) to argue that this bifurcation mechanism (Schut and Adams 2009) represents a universal mechanism for production of molecular hydrogen and formate from NADH by organisms capable of syntrophy.

However, convincing evidence for the involvement of chemiosmotic energy for hydrogen production from butyryl-CoA oxidation was obtained with inverted membrane vesicle preparations of *S. wolfei* (Wallrabenstein and Schink 1994). The need for a chemiosmotic gradient to make hydrogen from electrons derived from butyryl-CoA oxidation argues that an ion-translocating membrane complex (or complexes), rather than electron-bifurcating complexes, are involved in reverse electron transfer in *S. wolfei*. Hydrogenase inhibitors, such as cyanide or carbon monoxide, but not the formate dehydrogenase inhibitor, hypophosphate, inhibited syntrophic butyrate metabolism, but not crotonate metabolism, by *S. wolfei* (Seiber 2013). This finding additionally implicates the need for interspecies hydrogen transfer during syntrophic butyrate metabolism.

Here, I identified a membrane protein complex (Bt6; Figure 2) in *S. wolfei* cells grown syntrophically on butyrate that was not observed in membranes of *S. wolfei* cells grown axenically or in coculture on crotonate. I identified peptides associated with an FeS oxidoreductase (Swol_0698 gene product), Etf alpha- and beta-subunits (Swol_0696-97 gene products) and those associated with a cytochrome *b*-linked [FeFe]-hydrogenase (*hydIIABC* or Swol_1925-27 gene products). The subunit composition of the Bt6 complex suggests that it serves as the membrane input module for electrons derived from butyryl-CoA oxidation, which are then used to produce hydrogen.

Moreover, I was able to link reduction of tetrazolium red with hydrogen as electron donor to a membrane complex which contained peptides encoded by *hydIIABC.* Additionally, the differential expression of *hydIIABC* and Swol_0698 when *S. wolfei* was grown syntrophically on butyrate with *M. hungatei* or *Dehalococcoides* sp. argues strongly for the importance of the FeS oxidoreductase and *hydIIABC* in syntrophic butyrate metabolism. However, a role for formate in syntrophic butyrate metabolism cannot be excluded (Dong and Stams 1995; Schmidt *et al.* 2013; Stams and Dong 1995).

Based on the evidence presented, I propose two models for reverse electron transfer during hydrogen-linked, syntrophic butyrate oxidation by *S. wolfei* (Figure 6). In the first model, (Figure 6A) the FeS oxidoreductase and *hydIIABC* gene products form a complex where electrons from butyryl-CoA are transferred to the integral membrane protein, FeS oxidoreductase (Swol_0698 gene product) by *etfAB* (Swol_0696-97) gene products. Physical association between the FeS oxidoreductase, a presumed integral membrane protein, and cytochrome *b* (*hydIIC* or Swol_1927 gene product) would allow for direct transfer of electrons to the [FeFe]-hydrogenase (*hydIIAB* or Swol_1925-26 gene products). I propose an alternative model (Figure 6B) in which electrons are again funneled to the membrane from butyryl-CoA oxidation to the FeS oxidoreductase via *etfAB* gene products. In this model, however, the FeS oxidoreductase couples Etf oxidation to the reduction of menaquinone to menaquinol. Menaquinol would then be oxidized by cytochrome *b* (Swol_1927 gene product) in the membrane and cytochrome *b* would transfer the electrons to the *hydIIAB* gene products to form hydrogen. The *hydIIAB* gene products are predicted to be externally oriented.

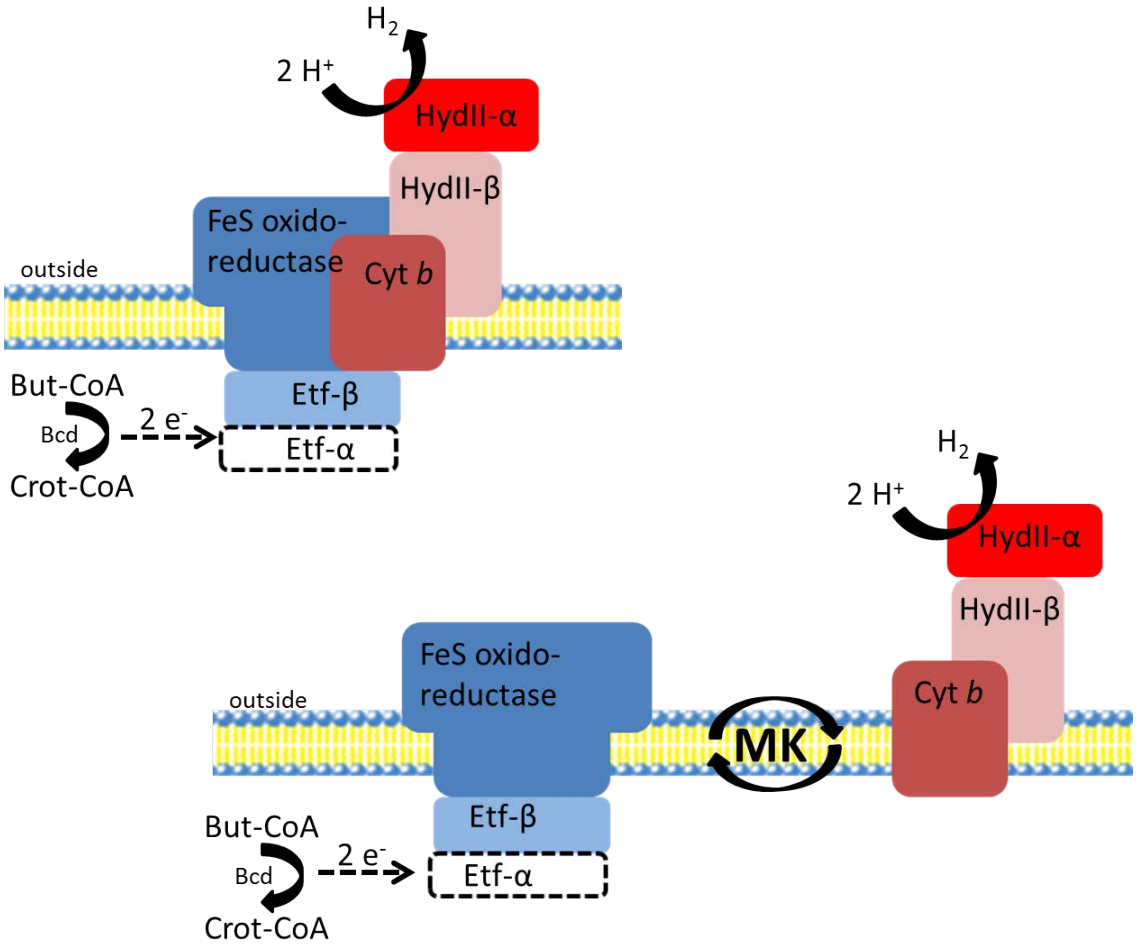

Figure 6: Two models for reverse electron transfer during syntrophic butyrate oxidation by *S. wolfei.* In both cases, electrons from butyryl-CoA dehydrogenase are transferred to the FeS oxidoreductase (Swol_0698) by electron transferring flavoproteins alpha and beta (Etfαβ). A. FeS oxidoreductase and hydrogenase form one complex. Electrons travel from FeS oxidoreductase through the physically adjacent cytochrome *b* to a membrane-anchored, outward-facing [FeFe]-hydrogenase. B. FeS oxidoreductase and cytochrome *b*-linked [FeFe]-hydrogenase form separate complexes. Electrons from FeS oxidoreductase are used to reduce menaquinone with protons consumed outside the cell. The cytochrome *b*-linked [FeFe]-hydrogenase oxidized menaquninol with protons released on the inside of the cell. This mechanism provides greater metabolic versatility for the cell as the menaquinone pool could interact with a hydrogenase (depicted here) or formate dehydrogenase depending on the metabolic needs of the cell. ETF-α = electron transferring flavoprotein – alpha subunit (Swol_0697), ETF-β = electron transferring flavoprotein – beta subunit (Swol_0696), FeS oxidoreductase (Swol_0698), Cyt-B = cytochrome-*b* (Swol_1927), Hyd-α = HydII alpha subunit (Swol_1925), Hyd-β = HydII beta subunit (Swol_1926).

In both models, proton consumption by hydrogenase would occur outside the cell thus allowing the use of a proton gradient to drive reverse electron transfer. The presence of a subunit of a sodium-transporting, two-sector ATPase (Swol_2384 gene product) suggests that the Bt6 complex described in the first model (Figure 6A) may be an ion pump. The inward movement of sodium or another ion could supply energy to drive reverse electron transfer. With the second model (Figure 6B), if menaquinone binds to the FeS oxidoreductase at the outside face of the membrane and menaquinol binds to cytochrome *b* at the inside face of the membrane, a reverse quinone-loop, net translocation of two protons from the outside to the inside of the membrane would occur which would supply additional chemiosmotic energy for reverse electron transfer. In either case, both models predict the use of the proton gradient for reverse electron transfer.

Our finding here that the Swol_0698 gene product, and peptides coded for by *etfAB* and *hydIIABC* were codetected in an approximately 162 kDa band (Bt6) could be explained by comigration of separate complexes rather than a single physical complex. The presence of two complexes linked by the menaquinone pool (model 2; Figure 6B) is attractive given the finding by Schmidt *et al.* (2013) that formate was the dominant interspecies electron carrier in cells of *S. wolfei* grown syntrophically on butyrate. The energetics of formate production are much the same as for hydrogen production – though in principle the partner organism (in our system *M. hungatei)* would get a small increase in its share of free energy in a system based on interspecies formate transfer. The ability to use both hydrogen or formate as an interspecies electron carrier has been well documented (Dong and Stams 1995; Friedrich and Schink 1993; Jackson *et al.*

1999; Li *et al.* 2011; Luo *et al.* 2002; McInerney *et al.* 1979; McInerney *et al.* 1981; McInerney *et al.* 1981; McInerney *et al.* 2007; McInerney *et al.* 2009; McInerney *et al.* 2008; Muller *et al.* 2010; Schink 1997; Schmidt *et al.* 2013; Schöcke and Schink 1997; Sieber *et al.* 2013; Stams and Dong 1995; Stams and Plugge 2009; Struchtemeyer *et al.* 2011; Walker *et al.* 2012; Wallrabenstein and Schink 1994; Worm *et al.* 2011) though there is no known mechanism for switching between hydrogen or formate consumption.

A system based around a reverse quinone-loop is an enticing way to explain this metabolic versatility of syntrophic organisms with respect to the preferred electron carrier. Menaquinone, and its reduced form, menaquinol, are soluble in the lipophilic portion of the membrane bilayer and, as such, are freely diffusible in three-dimensional space around the membrane. Depending on the metabolic conditions faced by the cell, menaquinol could interact with a membrane-bound formate dehydrogenase or membrane-bound hydrogenase. This would allow flexibility for the organism to modulate interspecies electron carriers depending on the needs of the consortium. In conditions where there is low cell-density, or a low density of methanogens relative to *S. wolfei*, intercellular distances would be greater between *S. wolfei* and cells of *M. hungatei* and formate transfer would be preferred over hydrogen transfer (Dong and Stams 1995). In conditions where there is high cell-density, for example in late log phase, a hydrogen-based economy would be preferred by *S. wolfei* because there is a slight energetic advantage and intercellular distances between cells of *S. wolfei* and cells of *M. hungatei* are lower. If this phenomenon is density dependent, it therefore is conceivable that there is an inflection point where a hydrogen based economy becomes more beneficial to the overall community and vice versa. Moreover, hydrogen was

shown to be essential for syntrophic cooperation (Sieber *et al.* 2013) and high-cell-density more closely mimics the natural environment of these associations.

I did notice one particular finding, with respect to whole cell shotgun proteomics, which warrants further consideration. Clustered regularly interspaced short palindromic repeats (CRISPR) are gene loci which confer adaptive immunity to microbial organisms. Here, I observed a CRISPR associated helicase only under butyrate-degrading conditions. Moreover, a relatively high number of CRISPR regions (6) were detected on the *S. wolfei* chromosome (Sieber *et al.* 2010). In principle, the primary role of the CRISPR system is for immunity against viral nucleic acid attack. However, I am not aware of studies which indicate CRISPR specificity only against viral DNA, and recently extensive parallel gene transfer in archaea has been observed in CRISPR regions (Brodt *et al.* 2011). In principle, a tight physical association between *S. wolfei* and *M. hungatei* would allow for a more efficient fatty acid oxidizing system and it is known DNA is an important component of biofilms (Gloag *et al.* 2013). Moreover, extracellular DNA has been shown to facilitate the organizational structure of biofilms (Gloag *et al.* 2013). It seems reasonable, therefore, to suggest that the high number of CRISPR regions and the detection of the CRISPR helicase only during growth on butyrate signals physical associations between *S. wolfei* and *M. hungatei*, a topic which has not received attention.

Perspectives

Syntrophic associations, such as that of *S. wolfei* and *M. hungatei*, are essential for the global anaerobic carbon cycle. Reverse electron transfer, alone, is not synonymous with syntrophy – however it is essential for syntrophic fatty-acid oxidation since electrons derived from acyl-CoA intermediates must be shifted to a potential at which hydrogen or formate production can occur. The release of the sequenced and annotated genomes from several organisms capable of syntrophy (McInerney *et al.* 2007; Plugge *et al.* 2012; Sieber *et al.* 2010) have advanced our understanding of reverse electron transfer in these organisms. Here, codetection of an FeS oxidoreductase (Swol_0698 gene product) with Etf subunits, suggests these may complex together to form the electron input module and deliver electrons derived from butyryl-CoA oxidation to the membrane. I propose two mechanisms for the reduction of protons to hydrogen based on our findings here. The Etf subunits may complex with the Swol_0698 and *hydIIABC* gene products, forming a single physically-associated complex which catalyzes the reduction of protons to hydrogen as described earlier (Figure 6A). Alternatively, preliminary evidence from our lab suggests menaquinone is reduced by hydrogen in membrane enrichments of *S. wolfei* (Kung et al, unpublished). In this mechanism, partitioning of proton consumption and release would allow chemiosmotic energy to be coupled to the shift in the redox potential of electrons derived from butyryl-CoA (Figure 6B).

Chapter 3: Membrane protein complexes of the syntrophic fatty and aromatic acid-oxidizing bacterium *Syntrophus aciditrophicus*

Abstract

The activated form of benzoate, benzoyl-CoA, is a central intermediate in the anaerobic decomposition of many aromatic ring-containing compounds. Under physiological conditions, the oxidation of benzoate to acetate, carbon dioxide and hydrogen is an energy requiring process. When hydrogen partial pressures or formate concentrations are kept extremely low by hydrogen or formate consuming partner organisms, benzoate oxidation becomes favorable. This relationship is known as syntrophy. The production of hydrogen (E' = -260 mV at 1 Pa) or formate (E' = -290 mV at 1 μM) with electrons derived from the high potential donor, glutaryl-CoA ($E^{0'}$ = -10 mV), is an essential feature of syntrophic benzoate oxidation by *Syntrophus aciditrophicus* and requires energy to overcome a ΔE of 250-280 mV. This process is known as reverse electron transfer and the process is not well understood. The presence of genes coding for electron confurcating acyl-CoA dehydrogenase provide a candidate strategy, but it is unclear from where the reduced ferredoxin is derived. The genome of *S. aciditrophicus* was found to contain a gene cluster coding for an Rnf-like complex. Rnf is known to couple the reduction of NADH with electrons derived from ferredoxin to the formation of a sodium ion gradient in *Acetobacter woodii*. Here, I hypothesized that reverse electron transfer is accomplished by an Rnf-like complex in *S. aciditrophicus*. I used blue-native gel electrophoresis to separate membrane protein complexes and peptide mass fingerprint analysis to determine the proteins present in each membrane complex. To test for the ability of *S. aciditrophicus* membrane fractions to catalyze the predicted Rnf-like activity, I looked for the ability of *S. aciditrophicus* to reduce the low potential viologen dyes benzyl viologen ($E^{0'}$ = -360

mV) or methyl viologen ($E^{0'}$ = -460 mV) with electrons derived from NADH ($E^{0'}$= -320 mV). I also partially purified the Rnf-like activity from solubilized membrane fractions of *S. aciditrophicus* using size exclusion chromatography. A total of 32 membrane complexes were identified from membrane fractions of *S. aciditrophicus* grown in pure culture on either crotonate or crotonate + benzoate, or in methanogenic coculture grown on either crotonate, benzoate or cyclohexane carboxylate. Peptide mass fingerprint analysis revealed the presence of peptides derived from an Rnf-like complex in membrane complexes. This is predicted to be an important source of reduced ferredoxin for electron confurcating acyl-CoA dehydrogenases. Additionally, peptides derived from a sodium-dependent ATP synthase and peptides from a sodium-translocating glutaconyl-CoA decarboxylase were detected. Both are predicted to be linked to the formation of a sodium ion gradient and argue for the importance of sodium in *S. aciditrophicus* bioenergetics. Peptides derived from the Syn_02638 gene product, which encodes a putative FeS oxidoreductase, were detected and were codetected with peptides derived from glutaconyl-CoA decarboxylase and/or peptides derived from acyl-CoA dehydrogenases. In this study, I also observed higher activity for an Rnf-like activity in *S. aciditrophicus* cells grown syntrophically, and peptides derived from Rnf subunits were detected in partially purified membrane fractions catalyzing an Rnf-like activity. Taken together, these data argue for the importance of an Rnf-like complex as a source for reduced ferredoxin for confurcating acyl-CoA dehydrogenases or for the production of hydrogen/formate by ferredoxin dependent hydrogenase/formate dehydrogenase enzymes.

Introduction

In the absence of other terminal electron accepting processes, complex organic matter is degraded to carbon dioxide and methane (Achtnich *et al.* 1995). A variety of fatty and aromatic acid and alcohol intermediates are produced as end products of fermentative bacteria that must be converted to methanogenic substrates (Crable *et al.* 2011; McInerney *et al.* 2009; McInerney *et al.* 2008). Degradation of fatty and aromatic acids is essential for efficient methane production from complex waste streams (McInerney *et al.* 2009; McInerney *et al.* 2008). Many aromatic ring-containing substrates are metabolized to benzoyl-CoA prior to ring cleavage. Therefore, the activated form of benzoate, benzoyl-CoA, is a central intermediate in the anaerobic decomposition of many aromatic ring-containing compounds (Evans and Fuchs 1988).

Syntrophus aciditrophicus, a member of the Deltaproteobacteria class of microorganisms is known to degrade benzoate in syntrophic cocultures (Jackson *et al.* 1999; McInerney *et al.* 2007) and has been shown to couple reduction of benzoate to cyclohexane carboxylate with the degradation of crotonate (Mouttaki *et al.* 2008). Initial studies with *S. aciditrophicus* grown on benzoate in pure culture with no electron donor (e.g. crotonate), suggested the organism fermented only 3.9% of benzoate supplied in pure culture (Jackson *et al.* 1999). A later study found that *S. aciditrophicus* was able to ferment benzoate supplied at a starting concentration of 1.6 mM to acetate (1.5 moles per mole benzoate) and cyclohexane carboxylate (0.5 moles per mole benzoate) (Elshahed and McInerney 2001).

Hydrogen accumulation to approximately 100 Pa was noted in both studies (Elshahed and McInerney 2001; Jackson and McInerney 2002). This, coupled with the

observation that the final concentration of benzoate in benzoate fermenting pure cultures was six-fold higher than in benzoate-oxidizing syntrophic cocultures, that hydrogen inhibited the fermentation of benzoate at 10.2 kPa and that *S. aciditrophicus* was unable to completely metabolize benzoate to acetate, carbon dioxide and hydrogen in pure culture (Elshahed and McInerney 2001) reflect the importance of hydrogen consumption during benzoate degradation. Furthermore, the conversion of cyclohexane carboxylate to acetate, carbon dioxide, hydrogen and formate occurs only when a hydrogen and/or formate-using microorganism is present (Elshahed *et al.* 2001).

The initial step in syntrophic benzoate oxidation, activation to benzoyl-CoA, is catalyzed by an AMP-forming benzoate CoA ligase (James et al unpublished). The aromatic ring is then reduced by an ATP-independent class II benzoyl-CoA reductase to cyclohexa-1,5-diene-1-carboxyl-CoA (Kung *et al.* 2009; Loffler *et al.* 2011). Cylohexa-1,5-diene-1-carboxyl-CoA serves as a branch point between the two known pathways for benzoate degradation. In *Rhodopseudomonas palustris*, cyclohexa-1,5-diene-1-carboxyl-CoA is reduced to cyclohex-1-ene-1-carboxyl-CoA, which is degraded to pimelyl-CoA by a series of reactions resembling fatty-acid beta oxidation (Egland *et al.* 1997; Pelletier and Harwood 2000). In *Thauera aromatic*a, cyclohexa-1,5-diene-1-carboxyl-CoA is not further reduced like in *R. palustris*, but instead is degraded to 3-hydroxypimelyl-CoA by a series of reactions resembling fatty-acid beta oxidation (Laempe *et al.* 1998; Laempe *et al.* 1999). 3-hydroxypimelyl-CoA is then beta-oxidized to acetyl-CoA (Laempe *et al.* 1998; Laempe *et al.* 1999).

The genome of *S. aciditrophicus* contains genes coding for the enzymes necessary for benzoate degradation via the pathway analogous to *T. aromatica*

(McInerney *et al.* 2007) and recent studies suggest benzoate fermentation proceeds via this pathway in *S. aciditrophicus* (Kung *et al.* 2009; Loffler *et al.* 2011; Peters *et al.* 2007). Moreover, the syntrophic degradation of cyclohexane carboxylate to acetate, carbon dioxide, hydrogen and/or formate likely involves the activation of cyclohexane carboxylate to its CoA derivative followed by two consecutive oxidation-reduction reactions converting cyclohexane-1-carboxyl-CoA to cyclohexa-1,5-diene-1-carboxyl-CoA (Kung *et al.* 2013). The latter compound is believed to be degraded by the same enzymes that metabolize this compound during benzoate metabolism (Kung *et al.* unpublished data).

A challenge for *S. aciditrophicus*, then, is the production of hydrogen or formate with electrons derived from glutaryl-CoA, whose midpoint redox potential is about E' = -10 mV compared to a redox potential of about E' = -260 mV for the H^+/H_2 couple at one Pascal hydrogen (Elshahed *et al.* 2001; Kuntze *et al.* 2008; Peters *et al.* 2007). The second enigma is how reduced ferredoxin is made. None of the redox reactions involved in crotonate, benzoate or cyclohexane-1-carboxylate metabolism are known to produce reduced ferredoxin. Rather, if the acyl-CoA dehydrogenases involved in glutaryl-CoA, cyclohex-1-ene-1-carboxyl-CoA and cyclohexane-1-carboxyl-CoA oxidation formed during benzoate (for glutaryl-CoA) or cyclohexane-1-carboxylate (all three compounds) metabolism involved electron bifurcation, then reduced ferredoxin would be required for each reaction.

The genome of *S. aciditrophicus* contains genes predicted to code for an Rnf-like complex analogous to that involved in nitrogen fixation by *Rhodobacter* sp. (McInerney *et al.* 2007). This complex is detected in the genome of the

phylogenetically related syntrophic propionate-oxidizing bacterium *Syntrophobacter fumaroxidans* strain MPOB (Plugge *et al.* 2012). In fermentative anaerobes, Rnf couples the oxidation of ferredoxin to the reduction of NAD^+ to NADH yielding energy in the form of a sodium gradient (Biegel *et al.* 2011; Muller *et al.* 2008). It is thought, however, that in syntrophic bacteria, Rnf-like complexes function to use the sodium gradient to drive the unfavorable oxidation of NADH coupled to the reduction of ferredoxin (McInerney *et al.* 2007). The low potential of ferredoxin would allow thermodynamically favorable reduction of protons to hydrogen and/or thermodynamically favorable reduction of carbon dioxide to formate. Also, the reduced ferredoxin could be used to drive electron bifurcation or biosynthetic processes such as the synthesis of pyruvate from acetyl-CoA and CO_2.

In this study, we identify membrane protein complexes in *S. aciditrophicus* grown axenically on crotonate and in methanogenic coculture on crotonate and benzoate involved in reverse electron transfer and energy conservation. I further demonstrate that *S. aciditrophicus* has an Rnf-like activity that could produce reduced ferredoxin needed for electron bifurcation and biosynthesis.

Materials and Methods

Cell Culture, growth and harvesting

Syntrophus aciditrophicus strain SB (ATCC# 700169) in pure-culture and in coculture with *Methanospirillum hungatei* strain JF1 (ATCC# 27890) were obtained from our culture collection. Cultures were grown in a defined basal medium with an 80% N_2:20% CO_2 gas phase with crotonate (20 mM), benzoate (12 mM), crotonate (20

mM) + benzoate (12 mM), or cyclohexane carboxylate (10 mM) as substrate. The basal medium is described elsewhere (Tanner 2002) and was composed of the following salts in final concentration: sodium chloride (0.8 mg/L), ammonium chloride (1 mg/L), potassium chloride (1 mg/L), potassium phosphate (0.1 mg/L) magnesium sulfate heptahydrate (0.2 mg/L), calcium chloride dihydrate (0.04 mg/L). The basal medium was composed of the following vitamins in final concentration: pyridoxine hydrochloride (0.1 mg/L), thiamine hydrochloride (0.05 mg/L), riboflavin (0.05 mg/L), calcium pantothenate (0.05 mg/L), thioctic acid (0.05 mg/L), *para*-aminobenzoic acid (0.05 mg/L), nicotinic acid (0.05 mg/L), vitamin B_{12} (0.05 mg/L), mercaptoethanesulfonic acid (0.05 mg/L), biotin (0.02 mg/L), and folic acid (0.02 mg/L). The basal medium was composed of the following metals in final concentration: nitrilotriacetic acid (0.01 mg/L), manganese (II) sulfate monohydrate (0.005 mg/L), ammonium iron (II) sulfate hexahydrate (0.004 mg/L), cobalt (II) chloride hexahydrate (0.001 mg/L), zinc sulfate heptahydrate (0.001 mg/L), copper (II) chloride dihydrate ($1 \cdot 10^{-5}$ mg/L), nickel (II) chloride ($1 \cdot 10^{-5}$ mg/L), sodium molybdate dihydrate ($1 \cdot 10^{-5}$ mg/L), sodium selenite ($1 \cdot 10^{-5}$ mg/L) and sodium tungstate ($1 \cdot 10^{-5}$ mg/L).

One liter of sterile medium in a sealed anaerobic 2-L bottle was inoculated with 200 ml of *S. aciditrophicus* in pure culture or coculture grown in the same medium. All cultures except for those grown syntrophically on cyclohexane carboxylate were transferred a minimum of three times as one-liter cultures prior to harvesting. Cultures grown on cyclohexane carboxylate were established with a 200 ml inoculum from benzoate grown coculture and this was transferred at least once before harvesting. Cultures were incubated at 37^0C and growth was monitored via measuring the OD_{600}

with time. Substrate utilization was monitored via high-pressure liquid chromatography (Sieber *et al.* 2010). The cultures were harvested when 50 to 70% of the substrate was used. Cells were harvested anaerobically in 1-L centrifuge vessels via centrifugation at 7,000 • *g* for 20 min at 4^{o}C. The cells were washed twice by centrifugation and resuspension of the pellet with anoxic 50 mM potassium phosphate buffer (pH of 7.2) as described above. Cell pellets were stored frozen in liquid nitrogen.

Cells of *S. aciditrophicus* grown in coculture were separated from *M. hungatei* by Percoll gradient centrifugation. Frozen cell pellets were thawed and suspended in a 6:3 ratio of standard isotonic Percoll to 50 mM potassium phosphate buffer (pH of 7.2) which was prepared anaerobically. Cell suspensions were transferred into sealed anaerobic disposable centrifuge tubes and centrifuged at 20,000 • *g*, for 40 min at 4^{0}C (Beaty *et al.* 1987; Sieber *et al.* 2013). Contamination of *S. aciditrophicus* cells with *M. hungatei* cells was determined microscopically and fractions containing less than one *M. hungatei* cell per 100 *S. aciditrophicus* cells were pooled. Pooled fractions were diluted 500-fold in 50 mM potassium phosphate buffer (pH 7.2) and centrifuged at 7,000 • *g* for 20 minutes to dilute out remaining Percoll. After separation, cells were used immediately.

Cell lysis, cell free extracts and membrane purification

Cells were lysed using French pressure and membrane fractions were obtained by ultracentrifugation. Cell pellets of purified *S. aciditrophicus* were resuspended in either 4 ml of lysis buffer for blue-native polyacrylamide gel electrophoresis (described below) or 4 ml of potassium phosphate (pH 7.2). Cells were lysed by passage through a

French pressure cell at an internal pressure of 138,000 kPA. After one pass, unbroken cells and cell debris were removed by centrifugation at 8,000 • *g* for two min at ambient temperature in sealed cryovial tubes. The resulting supernatant was decanted into disposable polyallomer centrifuge tubes and the soluble and insoluble fractions were separated by ultracentrifugation at 132,000 • *g*, 60 min, 4^0C. The supernatant was decanted and the insoluble pellet was washed by resuspending in 50 mM potassium phosphate (pH 7.2) and ultracentrifuged as above.

The supernatant was decanted and the remaining pellet (membrane fraction) was resuspended in approximately 250 µl of anaerobically prepared lysis buffer containing 0.5% n-dodecyl-β-maltoside (DDM) to obtain the solubilized membrane fraction or in 250 µl of potassium phosphate (pH 7.2) to obtain a suspension of membrane vesicles. Protein quantification was done using the Pierce BCA assay. Solubilized membrane fractions were stored in small (25 µl) aliquots at -20^0C in sealed microcentrifuge tubes. Suspensions of membrane vesicles were stored in sealed tubes on ice until used for enzyme activity assays (see below). All manipulations were done in an anaerobic chamber and all buffers except lysis buffer, were boiled and degassed with 80% N_2:20% CO_2. Lysis buffer was heated to 50^0C and degassed with 80% N_2:20% CO_2. Centrifugation and ultracentrifugation steps were performed in sealed anaerobic tubes.

Blue-Native polyacrylamide gel electrophoresis (BN-PAGE)

Blue native polyacrylamide gel electrophoresis (BN-PAGE) was usually conducted aerobically. *S. aciditrophicus* cells were obtained from pure cultures or separated from *M. hungatei* cells by Percoll separation (see cell culture, growth and

harvesting). The purified *S. aciditrophicus* cells were resuspended in 4 ml of lysis buffer described elsewhere (Swamy *et al.* 2006)., which contained 20 mM 2,2-Bis(hydroxymethyl)-2,2',2''-nitrilotriethanol (Bis-tris), ε-aminocaproic acid (500 mM), NaCl (20 mM), ethylenediaminetetraacetic acid (EDTA)(10 mM) and glycerol (10% v/v). The pH of the lysis buffer was adjusted to within 0.2 pH units of pH 7.2 with 1 N hydrochloric acid. The pH was further adjusted to pH 7.2 with 0.1 N hydrochloric acid.

BN-PAGE was conducted using the methods of Schägger and von Jagow (Schagger and von Jagow 1991) and Swamy et al. (Swamy *et al.* 2006) with the following modifications. Precast 4-16% polyacrylamide Bis-tris gels (Life Technologies™) were used. The cathode buffer (Swamy *et al.* 2006) was prepared as a 10X stock solution containing 15 mM Bis-tris, 50 mM tricine, and 0.02% Coomassie blue G250 (w/v). The anode buffer (Swamy *et al.* 2006) was prepared as a 10X stock solution containing 50 mM Bis-tris. Both buffers were adjusted to within 0.2 pH units of pH 7.0 with 1 N hydrochloric acid and then adjusted to pH 7.0 with 0.1 N hydrochloric acid. Buffers were stored at 4^{o}C. Prior to use, buffers were diluted 1:10 with deionized H_2O. The solubilized membrane fraction (ranging from 2 to 35 µg protein) was thawed and mixed with equal parts (v:v) of BN-PAGE sample buffer. BN-PAGE sample buffer was prepared by diluting one milliliter of cathode buffer, described above, with seven milliliters of deionized nanopure water and two milliliters of electrophoresis grade glycerol (≥ 99%). Gels were run at a constant 130 V for several hours until the dye front migrated to the bottom of the gel. Gels were fexed and destained in a solution containing 50% methanol (v/v) and 7% acetic acid (v/v), washed with nanopure water, and then stained with either Imperial stain (ThermoFisher),

SilverStain (Pierce) or SyproRuby (Thermofisher) according to manufacturer's instructions.

Tryptic digests and peptide mass fingerprinting

Predominant protein bands and protein bands that were unique to a given growth condition were selected for proteomic analysis. Protein bands of interest were first manually excised, washed and digested with trypsin. Gel slices were washed first in a solution of 50 mM sodium bicarbonate and 50% acetonitrile (v/v) in nanopure water and then in 100% acetonitrile. This step was performed three times. Disulfide bonds were reduced by incubation of the gel slice in 10 mM dithiothreitol (DTT) at 60°C for 1 hr. Free sulfhydryl bonds were blocked by incubating the gel slice in 50 mM iodoacetamide at 45°C for 45 min in the dark, followed by washing three times in alternating solutions of 100 mM sodium bicarbonate in nanopure water and 100% acetonitrile. The slices were dried and then individually incubated in a 20 ng/µl solution of porcine trypsin (Promega, Madison, WI, USA) for 45 min at 4°C, followed by incubation at 37°C for 4 to 6 hr in the same solution. Afterwards, the solution with the digested protein was transferred into a fresh collection tube. The gel slice was then incubated for 10 min in a solution of 50% acetonitrile:1% trifluoroacetic acid. The solution was removed and combined with the previously collected digested protein solutions from that gel. The gel was washed with a solution of 50% acetonitrile:1% trifluoroacetic acid a total of three times. The solution containing the digested gel peptides was then spun to dryness using a rotary evaporator at 30^0C.

Peptide sequencing was accomplished by colleagues at Univ. of California, Los Angeles, with a nano-liquid chromatography tandem mass spectrometer (nano LC-

MS/MS) (QSTAR Pulsar XL, Applied Biosystems, Foster City, CA, USA) equipped with nanoelectrospray interface (Protana, Odense, Denmark) and LC Packings (Sunnyvale, CA, USA) nano-LC system. The nano-LC was equipped with a homemade precolumn (150 × 5 mm) and analytical column (75 × 150 mm) packed with Jupiter Proteo C12 resin (particle size 4 mm, Phenomenex, Torrance, CA, USA). The dried digested peptides were resuspended in 1% formic acid solution. Six microliters of the sample solution was loaded to the precolumn for each LC-MS/MS run. The precolumn was washed with the loading solvent (0.1% formic acid) for 4 min before the sample was injected onto the liquid chromatography column. The eluents used for liquid chromatography were 0.1% formic acid (solvent A) and 95% acetonitrile containing 0.1% formic acid. The flow rate was 200 nl/min, and the gradient used was: 3% B to 35% B in 72 min, 35% B to 80% B in 18 min, followed by 80% B for 9 min. The column was then equilibrated with 3% B for 15 min prior to the next run. Electrospray ionization was performed using a 30 mm (internal diameter) nanobore stainless steel online emitter (Proxeon, Odense, Denmark) and a voltage set at 1900 V. Peptide sequences were searched against the NCBI genomes for *S. wolfei, S. aciditrophicus* and *M. hungatei* using MASCOT software versions 2.1.0 and 2.1.04 (Matrix Science, London, UK). Peptides were required to have a rank = 1 and a score >18.

Enzyme Assays

Rnf-like and NADH:quinone oxidoreductase (Nqo)-like activities, hydrogenase and formate dehydrogenase were assayed using suspensions of membrane vesicles (see cell lysis, cell free extracts and membrane purification) of *S. aciditrophicus* grown as described (see cell culture, harvesting and separation). Except where indicated, the

vesicles were not incubated in the presence of dodecyl maltoside. To test for the ability of membrane suspensions to catalyze Rnf-like reverse electron transfer, I followed NADH (E_0' = -320 mV) dependent reduction of benzyl viologen (E_0' = -360 mV) or methyl viologen (E_0' = -460 mV). I tested for the ability of the membrane fraction to catalyzed the more thermodynamically favorable oxidation of benzyl viologen with NAD^+ as well as for NADH dependent reduction of 2,6-dichlorophenolindophenol to test for Nqo-like activities.

Assays were performed in either sealed anaerobic cuvettes in volumes of 700-1,200 µl or in volumes of 280-320 µl in a 96-well plate in the anaerobic chamber. Reaction buffers contained indicator dyes at final concentrations of either 1 mM benzyl or methyl viologen or 200 µM 2,6-dichlorophenolindophenol. Benzyl or methyl viologen was pre-reduced with sodium dithionite to an OD_{600} (described below) of either 0.2 or 1.2 absorbance units to monitor reduction or oxidation of the indicator, respectively. Except in cases where hydrogen served as the electron donor, reactions were started with the addition of NADH, NAD^+ or formate to 1 mM from a 100 mM stock solution. In assays where hydrogen served as the electron donor, cuvettes were first pressurized to 138 kPa with hydrogen and the assays were started with the addition of suspensions of membrane vesicles. A minimum of five assays were conducted for each activity and the amount of protein was varied (from 2-40 µg protein per reaction). Where indicated, suspensions of membrane vesicles were solubilized with the detergent dodecyl maltoside to 0.5%.

The reduction of benzyl viologen, methyl viologen or 1,6-dichlorophenol indophenol was monitored spectrophotometrically at an optical density of 600 nm

(OD_{600}) with either a Shimadzu spectrophotometer or a 96-well plate reader. Graphs of OD_{600} versus time were plotted, and activity measurements were taken from the linear portion of the graph for each assay. Total indicator oxidized or reduced was calculated using the following molar extinction coefficients (ε) of the indicators as follows: ε = 7,800 mM • cm^{-1} for benzyl viologen, ε = 8,250 mM • cm^{-1} for methyl viologen and ε = 21,000 mM • cm^{-1} for 2,6-dichlorophenolindophenol. Specific activities were calculated from these values in the form of µmol • min^{-1} • mg^{-1} with the amount of protein determined as detailed before (see cell lysis, cell free extracts and membrane purification).

Size exclusion protein enrichment and SDS-PAGE

A total of 500-1,500 µg of protein from *S. aciditrophicus* membrane vesicles from cells grown in pure culture on crotonate suspended in 250 µl potassium phosphate (pH 7.2) were solubilized with the addition of dodecylmaltoside to 0.5% and separated chromatographically

on a GE Superdex 200 gel filtration/size exclusion column in an anaerobic chamber. Potassium phosphate (50 mM) (pH 7.2) with the addition of dodecyl maltoside to 0.1% served as the elution buffer. Hydrogenase activity was tested as before (see enzyme assays) for each fraction using 200 µl of 1 mM benzyl viologen in 50 mM potassium phosphate (pH 7.2) as the reaction buffer and ambient hydrogen as the electron source. Each reaction was started with the addition of 10 µl aliquots from the corresponding fraction. Rnf-like activity was analyzed in essentially the same manner, though the reaction was started with the addition of 10 µl of 100 mM NADH in 50 mM potassium

phosphate (pH 7.2). Assays were conducted in the anaerobic chamber in 7 ml fractionation tubes.

Small, 35 µl, aliquots of fractions testing positive for the Rnf-like activity were electrophoretically separated on a 4-16% acrylamide gradient gel via BN-PAGE as previously described (see blue-native polyacrylamide gel electrophoresis), or pooled and concentrated in an Amicon filtration system under nitrogen atmosphere with a 3,000 kDa molecular weight cutoff filter. Aliquots of pooled, concentrated fractions and unconcentrated fractions were resuspended in Laemmli sample buffer (Bio-Rad). For sodium dodecyl sulfate polyacrylamide gel electrophoresis, samples were heated for thirty seconds in five- to ten-second intervals and electrophoretically separated on a polyacrylamide gel containing 12% polyacrylamide, 375 mM tris(hydroxymethyl)aminomethane (Tris), 0.1% sodium dodecyl sulfate with the addition of 100 µl 10% ammonium persulfate as catalyst per 10 ml gel buffer. Polymerization was started with the addition of 8 µl tetramethylenediamine per 10 ml gel buffer and the gel was cast using our casting apparatus (Hoeffer) with 1 mm spacers. The gel was run at 130 V with a running buffer containing 50 mM Tris, 250 mM glycine and 0.1% sodium dodecyl sulfate until the dye front was within 3-5 mm of the bottom of the gel. The gel was fixed, washed and stained as discussed previously (see blue-native polyacrylamide gel electrophoresis).

In-gel trypsin digestion of chromatographically separated proteins with reduction and alkylation

Protein bands were excised from the gel and sent to the University of Oklahoma Health Sciences Center for digestion by trypsin. Excised bands were cut into pieces and fully destained with 25 mM ammonium bicarbonate in 50% acetonitrile in ultrapure water (v/v). Destaining solution was removed and gel pieces were reduced by adding 55 mM Tris[2-carboxyethyl]phosphine (Thermo Fisher 89671E), 25 mM ammonium bicarbonate in ultra-pure water and incubating at 60°C for 10 minutes. Reducing buffer was removed and gel pieces were alkylated by adding 100 mM iodoacetamide (Thermo Fisher 89671F), 25 mM ammonium bicarbonate in ultra-pure water and incubating at room temperature, in the dark, for 1 hour. After removing alkylation buffer, the gel pieces were washed twice with 25 mM ammonium bicarbonate in 50% acetonitrile in ultra-pure water (v/v) then dehydrated with 100% acetonitrile. After acetonitrile was removed and gel pieces allowed to dry, 100 ng of trypsin was added in 10 µl of 25 mM ammonium bicarbonate in ultra-pure water. The gel pieces were allowed to swell and an additional 25 µl of 25 mM ammonium bicarbonate in ultra-pure water was added to cover. Gel pieces were incubated at 30°C overnight (16 hours). The digest solution was removed to a new tube and 25 µl of 100% acetonitrile was added to the gel pieces. Once gel pieces were dehydrated, the acetonitrile was removed and added to the tube containing the digest solution. The digest solution containing peptides was then completely dried using a speed-vac.

Peptide mass fingerprint analysis of partially purified fractions

Sequence analysis for bands obtained by SDS-PAGE (described above) was performed by the University of Oklahoma Health Sciences Center Proteomics Core

Facility. Samples were analyzed using a Dionex Ultimate 3000 nanoscale HPLC system connected to Applied Biosystems QSTAR Elite mass spectrometer. Peptides were separated on a C18 column consisting of 3-micron particles packed in a column of 75 microns internal diameter by 150 mm length. Collected data were submitted to a MASCOT search using the University of Oklahoma Health Sciences Center Proteomics Core Facility's in house NCBInr database to identify peptides present in the original sample. Full details regarding the peptide mass fingerprint analysis conducted on partially purified protein fractions are available from the University of Oklahoma Health Sciences Center Proteomics Core Facility, 975 NE 10th Street, BRC1106, Oklahoma City, OK 73104.

Results

Protein complexes identified from S. aciditrophicus membrane enrichments

During the syntrophic oxidation of benzoate and cyclohexane carboxylate by *S. aciditrophicus*, electrons derived from acyl-CoA intermediates of benzoate and cyclohexane carboxylate oxidation are at a relatively high midpoint redox potential relative to hydrogen or formate. Kung and colleagues (2013) speculated that the thermodynamically favorable reduction of NAD^+ by reduced ferredoxin provides energy for the reduction of NAD^+ with electrons derived from these intermediates in a process known as electron confurcation. However, the source of reduced ferredoxin remains unclear. The genome of *S. aciditrophicus* was found to contain genes encoding

a membrane bound Rnf-like complex which could function to use ion gradients to drive the reduction of ferredoxin with electrons derived from NADH.

To identify membrane bound protein complexes, solubilized membrane fragments *S. aciditrophicus* were electrophoretically separated using single dimension blue-native polyacrylamide gel electrophoresis (BN-PAGE). A total of 32 membrane complexes (Figure 7) were detected from the five growth conditions. I was able to

NativeMark MW Stds
Crotonate pure culture
Crotonate + benzoate pure culture
Crotonate + M. hungatei
Benzoate + M. hungatei
Cyclohexane carboxylate + M. hungatei
kDa
1,048
720
480
242
146
66
CroPC1
CroPC2
CroPC3
CroPC4
CroPC5
CroPC6
CroBz1
CroBz2
CroBz3
CroBz4
CroBz5
CroBz6
CroBz7
CroBz8
CroCC1
CroCC2
CroCC3
CroCC4
CroCC5
CroCC6
CroCC7
Bz1
Bz2
Bz3
Bz4
Bz5
Bz6
Bz7
CHC1
CHC2
CHC3
CHC4
CHC5

Figure 7: Separation of membrane protein complexes by blue-native polyacrylamide gel electrophoresis (BN-PAGE). Membrane fractions were electrophoretically separated using non-denaturing BN-PAGE. A total of 32 complexes were detected. Six complexes were detected during growth in pure culture on crotonate, eight complexes were detected during growth in pure culture on crotonate + benzoate, seven complexes were detected during growth in coculture on crotonate, seven complexes were detected during growth in coculture on benzoate and five complexes were detected during growth in coculture on cyclohexane carboxylate. Corresponding apparent molecular weight (MW_{app}) for each band is given in Table 5.

Table 5: Peptides detected from non-denaturing blue-native PAGE separation of solubilized *S. aciditrophicus* membranes. Observed bands were excised, digested with trypsin and peptides sequenced by peptide mass fingerprint analysis. Unique peptides correspond to the number of unique peptides detected by peptide mass fingerprint analysis from the respective band. Peptides were identified by a MASCOT search using the NCBInr database. Scores represent the score returned by MASCOT. TMH = predicted transmembrane helices, MW_{app} apparent molecular weight for the indicated band, MW_p = molecular weight of the predicted amino acid sequence for the respective locus tag, pI = isoelectric point of the predicted amino acid sequence for the respective locus tag.

Band # (MW_{app})	Locus Tag	Annotation	Unique Peptides	Score	TMH	Signal Peptide	MW_p	pI
CroPC1	Syn_00547	ATP synthase delta chain	6	181	No	No	20	8.7
(731 kDa)	Syn_03116	unknown function	4	153	Yes	Yes	48	4.4
	Syn_00544	ATP synthase beta chain	3	89	No	No	51	4.5
	Syn_00198	outer membrane porin protein	2	63	Yes	Yes	47	5.2
	Syn_00549	ATP synthase B chain	2	60	Yes	No	19	8.9
	Syn_00545	ATP synthase gamma chain	2	58	No	No	33	6.6
CroPC2	Syn_03116	unknown function	4	203	Yes	Yes	48	4.4
(569 kDa)	Syn_00546	ATP synthase alpha chain	7	128	No	No	55	5.2
	Syn_00198	outer membrane porin protein	2	94	Yes	Yes	47	5.2
	Syn_01156	ATP-dependent protease La	5	75	No	No	93	4.9
	Syn_00063	DNA-directed RNA polymerase beta' chain	3	68	No	No	154	8.2
	Syn_00846	transmembrane symporter	2	60	Yes	Yes	53	9.8
	Syn_02772	proton translocating pyrophosphatase	2	55	Yes	No	72	5.3
	Syn_01662	Rnf, subunit C	2	42	Yes	Yes	34	8.8
	Syn_02770	proton translocating pyrophosphatase	3	34	Yes	Yes	87	5.0

CroPC3	Syn_03116	unknown function	5	190	Yes	Yes	48	4.4
(481 kDa)	Syn_00897	Inosine-5'-monophosphate dehydrogenase	6	159	No	No	53	7.6
	Syn_03223	chaperonin GroEL , truncated	4	101	No	No	58	4.7
	Syn_01662	Rnf, subunit C	3	87	Yes	Yes	34	8.8
	Syn_02772	proton translocating pyrophosphatase	2	67	Yes	No	72	5.3
	Syn_02770	proton translocating pyrophosphatase	3	40	Yes	Yes	87	5.0
CroPC4	Syn_02772	proton translocating pyrophosphatase	3	116	Yes	No	72	5.3
(337 kDa)	Syn_02896	4-hydroxybenzoate--CoA ligase / benzoate--CoA ligase	4	105	No	No	59	5.6
	Syn_02770	proton translocating pyrophosphatase	2	104	Yes	Yes	87	5.0
	Syn_03116	unknown function	4	90	Yes	Yes	48	4.4
	Syn_00546	ATP synthase alpha chain	2	37	No	No	55	5.2
CroPC5	Syn_01654	BamA	6	284	No	No	43	6.7
(262 kDa)								
CroPC6	Syn_00480	Glutaconyl-CoA decarboxylase	6	243	No	No	42	4.9
(152 kDa)	Syn_02772	proton translocating pyrophosphatase	4	159	Yes	No	72	5.3
	Syn_02638	FeS oxidoreductase	5	137	Yes	No	79	5.4

	Syn_01303	Membrane protein, unknown function	2	94	Yes	No	15	4.8
	Syn_02770	proton translocating pyrophosphatase	2	74	Yes	Yes	87	5.0
	Syn_01653	putative enoyl-CoA hydratase	3	63	No	No	28	5.4
	Syn_02157	argininosuccinate synthase	2	43	No	No	45	5.1
	Syn_03002	Membrane protein, unknown function	2	23	Yes	Yes	22	9.7
CroBz1	Syn_00546	ATP synthase alpha chain	21	424	No	No	55	5.2
(732 kDa)	Syn_00547	ATP synthase delta chain	7	183	No	No	20	8.7
	Syn_03116	unknown function	4	126	Yes	Yes	48	4.4
	Syn_00549	ATP synthase B chain, sodium ion specific	3	111	Yes	No	19	8.9
	Syn_00544	ATP synthase beta chain	6	110	No	No	51	4.5
	Syn_00198	outer membrane porin protein	3	62	Yes	Yes	47	5.2
	Syn_00545	ATP synthase gamma chain	2	50	No	No	33	6.6
	Syn_02896	4-hydroxybenzoate--CoA ligase / benzoate--CoA ligase	2	41	No	No	59	5.6
	Syn_02772	proton translocating pyrophosphatase	2	24	Yes	No	72	5.3
CroBz2	Syn_00546	ATP synthase alpha chain	15	229	No	No	55	5.2
(580 kDa)	Syn_03116	unknown function	4	221	Yes	Yes	48	4.4

	Syn_00198	outer membrane porin protein	8	219	Yes	Yes	47	5.2
	Syn_00544	ATP synthase beta chain	4	96	No	No	51	4.5
	Syn_00547	ATP synthase delta chain	4	86	No	No	20	8.7
	Syn_02772	proton translocating pyrophosphatase	3	70	Yes	No	72	5.3
	Syn_02770	proton translocating pyrophosphatase	3	57	Yes	Yes	87	5.0
	Syn_01156	ATP-dependent protease La	3	40	No	No	93	4.9
	Syn_02074	acriflavin resistance plasma membrane protein	3	33	Yes	Yes	117	7.7
CroBz3	Syn_03116	unknown function	6	232	Yes	Yes	48	4.4
(451 kDa)	Syn_02770	proton translocating pyrophosphatase	5	201	Yes	Yes	87	5.0
	Syn_02772	proton translocating pyrophosphatase	4	180	Yes	No	72	5.3
	Syn_01659	Rnf, subunit E	4	171	Yes	Yes	35	9.0
	Syn_00198	outer membrane porin protein	5	150	Yes	Yes	47	5.2
	Syn_01662	Rnf, subunit C	4	94	Yes	Yes	34	8.8
	Syn_01664	Rnf, NADH-binding subunit	5	87	No	No	47	6.8
	Syn_03223	chaperonin GroEL , truncated	4	74	No	No	58	4.7
	Syn_00549	ATP synthase B chain	2	63	Yes	No	19	8.9
	Syn_02896	4-hydroxybenzoate--CoA ligase / benzoate--CoA ligase	3	50	No	No	59	5.6
	Syn_00231	glycogen phosphorylase	2	30	No	No	97	6.9

CroBz4 (337 kDa)	Syn_02896	4-hydroxybenzoate--CoA ligase / benzoate--CoA ligase	10	315	No	No	59	5.6
	Syn_03116	unknown function	4	220	Yes	Yes	48	4.4
	Syn_02770	proton translocating pyrophosphatase	7	197	Yes	Yes	87	5.0
	Syn_02772	proton translocating pyrophosphatase	4	162	Yes	No	72	5.3
	Syn_00481	glutaconyl-CoA decarboxylase	7	154	No	No	65	7.0
	Syn_01431	glutaconyl-CoA decarboxylase beta subunit	5	93	Yes	Yes	48	8.9
	Syn_02382	glutamate dehydrogenase	2	60	No	No	50	6.0
	Syn_01659	Rnf, subunit E	2	59	Yes	Yes	35	9.0
	Syn_00549	ATP synthase B chain	2	48	Yes	No	19	8.9
	Syn_00545	ATP synthase gamma chain	2	36	No	No	33	6.6
	Syn_01524	protein translocase subunit	3	27	Yes	Yes	59	6.7
CroBz5 (267 kDa)	Syn_01654	BamA	12	410	No	No	43	6.7
	Syn_02770	proton translocating pyrophosphatase	6	186	Yes	Yes	87	5.0
	Syn_02772	proton translocating pyrophosphatase	5	179	Yes	No	72	5.3
	Syn_01431	glutaconyl-CoA decarboxylase beta subunit	3	90	Yes	Yes	48	8.9
	Syn_01303	hypothetical membrane protein	2	87	Yes	No	15	4.8

	Syn_00549	ATP synthase B chain	2	49	Yes	No	19	8.9
	Syn_01310	3-hydroxyacyl-CoA dehydrogenase	2	33	No	Yes	31	6.6
CroBz6	Syn_02772	proton translocating pyrophosphatase	4	154	Yes	No	72	5.3
(221 kDa)	Syn_00546	ATP synthase alpha chain	5	127	No	No	55	5.2
	Syn_01303	hypothetical membrane protein	2	118	Yes	No	15	4.8
	Syn_02586	acyl-CoA dehydrogenase	2	89	No	No	42	5.6
	Syn_02638	FeS oxidoreductase	2	75	Yes	No	79	5.4
	Syn_02770	proton translocating pyrophosphatase	3	73	Yes	Yes	87	5.0
CroBz7	Syn_00480	Glutaconyl-CoA decarboxylase	5		No	No	42	4.9
(152 kDa)	Syn_02638	FeS oxidoreductase	6		Yes	No	79	5.4
CroCC1	Syn_02896	4-hydroxybenzoate--CoA ligase / benzoate--CoA ligase	3	71	No	No	59	5.6
(903 kDa)	Syn_02180	membrane protease subunit, stomatin/prohibitin -like protein	2	68	Yes	Yes	28	5.2
	Syn_00603	formate dehydrogenase major subunit	5	67	No	No	93	7.7
	Syn_03116	unknown function	4	53	Yes	Yes	48	4.4
	Syn_02180	membrane protease subunit, stomatin/prohibitin -like protein	2	50	Yes	Yes	28	5.2

CroCC2	Syn_02770	proton translocating pyrophosphatase	3	59	Yes	Yes	87	5.0
(330 kDa)	Syn_00628	Rnf subunit	2	57	Yes	Yes	30	6.7
	Syn_01664	Rnf, NADH-binding subunit	4	48	No	No	47	6.8
	Syn_00545	ATP synthase gamma chain	2	39	No	No	33	6.6
	Syn_01659	Rnf, subunit E	2		Yes	Yes	35	9.0
	Syn_01662	Rnf, subunit C	4		Yes	Yes	34	8.8
	Syn_02772	proton translocating pyrophosphatase	4		Yes	No	72	5.3
	Syn_02896	4-hydroxybenzoate--CoA ligase / benzoate--CoA ligase	4		No	No	59	5.6
	Syn_03116	unknown function	4		Yes	Yes	48	4.4
CroCC3	Syn_03116	unknown function	4	174	Yes	Yes	48	4.4
309	Syn_03116	unknown function	4	174	Yes	Yes	48	4.4
	Syn_02772	proton translocating pyrophosphatase	4	124	Yes	No	72	5.3
	Syn_02770	proton translocating pyrophosphatase	6	90	Yes	Yes	87	5.0
	Syn_02770	proton translocating pyrophosphatase	7	89	Yes	Yes	87	5.0
	Syn_02772	proton translocating pyrophosphatase	6	84	Yes	No	72	5.3
	Syn_02896	4-hydroxybenzoate--CoA ligase / benzoate--CoA ligase	5	74	No	No	59	5.6
	Syn_00545	ATP synthase gamma chain	3	53	No	No	33	6.6

	Syn_02896	4-hydroxybenzoate--CoA ligase / benzoate--CoA ligase	4	50	No	No	59	5.6
CroCC4	Syn_02770	proton translocating pyrophosphatase	8	204	Yes	Yes	87	5.0
165	Syn_02638	FeS oxidoreductase	5	188	Yes	No	79	5.4
	Syn_02772	proton translocating pyrophosphatase	7	172	Yes	No	72	5.3
	Syn_02770	proton translocating pyrophosphatase	6	128	Yes	Yes	87	5.0
	Syn_02638	FeS oxidoreductase	6	116	Yes	No	79	5.4
	Syn_02772	proton translocating pyrophosphatase	4	92	Yes	No	72	5.3
CroCC7	Syn_00546	ATP synthase alpha chain	11	181	No	No	55	5.2
(60 kDa)	Syn_00547	ATP synthase delta chain	6	74	No	No	20	8.7
	Syn_01909	chaperonin GroEL	2	57	No	No	58	5.1
	Syn_03223	chaperonin GroEL , truncated	2	56	No	No	58	4.7
	Syn_01028	bacterial regulatory protein, LuxR family	2	52	No	No	36	5.9
	Syn_00544	ATP synthase beta chain	4	48	No	No	51	4.5
	Syn_02772	proton translocating pyrophosphatase	3	38	Yes	No	72	5.3
	Syn_03255	SSU ribosomal protein S7P	2	33	No	No	18	10.9

Bz4 (351 kDa)	Syn_03116	unknown function	2	84	Yes	Yes	48	4.4
Bz5 (240 kDa)	Syn_03116	unknown function	4	168	Yes	Yes	48	4.4
	Syn_01654	BamA	2	46	No	No	43	6.7
Bz6 (216 kDa)	Syn_03116	unknown function	3	170	Yes	Yes	48	4.4
Bz7 (92 kDa)	Syn_02638	FeS oxidoreductase	4	115	Yes	No	79	5.4
CHC2 (351 kDa)	Syn_03116	unknown function	2	72	Yes	Yes	48	4.4
CHC3 (251 kDa)	Syn_03116	unknown function	4	144	Yes	Yes	48	4.4
	Syn_01654	BamA	3	58	No	No	43	6.7
CHC4 (216 kDa)	Syn_03116	unknown function	4	156	Yes	Yes	48	4.4

CHC5 (95 kDa)	Syn_02638	FeS oxidoreductase		3	100	Yes	No	79	5.4

positively identify *S. aciditrophicus* -derived peptides from 26 of these bands using peptide mass fingerprint analysis. Three of these complexes (Bz1/CHC1, Bz6/CHC4, and Bz7/CHC5) appeared unique to growth under syntrophic conditions – benzoate- and cyclohexane carboxylate-oxidizing conditions – and are, therefore, presumed to be formed specifically during syntrophic growth.

Peptides corresponding to the Rnf-like complex were detected in two high molecular weight bands during growth in pure culture on crotonate (CroPC2 and CroPC3) and in one band from cells grown axenically on crotonate with benzoate as electron acceptor (CroBz3) (Figure 7, Table 5). A similar molecular weight band was observed from cells grown in coculture on benzoate though we were unable to positively identify any peptides derived from *S. aciditrophicus.*

S. aciditrophicus was found to contain two gene clusters predicted to code for a sodium-dependent ATP synthase (Syn_00543-00549 and _02101-02105) (McInerney *et al.* 2007). Here, only peptides corresponding to the ATP synthase Syn_00543-00549 were detected. In total, peptides derived from these genes were found in a total of seven bands (CroPC1-2, 4 and CroBz1-6) with molecular weights of > 220 kDa. All of these were detected from cells grown axenically on crotonate or on crotonate with benzoate as electron acceptor (Figure 7, Table 5). Additionally, peptides derived from a proton translocating pyrophosphatase were highly abundant and detected in a total of ten bands from cells grown in pure culture on crotonate and in pure cultures grown on crotonate + benzoate (CroPC2-4,6 and CroBz1-6) (Figure 7, Table 5).

In addition to an Rnf-like complex, the genome of *S. aciditrophicus* was found to contain genes encoding glutaconyl-CoA decarboxylase (Syn_00479-81). These

genes were not linked on the chromosome to those predicted to code for the sodium transporting membrane subunit, Syn_00115 or Syn_01431. Here, we detected subunits derived from the gene products of Syn_00480 (CroPC6) and Syn_00481 (CroBz3, CroBz4 and CroBz5) (Table 5) and codetected peptides derived from the gene product of a candidate membrane component encoding gene, Syn_01434 (Table 5) with peptides derived from the Syn_00481 gene product (CroBz4). This suggests that the gene product coded for by Syn_01431 recruits the glutaconyl-CoA decarboxylase subunits to the enzyme. McInerney and colleagues (2007) as well as others (Wischgoll *et al.* 2009) suggest glutaryl-CoA is oxidized to glutaconyl-CoA in *S. aciditrophicus,* rather than decarboxylated to crotonyl-CoA, and our findings here are consistent with this hypothesis.

Copurification of an FeS oxidoreductase with NADH:acceptor oxidoreductase activity in the syntrophic butyrate-oxidizing bacterium *Syntrophomonas wolfei* (Muller *et al.* 2009; Schmidt *et al.* 2013) led to speculation that this FeS oxidoreductase may be a module for electron input into the membrane during the oxidation of acyl-CoA intermediates. Here, peptides corresponding to the analogous FeS oxidoreductase (Syn_02638) were detected in lower molecular weight bands from cells grown in pure culture on crotonate (CroPC6), cells grown in pure culture on crotonate + benzoate (CroBz6), cells grown in coculture on benzoate (Bz7) and cells grown in coculture on cyclohexane carboxylate (CHC5). Interestingly, only peptides derived from the Syn_02638 gene product were detected in CHC5 (Figure 7, Table 5). The gene locus coding for this protein is located adjacent to genes coding for alpha- and beta- subunits of electron transferring flavoprotein subunits (Syn_02636 and 37 gene products,

respectively). I did not detect peptides derived from either electron transferring flavoprotein subunit in membrane complexes separated by BN-PAGE.

Peptides from *M. hungatei*, but not *S. aciditrophicus*, were detected from an approximately 950 kDa band (Bz1) derived from cells grown syntrophically on benzoate and we were unable to positively identify any peptides from the analogous band (CHC1) derived from cells grown in syntrophic coculture on cyclohexane carboxylate (Figure 7). Peptides derived from Syn_01654 were detected in an ~240 kDa band (Bz5) during growth on benzoate (Figure 7, Table 5). Syn_01654 has recently been shown to code 6-hydroxycyclohex-1-ene-1-carboxyl-CoA hydrolase (Kuntze *et al.* 2008) and is necessary for benzoate degradation in a pathway analogous to that of *Thauera aromatica* (Breese *et al.* 1998). A slightly larger band (~260 kDa) was observed from the axenic growth conditions on crotonate or crotonate + benzoate (CroPC5 and CroBz5) and peptides corresponding to Syn_01664 gene product were likewise detected (Figure 7, Table 5).

Presence of NADH-dependent reduction of benzyl viologen

Several subunits derived from genes predicted to encode an Rnf-like complex were detected in membrane fractions from *S. aciditrophicus* grown in pure culture on crotonate (Table 5). The presence of Rnf-like subunits suggested that *S. aciditrophicus* uses this enzyme to produce reduced ferredoxin. I therefore tested if *S. aciditrophicus* membranes catalyze the predicted Rnf-like activity, the reduction of a low potential electron acceptor using NADH as the electron donor. For these experiments, benzyl

viologen ($E^{0'}$ = -360 mV) (Michaelis and Hill 1933) and methyl viologen ($E^{0'}$ = -450 mV) (Michaelis and Hill 1933) served as low potential electron acceptors.

Both hydrogenase and formate dehydrogenase activities are oxygen-labile in *S. aciditrophicus* and the detection of both activities shows that active fractions were obtained (Table 6). *S. aciditrophicus* membrane fractions, which were not

Table 6: Specific activities of hydrogenase, formate dehydrogenase and Rnf- and Nqo-like activity in *S. aciditrophicus* membrane fractions. Cells were grown in pure culture on crotonate or in pure culture on crotonate + benzoate. For assays where hydrogen was not the electron donor, membrane fractions (2-40 µg protein) were diluted into a reaction buffer containing 1 mM of either benzyl viologen, methyl viologen or 200 µM 2,6-dichlorophenolindophenol and the activity was started with the addition of NAD^+, NADH or formate to 1 mM. Where hydrogen was the electron donor, the sealed anaerobic cuvette containing the reaction buffer was pressurized to 138 kPa H_2 and the reaction was started with the addition of the membrane fraction. The increase in absorbance (oxidized methyl and benzyl viologen) or decrease in absorbance (reduced methyl and benzyl viologen and 2,6-dichlorophenolindophenol) was measured spectrophotometrically at 600 nm. Where indicated, membrane fractions were solubilized in buffer containing 0.5% dodecyl maltoside (DDM).

	Specific activity (µmol • min^{-1} • mg^{-1})	
	Crotonate	Crotonate + benzoate
Hydrogen + oxidized benzyl viologen	0.4 ± 0.1	0.06 ± < 0.1
Formate + oxidized benzyl viologen	0.5 ± 0.1	0.2 ± < 0.1
NADH + oxidized benzyl viologen [•]	3.3 ± 0.7	7.9 ± 1.0
NADH + oxidized methyl viologen [•]	0.1 ± < 0.1	Not performed
NADH + oxidized benzyl viologen [•] (solubilized with DDM)	Not performed	1.9 ± < 0.1
NAD^+ + reduced benzyl viologen	1.2 ± 0.6	2.1 ± 0.1
NAD^+ + methyl viologen	5.9 ± 1.4	Not performed
NADH + 2,6-dichlorophenolindophenol [¨]	1.33 ± <0.1	1.66 ± 0.11

[•] Reaction represents an Rnf-like activity

[¨] Reaction represents an Nqo-like activity

treated with detergent, from cells grown in pure culture on either crotonate or crotonate and benzoate reduced benzyl viologen with NADH as electron donor (Table 6). Surprisingly, the specific activity for NADH-dependent reduction of benzyl viologen was higher than the specific activity of the thermodynamically favorable direction, NAD^+-dependent oxidation of benzyl viologen pre-reduced with trace amounts of sodium dithionite (Table 6). As predicted, the rate of NAD^+ -dependent oxidation of the lower potential acceptor methyl viologen was higher than NADH-dependent reduction of methyl viologen, though our ability to detect an NADH –dependent activity with methyl viologen further confirms the ability of membrane fractions to catalyze reverse electron transfer. The addition of the detergent, dodecylmaltoside, decreased Rnf-like specific activity by approximately 60% (Table 6), consistent with the need for an intact membrane to maintain ion gradients to drive reverse electron transfer.

Components of Rnf are phylogenetically related to components of sodium-pumping, NADH-ubiquinone oxidoreductases (Nqo) and proton-pumping, NADH-ubiquinone oxidoreductases (NADH dehydrogenase, Ndh-1; complex 1). I tested whether S. *aciditrophicus* membranes contained Ndh or Nqo activity with the use of 2,6-dichlorophenolindophenol (DCPIP) ($E^{0'}$ = +220 mV). Membrane fractions of *S. aciditrophicus* were able to reduce DCPIP with electrons derived from NADH; however, the specific activity for this assay in membrane fractions from cells grown in pure culture on crotonate and in pure culture on crotonate + benzoate was only 30% of the specific activity detected for the Rnf-like activity.

The need for reverse electron transfer is most apparent when *S. aciditrophicus* grows syntrophically where electrons derived from the oxidation of acyl-CoA intermediates ($E^{0'}$ = -10 mV) (Sato *et al.* 1999) and NADH ($E^{0'}$ = -320 mV) are used to produce hydrogen (E' = -260 mV at 1 Pa H_2) or formate (E' = -290 mV at 1 µM formate) (McInerney *et al.* 2007). Membrane fractions from *S. aciditrophicus* cells grown axenically on crotonate and syntrophically on either benzoate or cyclohexane carboxylate were tested for the predicted Rnf-like activity. Here, assays were performed in the anaerobic chamber using a 96-well plate reader to reduce the likelihood of air inactivation. Because of this, background benzyl viologen reduction was observed in unamended controls that lacked an electron donor due to presence of hydrogen in the chamber atmosphere (less than 5%) (Table 7). The background activity represents

Table 7: Specific activities of hydrogenase, formate dehydrogenase and Rnf-like activity in *S. aciditrophicus* membrane fractions. Cells were grown in pure culture on crotonate, coculture on benzoate or in coculture on cyclohexane carboxylate. Membrane fractions (2-40 µg protein) were diluted into a reaction buffer containing 1 mM benzyl viologen and started with the addition of NADH or formate to 1 mM. Assays were conducted in an anaerobic chamber with a background hydrogen concentration of less than 5%. The increase in absorbance was measured spectrophotometrically at 600 nm. Values for assays with formate or NADH as electron donor are the difference of total activity and the activity obtained with background hydrogen as electron donor.

	Specific activity (µmol • min^{-1} • mg^{-1})		
	Crotonate pure culture	Benzoate coculture	Cyclohexane carboxylate coculture
Background hydrogen + oxidized benzyl viologen	0.4 ± 0.1	0.4 ± 0.1	2.2 ± 0.6
Formate + oxidized benzyl viologen	15.2 ± 3.7	8.5 ± 2.7	5.2 ± 2.7
NADH + oxidized benzyl viologen $^{\cdot}$	9.0 ± 1.9	16.1 ± 3.3	13.5 ± 5.6

$^{\cdot}$ Activity represents an Rnf-like activity

hydrogenase activity in the membrane. Hydrogenase activity in membranes of *S. aciditrophicus* grown axenically on crotonate measured in the chamber with the 96-well plate reader (Table 7) was within the same range as measured using sealed cuvettes (Table 6), showing that the different assay conditions did not affect the activity of this important enzyme. Formate dehydrogenase activity (formate-dependent, benzyl viologen reduction activity) was much higher than hydrogenase activity for all growth conditions tested (Table 7). Very high specific activities for the predicted Rnf-like activity were detected in membranes from syntrophically grown *S. aciditrophicus*, 16.47 ± 3.31 μmol•min^{-1}•mg^{-1} for benzoate-grown cells and 15.65 ± 5.57 μmol•min^{-1}•mg^{-1} for cyclohexane carboxylate-grown cells, respectively (Table 7). These specific activities were approximately 1.8-fold and 1.7-fold higher, respectively, than the specific activity of cells grown axenically on crotonate (9.34 ± 1.93 μmol•min^{-1}•mg^{-1}) (Table 7). The elevated levels of NADH-dependent, benzyl viologen reduction activity during syntrophic growth is consistent with the need for reverse electron transfer during syntrophic metabolism.

Partial purification of the NADH-dependent benzyl viologen reduction activity

The presence of a peptides corresponding to an Rnf-like complex and my observation that I could follow an activity in which electrons moved from a higher potential donor to a lower potential acceptor (NADH to benzyl viologen) led me to partially purify the enzyme(s) catalyzing this reaction. NADH-dependent benzyl viologen reducing activity was solubilized from *S. aciditrophicus* membrane fractions grown axenically on crotonate and separated using size-exclusion chromatography. A

total of forty fractions of one milliliter each were collected and assayed for NADH-dependent reduction of benzyl viologen. Three fractions reduced benzyl viologen with NADH as electron donor (Figure 8). Specific activity for the pooled fractions was low, $0.1 \pm <0.1$ μmoles • min^{-1} • mg^{-1}.

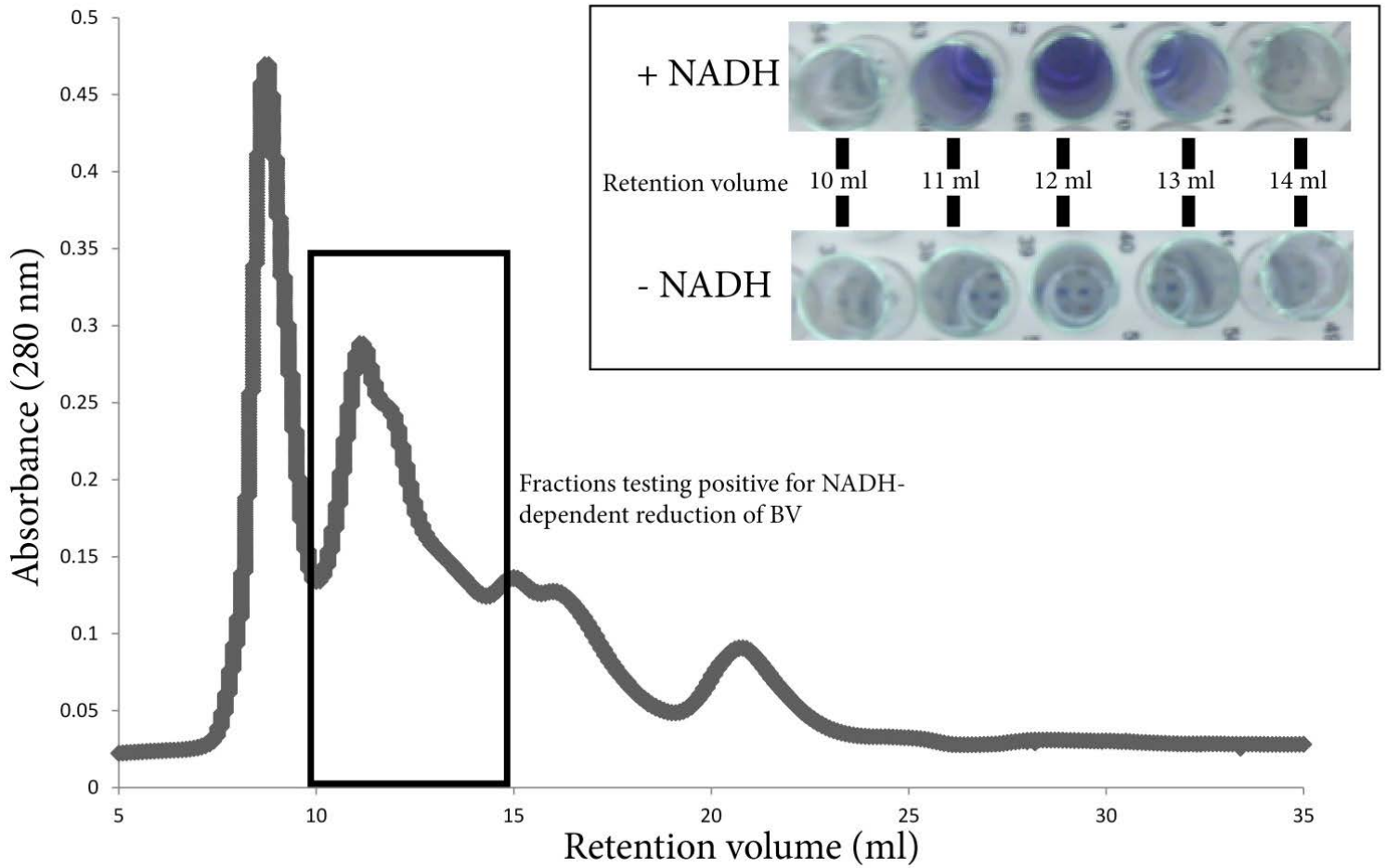
+ NADH
Retention volume
10 ml
11 ml
12 ml
13 ml
14 ml
- NADH
Fractions testing positive for NADH-dependent reduction of BV
Absorbance (280 nm)
Retention volume (ml)
0
0.05
0.1
0.15
0.2
0.25
0.3
0.35
0.4
0.45
0.5
5
10
15
20
25
30
35

Figure 8: Partial purification of the predicted Rnf-like activity from *S. aciditrophicus* membrane fractions from cells grown in pure culture on crotonate. Membrane fractions obtained via ultracentrifugation were solubilized in reaction buffer containing the detergent dodecyl maltoside. Activity was retained in fractions between 11 ml and 13 ml retention volume. Inset: NADH-dependent activity (above) versus background activity (below) at 30 min incubation. Background activity represents reduction of benzyl viologen with hydrogen (less than 5%) as electron donor.

The subunit composition of Rnf is not yet known, though preliminary data suggests that in *Acetobacter woodii*, the purified Rnf complex has an apparent molecular weight of 186 kDa (Biegel *et al.* 2011). Here, the fractions testing positive for NADH-dependent reduction of benzyl viologen eluted between 11 ml and 13 ml, which corresponds to an apparent molecular weight between 480 and 720 kDa. This corresponds to a molecular weight 2.5-3.8 –fold higher than that observed in *A. woodii* (Biegel *et al.* 2011). I observed two distinct bands from fractions separated by BN-PAGE with apparent molecular weights of ~120 kDa and ~160 kDa and a total of four bands were detected from fractions separated by SDS-PAGE (Figure 9).

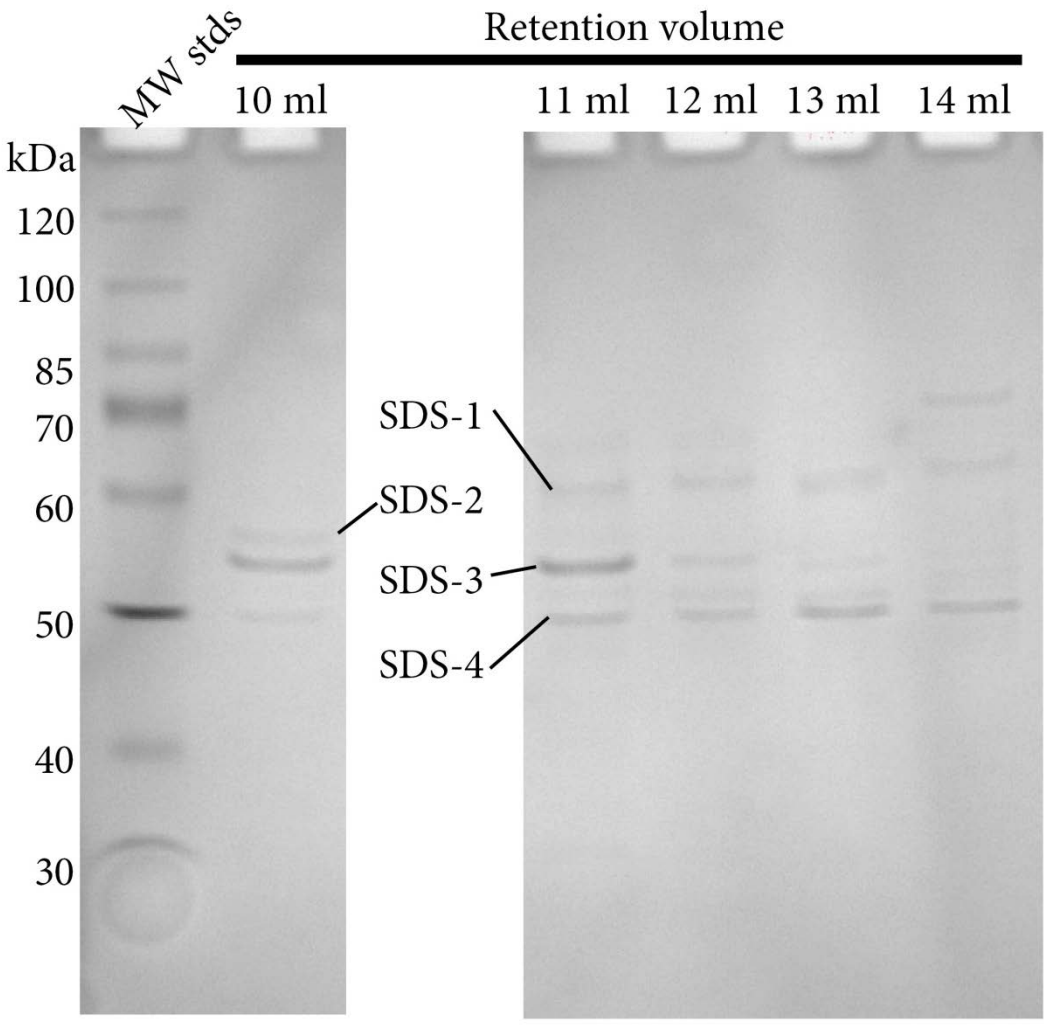

Figure 9: SDS-PAGE separation of fractions testing positive for predicted Rnf-like activity. Solubilized membranes of *S. aciditrophicus* were separated via size exclusion gel filtration and tested for NADH-dependent reduction of benzyl viologen. Fractions testing positive for the activity were concentrated and separated on a 10% polyacrylamide gel by SDS-PAGE. Four bands were excised and sequenced using peptide mass fingerprint analysis by LC-MS/MS. Corresponding apparent molecular weight (MW_{app}) is given in Table 8.

Table 8: Peptides detected from denaturing SDS-PAGE separation of *S. aciditrophicus* membrane fractions partially purified for Rnf-like activity. Observed bands were excised, digested with trypsin and peptides sequenced by peptide mass fingerprint analysis. Unique peptides correspond to the number of unique peptides detected by peptide mass fingerprint analysis from the respective band. Peptides were identified by a MASCOT search using the NCBInr database. Scores represent the score returned by MASCOT. TMH = predicted transmembrane helices, MW_{app} = apparent molecular weight for the indicated band, MW_p = molecular weight of the predicted amino acid sequence for the respective locus tag, pI = isoelectric point of the predicted amino acid sequence for the respective locus tag.

Band # (MW_{app})	Locus Tag	Annotation	Unique Peptides	Score	TMH	Signal Peptide	MW_p	pI
SDS-1	Syn_02896	4-hydroxybenzoate CoA ligase	17	1351	No	No	59	5.6
(71 kDa)	Syn_00481	Glutaconyl-CoA decarboxylase A subunit	1	247	No	No	65	7.0
	Syn_02770	Membrane bound pyrophosphatase	2	228	Yes	Yes	87	5.0
	Syn_02772	Membrane bound pyrophosphatase	1	164	Yes	No	72	5.3
	Syn_00123	D-3-phosphoglycerate dehydrogenase	1	98	No	No	57	5.4
SDS-2	Syn_00544	ATP synthase subunit beta	24	832	No	No	51	4.5
(63 kDa)	Syn_00546	ATP synthase subunit alpha	21	747	No	No	55	5.2
	Syn_00198	Porin	4	159	Yes	Yes	47	5.2
	Syn_02896	4-hydroxybenzoate CoA ligase	1	65	No	No	59	5.6
SDS-3	Syn_03116	Hypothetical protein	43	2608	Yes	Yes	48	4.4
(61 kDa)	Syn_00198	Porin	14	781	Yes	Yes	47	5.2
	Syn_00546	ATP synthase subunit alpha	3	101	No	No	55	5.2
	Syn_00544	ATP synthase subunit beta	4	101	No	No	51	4.5
	Syn_02772	Membrane bound pyrophosphatase	1	88	Yes	No	72	5.3
	Syn_01664	Rnf, NADH-binding subunit	1	85	No	No	47	6.8

SDS-4	Syn_00544	ATP synthase F_0F_1 subunit beta	10	841	No	No	51	4.5
(53 kDa)	Syn_00198	Porin	6	614	Yes	Yes	47	5.2
	Syn_00545	ATP synthase subunit gamma	6	563	No	No	33	6.6
	Syn_00546	ATP synthase F_0F_1 subunit alpha	2	501	No	No	55	5.2
	Syn_02637	Electron transfer flavoprotein alpha subunit	5	433	No	No	34	5.0
	Syn_1662	Rnf, subunit C	1	326	Yes	No	34	8.8
	Syn_01491	Flp pilus assembly protein	6	306	Yes	No	32	10.2
	Syn_03116	Hypothetical protein	2	204	Yes	Yes	48	4.4
	Syn_01402	Hypothetical protein	2	184	Yes	No	39	9.0
	Syn_01431	Glutaconyl-CoA decarboxylase subunit beta	1	154	Yes	No	48	8.9
	Syn_02140	Oxalate/formate antiporter	1	141	Yes	No	43	10.0
	Syn_00044	ComL family lipoprotein	2	141	Yes	No	28	9.5
	Syn_00202	Hypothetical protein	2	136	No	Yes	25	6.1
	Syn_01655	6-hydroxycyclohex-1-ene-1-carboxyl-CoA dehydrogenase	2	109	No	No	40	7.6
	Syn_00628	Rnf subunit	1	98	Yes	No	30	6.7
	Syn_03640	Hypothetical protein	3	93	Yes	Yes	8	6.6
	Syn_01774	Pili assembly protein	1	84	Yes	No	27	10.1

Syn_3141	Peptidylprolyl isomerase	1	70	Yes	No	40	10.3
Syn_01267	Hypothetical protein	1	64	Yes	No	29	9.1

I used peptide mass fingerprint analysis by LC-MS/MS to identify proteins present in bands obtained by SDS-PAGE. Peptides corresponding to five unique proteins were detected from a large band with a molecular weight of 71 kDa (SDS1). Seventeen peptides derived from a hydroxybenzoate-/benzoate-CoA ligase (Syn_02896) were detected (Table 8). This is an approximately 59 kDa protein which is predicted to be involved in benzoate degradation and is not predicted to contain transmembrane helices. Interestingly, this peptide was co-detected with peptides for a membrane-bound proton-translocating pyrophosphatase (Syn_02770, 72) (Table 8).

The most abundant peptides from a smaller 63 kDa band corresponded to alpha- and beta-subunits of a sodium dependent ATP synthase (Table 8). Forty-three total peptides derived from a hypothetical membrane protein (Syn_03116) were detected in a 61 kDa band along with peptides derived from a gene encoding a porin (Syn_00198), ATP synthase subunits and a membrane-bound proton-translocating pyrophosphatase – both of which were co-detected from higher molecular weight bands (SDS-1 and SDS-2) and the peptides may represent degradation products which comigrated with the hypothetical cell surface protein Syn_03116. A weak signal (Score = 85) was also detected in this band for peptides derived from an Rnf-like electron transport complex subunit (Syn_1664) (Table 8).

The lowest molecular weight band, at approximately 53 kDa, was the most diverse with peptides derived from 19 different genes represented (Table 8). The top six peptide matches (based on MASCOT score) included two different ATP synthase subunits, peptides derived from a gene encoding a porin and peptides derived from an electron transfer flavoprotein alpha-subunit and an Rnf-like complex, subunit C

(Syn_01662) (Table 8). Six peptides were detected for the gamma-subunit of ATP synthase (Syn_00545) in this band but were not previously detected in higher molecular weight bands (Table 8). Five unique peptides derived from a gene encoding the alpha-subunit of an electron transfer flavoprotein were detected (Syn_02673) along with one unique peptide derived from an Rnf-like complex subunit C (Syn_01662).

Discussion

The sequenced, annotated genome of *S. aciditrophicus* revealed possible strategies for the production of reduced ferredoxin required for syntrophic metabolism and biosynthesis (McInerney *et al.* 2007). A seven-gene cluster with similarity to genes coding for Rnf from *Rhodobacter capsulatus* was found. The gene sequence encoding RnfG differed from all other sequenced RnfG –like subunits except for those found in other organisms capable of syntrophic growth (McInerney *et al.* 2007). This suggested an Rnf-like complex could couple proton- or sodium ion-motive force to the reduction of ferredoxin with electrons derived from NADH as the physiological electron donor and further suggested that the RnfG-like subunit could be used as a functional probe for syntrophic metabolism (McInerney *et al.* 2007). Rnf-like components were identified in the genome of the closely related syntrophic propionate-oxidizing bacterium, *Syntrophobacter fumaroxidans* (Plugge *et al.* 2012), but not in the genome of the syntrophic butyrate-oxidizing bacterium, *Syntrophomonas wolfei* – a Gram-negative Clostridiales (Sieber *et al.* 2010). Transcripts of *rnfC* were detected from *S. fumaroxidans* under a variety of growth conditions (Worm *et al.* 2011) implicating its importance in the physiology of *S. fumaroxidans*.

To identify the proteins responsible for reverse electron transferring activities, solubilized membrane enrichments from axenically grown cells were separated by size exclusion chromatography. After solubilization and fractionation, several fractions retained NADH-dependent benzyl viologen activity. Strikingly, these fractions also tested positive for hydrogenase activity as benzyl viologen was reduced in the absence of NADH (under ~5% hydrogen atmosphere), albeit at a much slower rate. Peptides associated with Rnf-like components were detected in bands from *S. aciditrophicus* grown axenically on crotonate and from *S. aciditrophicus* grown axenically on crotonate and benzoate.

Membrane fractions of *S. aciditrophicus* were able to reduce benzyl viologen with NADH, showing that Rnf activity is present in *S. aciditrophicus* membranes (Table 6). Furthermore, the rate for NADH-dependent reduction of benzyl viologen was higher than the rate for NAD^+ -dependent oxidation of reduced benzyl viologen. These findings, coupled with the ability of membrane fractions to reduce the lower potential indicator, methyl viologen, suggest that membrane fractions of *S. aciditrophicus* possess a membrane enzyme or complex with the predicted function of an Rnf complex (McInerney *et al.* 2007). This NADH-dependent benzyl viologen reduction was observed in membrane enrichments of cells grown under all conditions tested. The observation made here, that NADH-dependent benzyl viologen reduction has a higher specific activity in membrane enrichments obtained from cells grown in syntrophic conditions relative to those grown axenically on crotonate, implicates this/these enzymes in syntrophic growth. Approximately 60% of activity was lost after incubation in the presence of the detergent, dodecyl maltoside, which is consistent with the

possibility that this activity is chemiosmotically linked. An Rnf-like complex is likely the only mechanism that *S. aciditrophicus* has to produce reduced ferredoxin because gene loci predicted to code for a Fix system were not detected (Sieber *et al.* 2012).

Genes encoding electron transferring flavoprotein alpha- and beta-subunits (Etf-α and Etf-β, respectively) were found coupled on the *S. aciditrophicus* chromosome with an FeS oxidoreductase. This arrangement has been observed in *Pelotomaculum thermopropionicum* and in *S. wolfei* (Sieber *et al.* 2010). This arrangement suggested that the electron transferring flavoproteins are involved in electron flow during the oxidation of acyl-CoA intermediates and could potentially involve a reverse Q-loop. Additionally, the work of Schink and colleagues showed that, under their growth conditions, *S. wolfei* possibly formed an ETFα/β/FeS complex which presumably shuttles electrons derived from butyrate to the membrane – ultimately leading to the reduction of carbon dioxide to formate (Muller *et al.* 2009). No analogous complex has been experimentally demonstrated in *S. aciditrophicus*. Here, peptides derived from the Syn_02638 gene product were found in bands under all conditions, though no peptides derived from the Etf-α or Etf-β were detected from BN-PAGE. Peptides for ETF-α were detected in an approximately 53 kDa band by SDS-PAGE (SDS-4) from fractions partially purified for Rnf-like activity (Figure 9, Table 8).

The genome of *S. aciditrophicus* also revealed the importance of sodium ion gradients to meet the bioenergetic requirements of the cell. Two predicted methylmalonyl-CoA/oxaloacetate decarboxylases (Syn_00115 and Syn_01431) were detected in the genome of *S. aciditrophicus* (McInerney *et al.* 2007). McInerney and colleagues (2007) raised the possibility that these could interact with glutaconyl-CoA

decarboxylases (Syn_00479-81) and couple the decarboxylation of glutaconyl-CoA to the formation of a sodium ion gradient. This is consistent with the suggestion that *S. aciditrophicus* oxidizes glutaryl-CoA to glutaconyl-CoA without concomitant decarboxylation to crotonyl-CoA (Wischgoll *et al.* 2009). Here, we detected peptides derived from Syn_01431 as well as peptides derived from the glutaconyl-CoA decarboxylase subunits encoded by Syn_00480-81. Additionally, two gene clusters which presumably code for sodium-dependent ATP synthases were detected (Syn_00543-49 and Syn_02101-05) in the genome of *S. aciditrophicus* (McInerney *et al.* 2007). I detected a large number of peptides derived from the genes coding for the ATP synthase, Syn_00543-49, but did not detect any peptides derived from Syn_02101-05 gene products. Taken together, the presence of a sodium-transporting glutaconyl-CoA decarboxylase and a presumably sodium-dependent ATP synthase further support the important role sodium ions play in meeting the overall bioenergetic demands of the cell.

The detection here of peptides associated with glutaconyl-CoA decarboxylase provides further evidence to support the degradation of benzoate by a pathway analogous to that of *T. aromatica.* Interestingly, though, cultures of *S. aciditrophicus* grown in coculture with *Methanospirillum hungatei* were previously shown to convert cyclohex-1-ene carboxylate to methane. In *R. palustris,* cyclohex-1-ene carboxylate is produced via two consecutive two-electron reductions of benzoyl-CoA. These data argued for a possible pathway for benzoate oxidation via a pathway analogous to *R. palustris* (Elshahed *et al.* 2001).

In addition to our above findings, a large number of unique peptides for a hypothetical membrane protein, Syn_03116 were detected from many bands. This protein has no assigned function, but results of a BLAST search revealed two putative domains which are externally oriented. These domains include a domain of 158 peptides with high similarity (41%) to the *Leishmania* S-adenosylhomocysteine hydrolyase and another, smaller domain (35 peptides) with high similarity to a dehydrogenase/reductase domain identified in *Brucella melitensis*. The predicted peptide sequence was submitted to the I-TASSER homology modeling server (Roy *et al.* 2010; Zhang 2007; 2008; 2009). The structure of Syn_03116 appeared similar to the structure of carboxylate ion porin proteins from, for example, *Pseudomonas* species. However, Syn_03116 is predicted to have an NAD^+ binding domain and is predicted to have high structural homology with the aldehyde oxidoreductase of *Desulfovibrio gigas*. Purification and analysis of this protein will further clarify its function. However, based on these findings we suggest this is likely a small molecule transport porin.

Chapter 4: The genome and proteome of *Methanospirillum hungatei* strain JF1: new insights into syntrophic metabolism and biological methane production

Abstract

Methanospirillum hungatei strain JF1 is a hydrogenotrophic methanogen belonging to the order Methanomicrobiales, whose members are commonly encountered in syntrophic associations with fermenting microorganisms. *M. hungatei* has a 3.5 MB circular genome with 3,239 protein-coding genes, 61% of which had an assigned function. *M. hungatei* has genes for five formate dehydrogenases, three membrane-bound hydrogenases, and one F_{420}-reducing hydrogenase, but lacks genes for a F_{420}-nonreducing hydrogenase catalytic subunit. Complete biosynthetic pathways were detected for all amino acids except histidine, and a his-tRNA was not detected. Proteomic analyses showed that *M. hungatei* expressed both hydrogenases and formate dehydrogenases and increased the relative abundance of core methanogenic machinery during syntrophic growth compared to pure culture growth on hydrogen and formate. The relative abundance of peptides associated with energy production and cofactor synthesis increased while those involved in translation decreased in syntrophically grown cells compared to axenically-grown cells. The above data are consistent with a strategy to maximize energy production efficiency and curtail biosynthesis during syntrophic growth.

Introduction

Methane is an important fuel and a potent greenhouse gas. Atmospheric methane concentration has increased since preindustrial times by a factor of 2.5 (Dlugokencky *et al.* 2011) despite large annual variability (Pison *et al.* 2013). Methane production from carbon dioxide occurs in anaerobic ecosystems where lower potential electron acceptors such as sulfate, nitrate, iron, etc. are absent (Achtnich *et al.* 1995). Biologically produced methane accounts for approximately 825 Tg of carbon released to the environment each year (Thauer *et al.* 2008). Methanogenesis occurs in diverse environments such as wetlands, rice paddies, sewage digesters and the intestinal tracts of mammals. The biological formation of methane is catalyzed by a physiologically specialized group of microorganisms, though the process of degrading complex organic material to methane relies on a multifaceted hierarchy of organisms living in close association with methanogens (Thauer *et al.* 2008). In anaerobic food networks, complex organic matter is degraded into simple monomeric compounds and further fermented to carbon dioxide, formate, acetate and hydrogen by primary fermenting bacteria (McInerney *et al.* 2009). A certain portion of the carbon fluxing through anaerobic food webs, however, is degraded to a variety of reduced organic acids and alcohols. These compounds are then utilized by the secondary fermenting microorganisms – generally known as the syntrophic metabolizers – with consequent production of acetate, carbon dioxide, formate and hydrogen. The production of acetate, carbon dioxide, formate and hydrogen by primary and secondary fermenting organisms represents the principle source of methanogenic substrates in anaerobic ecosystems (Crable *et al.* 2011).

In the absence of other electron accepting processes, consumption of formate or hydrogen by hydrogenotrophic methanogens is essential for the oxidation of fatty acids, aromatic acids and alcohols by organisms capable of syntrophy (McInerney *et al.* 2009). In most ecosystems, methanogens must eke out a living at very low hydrogen partial pressures (~10 pascal) or formate concentrations (<10 μM). As a result, the amount of energy available for growth for the methanogen is very low. In syntrophic lactate-degrading communities, total free energy change of -82.8 kJ/mol was observed (Walker *et al.* 2012). However, the free energy is not shared equally between the secondary fermenter and the methanogen and the amount of energy available to the methanogen is much less than that given above (Walker *et al.* 2012). Thus, methanogens live at or near the thermodynamic threshold for life (Walker *et al.* 2012).

The question, then, is what genetic and enzymatic systems allow methanogens to grow and metabolize in syntrophic associations where the free energy changes are close to the thermodynamic threshold for life? The physiological response of *Methanococcus maripaludis* in syntrophic coculture with the lactate oxidizer *Desulfovibrio vulgaris* has received considerable attention (Costa *et al.* 2010; Costa *et al.* 2013; Hendrickson and Leigh 2008; Hendrickson *et al.* 2008; Lupa *et al.* 2008; Walker *et al.* 2012). Transcriptional analysis of *M. maripaludis* showed an increase in transcript abundance for genes encoding core methanogenic machinery in response to syntrophic growth with a parallel decrease in transcript abundance for genes encoding biosynthetic machinery (Walker *et al.* 2012). In addition, there was an increase in transcript abundance for genes encoding enzymes that use H_2 directly rather than reduced deazoflavin (cofactor F_{420}) and this finding was supported by genetic evidence

showing that a F_{420}-dependent dehydrogenase mutant of *M. maripaludis* had improved syntrophic growth. When *Methanothermobacter thermoautotrophicus* was grown with fatty acid-oxidizing syntrophic metabolizers (Enoki *et al.* 2011; Luo *et al.* 2002), differential expression of isozymes of methyl-coenzyme M reductase (Mcr) occurred, and McrI was preferentially expressed during syntrophic growth. Also, a down regulation of biosynthetic enzyme systems consistent with the response of *M. maripaludis* in coculture (Walker *et al.* 2012) was noted. Additionally, Walker *et al* (2012) provided evidence for interspecies alanine transfer (Walker *et al.* 2012).

Methanospirillum hungatei strain JF1, like *M. maripaludis*, belongs to the physiologically described class of hydrogenotrophic methanogens that do not produce cytochromes (Thauer *et al.* 2008). Like *M. maripaludis, M. hungatei* readily partners with a number of secondary-fermenting organisms and catalyzes the terminal electron-accepting processes in many syntrophic associations including butyrate-oxidizing cocultures with *Syntrophomonas wolfei* (McInerney *et al.* 1981), benzoate-oxidizing cocultures with *Syntrophus aciditrophicus* (Elshahed *et al.* 2001) and propionate-oxidizing cocultures with *Syntrophobacter fumaroxidans* (Plugge *et al.* 2012). The butyrate-degrading syntrophic coculture of *S. wolfei* growing with *M. hungatei* has served as a model system to study syntrophic interactions for many years (McInerney *et al.* 1979; Muller *et al.* 2009; Schmidt *et al.* 2013; Sieber *et al.* 2010; Wallrabenstein and Schink 1994; Wofford *et al.* 1986) as it was the first stable fatty acid-oxidizing coculture isolated. In this system, butyrate oxidation is tightly coupled to methanogenesis and the free energy changes are very low (McInerney *et al.* 1981; McInerney *et al.* 2008). Thus, the association of *S. wolfei* with *M. hungatei* is an

excellent model to interrogate the physiological responses of *M. hungatei* to syntrophic growth. Here, I report the sequence and annotation of the *M. hungatei* JF1 genome. In addition, I use semi-quantitative label-free comparative proteomics to elucidate the physiological response of *M. hungatei* JF1 to growth in hydrogen replete pure culture and in syntrophic association with *S. wolfei* degrading either crotonate or butyrate.

Materials and Methods

Cell culture, growth and harvesting

Methanospirillum hungatei strain JF1 (ATCC# 27890) in pure-culture and in coculture with *Syntrophomonas wolfei* ssp. *wolfei* strain Göttingen (ATCC# BAA-1933) were obtained from our culture collection. *M. hungatei* was grown in pure culture in defined basal medium (Tanner 2002) with an 80% H_2:20% CO_2 gas phase as described previously (Beaty *et al.* 1987). *S. wolfei* and *M. hungatei* cocultures were grown in the above defined basal medium with either crotonate (20 mM) or butyrate (20 mM) as carbon sources. Cocultures were grown in 500-ml sealed glass bottles with 250-ml of medium (Beaty *et al.* 1987). The bottles were inoculated with 50 ml of *S. wolfei-M. hungatei* coculture grown in the same medium. Cocultures were transferred three times before proteomic analysis. All cultures were incubated at 37^{o}C and growth was monitored via OD_{600} readings at pre-defined time points. Substrate utilization was monitored via high-pressure liquid chromatography ((Beaty *et al.* 1987; Sieber *et al.* 2013). Cocultures were harvested at 50-70% substrate utilization. Cells were harvested via centrifugation at 4^{o}C and washed twice with 50 mM potassium phosphate buffer (pH 7.2). Cells of *M. hungatei* were separated from *S. wolfei* in sealed anaerobic tubes

at 20,000 • *g* in a 5:4 ratio of standard isotonic Percoll to 50 mM potassium phosphate (pH 7.2) (Beaty *et al.* 1987).

Genome sequencing

Pure cultures of *M. hungatei* were grown as described above and high molecular weight genomic DNA was isolated from cell pellets using the CTAB method described by JGI at http://www.jgi.doe.gov. Genomic DNA was sequenced at the Joint Genome Institute (JGI) using a combination of 3 kb, 8 kb and 40 kb Sanger shotgun DNA libraries. All general aspects of library construction and sequencing performed at the JGI can be found at http://www.jgi.doe.gov. The Phred/Phrap/Consed software package (http://www.phrap.com) was used to assemble all three libraries and to assess quality (Ewing and Green 1998; Ewing *et al.* 1998; Gordon *et al.* 1998). Possible misassemblies were corrected, and gaps between contigs were closed by editing in Consed, custom primer walks or PCR amplification (Roche Applied Science, Indianapolis, IN). The error rate of the completed genome sequence of *M. hungatei* is less than 1 in 50,000. Pair-wise graphical alignments of whole genome assemblies (e.g. synteny plots) were generated using the MUMmer system (Delcher *et al.* 1999; Delcher *et al.* 1999). The sequence of *M. hungatei* can be accessed using the GenBank Accession No. NC_007796.

Proteomic Sample Preparation

Duplicate cell pellets of the *M. hungatei* pure culture grown as above were prepared separately for shotgun proteomics analysis, generally following a protocol optimized for measurements on small bacterial samples (Thompson *et al.* 2008). Cell

pellets were lysed and proteins denatured by incubating each cell pellet overnight at 37^{o}C in 100 µL of 6 M guanidine and 10 mM dithiothreitol (DTT). Lysates were cooled to ambient temperature, and diluted with 50 mM tris(hydroxymethyl)aminomethane, 10 mM calcium chloride to decrease the guanidine concentration to ~ 1M. Ten micrograms of trypsin (sequencing grade, Promega, Madison WI) were added to each lysate, followed by a 5-hour incubation at 37^{o}C. An additional 10 µg of trypsin was added, followed by a further overnight incubation at 37^{o}C. Remaining disulfide bonds were reduced by adding additional DTT to a final concentration of 10 mM and incubation for 1 hour at 37^{o}C. Desalting was performed using reverse-phase solid-phase extraction cartridges (Sep-Pak Lite C18, Waters, Milford MA), with final elution using 0.1% formic acid in acetonitrile. Solvent transfer to aqueous 0.1% formic acid was performed by vacuum centrifugation, with final volume adjusted to 150 µL. Particulates and remaining cellular debris were removed by centrifugation through 0.45 µm pore filters (Ultrafree-MC, Millipore, Billerica MA). Samples were frozen at -80^{o}C until further use.

Duplicate cell pellets of Percoll-separated *M. hungatei* from cocultures with *S. wolfei*, as described above, were prepared for proteomics analysis using an SDS-based lysis protocol (Giannone *et al.* 2011). Pellets were suspended in 150 µL lysis buffer (4% SDS in 100 mM Tris-HCL, pH 8.0) and boiled for 5 min. Suspensions were sonicated (10 sec on/off cycles at 10% power for a total of 2 min; Branson ultrasonic disruptor) in a water bath. Samples were boiled for an additional 5 minutes, and centrifuged (10 minutes, 21000g) to provide a clear supernatant. Supernatants were adjusted to 20% trichloroacetic acid, vortexed, and placed at -80^{o}C for ~1.5 hr to

precipitate protein. Samples were thawed on ice and centrifuged (15 min, 21,000 • *g*, 4^{o}C). Pellets were washed twice with 500 µL cold acetone, centrifuging (5 min, 21,000 • *g*) after each wash. Residual acetone was removed in a centrifugal vacuum concentrator (SpeedVac). Pellets were suspended in 100 µL of 8M urea, 100 mM Tris-HCl for 20 min, followed by sonication (5 sec on, 10 sec off, at 10% power for a total of 2 min) in an ice water bath. Proteins were denatured by addition of DTT to 10 mM and incubation at ambient temperature for 45 min, and cysteines were carbamidomethylated by incubation with iodoacetamide at 20 mM in the dark for 45 min. Proteins were digested by adding 1 µg trypsin in 1 volume of a solution containing 100 mM Tris-HCl and 10 mM calcium chloride (pH 8.0) to 1 volume of sample and incubating at ambient temperature overnight. The same amount of trypsin was added again for an additional 4-hour digestion. Twenty microliters of a solution containing 4M NaCl and 2% formic acid in water were added to each digest, followed by filtration through a 10 kDa molecular weight cutoff filter.

LC-MS-MS Analysis

Tryptic peptide mixtures were analyzed by two-dimensional liquid chromatography/tandem mass spectrometry (2D LC-MS/MS), using the MudPIT approach (Washburn *et al.* 2001; Wolters *et al.* 2001) implemented as previously described in further detail (Hervey *et al.* 2007). Two LC-MS/MS analyses were performed on the tryptic digest from each cell pellet (2 biological replicates • 2 technical replicates). Aliquots (50 µL for *M. hungatei* pure culture; 100 µl for

cocultures) were loaded via a pressure cell (New Objective, Woburn MA) onto a "back" column fabricated from 150 µm (internal diameter) fused silica tubing (Polymicro Technologies, Phoenix AZ) packed with a ~4 cm long bed of reverse-phase chromatographic phase (Jupiter C18, 3µm particle size, Phenomenex, Torrance CA) upstream of a ~4 cm bed of strong cation exchange material (5µm particle size SCX, Phenomenex). Back columns for coculture samples were additionally desalted by flowing 95% H_2O, 5% acetonitrile, 0.1% formic acid (solvent A) at ~0.5 µL/min for 2 minutes followed by a linear gradient lasting 22 min to 30% H_2O, 70% acetonitrile, 0.1% formic acid, followed by re-equilibration in solvent A.

After sample loading, the back column was attached via a filter union (Upchurch Scientific, Oak Harbor WA) to a "front" analytical column fabricated from a 100 µm (internal diameter) PicoTip Emitter (New Objective), packed with a ~14 cm bed of reverse-phase material (Jupiter C18, 3 µm particle size, Phenomenex). Two-dimensional LC was performed via twelve step gradients of increasing salt (ammonium acetate) concentration, with the eluted peptides from each strong cation exchange step subsequently resolved via a separate reverse-phase gradient (Ultimate HPLC, LCPackings/Dionex, Sunnyvale CA). The LC eluent was interfaced via a nanospray source (Proxeon, Odense, Denmark) with a linear-geometry quadrupole ion trap mass spectrometer (LTQ for *M. hungatei* pure cultures, LTQ-XL for cocultures; ThermoFinnigan, San Jose CA). Data acquisition was performed in data-dependent mode under the control of XCalibur software. Up to 5 tandem mass spectra were acquired from the most abundant parent ions in full-scan mass spectra; dynamic

exclusion was enabled with a repeat count of 1, repeat duration of 60 seconds, and exclusion duration of 180 seconds.

Proteomics Data Analysis

Peptide identifications were obtained from tandem mass spectra using Sequest software (version 27) (Eng *et al.* 1994), and protein identifications were compiled from peptide identifications using DTASelect (version 1.9) (Tabb *et al.* 2002). A multiple-species protein FASTA file was constructed from individual FASTA files for *Syntrophomonas wolfei wolfei* Göttingen (NC_008346), *Methanospirillum hungatei* JF1 (NC_007796), and *Syntrophus aciditrophicus* SB (NC_007759), all downloaded from the DOE Joint Genome Institute website. The sequence-reversed analog of each protein sequence was appended to the FASTA file to allow estimation of the false discovery rate of peptide identification (Elias *et al.* 2007; Moore *et al.* 2002). Sequences of 36 common contaminant proteins were also appended to the FASTA file. Peptide identifications were retained for XCorr $\geq$1.8 (z=1), $\geq$2.5 (z=2), or $\geq$3.5 (z=3), with DeltaCN $\geq$0.08. Cysteine carbamidomethylation was specified as a static modification for cells grown as cocultures. Protein identifications required identification of two peptides. The false discovery rate for peptides was generally $\leq$1%.

Spectrum count values were adjusted to prevent duplicate contributions from tryptic peptides associated with more than one protein (Zhang *et al.* 2010). Estimates of protein abundance were calculated using normalized spectral abundance factors (NSAF) (Zybailov *et al.* 2006). To correct for the presence of protein from non-target organisms, such as *S. wolfei* and *S. aciditrophicus*, the NSAF values were corrected

such that the sum of NSAF values for peptides detected from the target organism equaled a value of 1.

NMDS

Nonmetric multidimensional scaling (NMDS) was performed with R (V. 2.15.0, R Development Core Team (2012)) in the Vegan package (Ver. 2.0-6 (Oksanen *et al.* 2007)). Before calculation of the dissimilarity matrix, proteins represented in less than two of the replicates were considered spurious and were replaced by zero. NMDS was calculated using the metaMDS() function with autotransformation flagged and Bray-Curtis dissimilarities. Because of the large disparity in protein abundances, protein abundance was square root transformed then a Wisconsin standardization was performed, which consists of dividing protein abundance by the maxima then standardizing for each replicate.

Results

General Overview:

Methanospirillum hungatei strain JF1 is a Gram-negative staining methanogen from the order Methanomicrobiales with a G+C content of 45.15%. A total of 3,239 putative protein-coding genes greater than 200 nucleotides in length were detected in the 3.5 Mb circular chromosome (Table 9). Approximately 86% of nucleotides are

Table 9: General features of *M. hungatei* strain JF1 genome

Category	Amount
DNA Total	3,544,738 bp
Coding DNA	306,474,743 bp (86.46%)
G+C Content	1,600,415 bp (45.15%)
DNA Scaffolds	1
Genes total number	3,307
Genes protein coding	3,239 (97.94%)
RNA genes	68
rRNA genes	
5S rRNA	6
16S rRNA	4
23S rRNA	4
tRNA	51
Genes with function prediction	2,108 (61.02%)
Genes without function prediction	1,221 (36.92%)

in putative protein-coding regions. A total of 68 RNA genes were detected including six 5S rRNA, four 16S rRNA, four 23S rRNA and 51 tRNA genes. Forty-three of the 51 tRNA genes have an identified function, which cover all amino acids except His. A total of 8 pseudo-tRNA genes without an identified function were detected. It is probable that one of these pseudo-tRNA genes encodes a tRNA for incorporation of pyrrolysine.

Of particular interest is the lack of a gene encoding His-tRNA. The histidine biosynthesis pathway from pyruvate is present with the exception that a gene for histidinol phosphate phosphatase (HisN) was not detected (see biosynthesis). Greater than 2% of detected codons are predicted to code for histidine (Table 10) and histidine

Table 10: Amino acid incorporation in *M. hungatei* strain JF1. Percent totals represent percent of codons theoretically coding for the indicated amino acid relative to the total number of amino acids coded across the genome.

Amino Acid	Total predicted	Percentage of total AA
Leucine	95375	9.19%
Isoleucine	88700	8.54%
Glycine	75848	7.31%
Alanine	72066	6.94%
Glutamate	70344	6.78%
Serine	69641	6.71%
Valine	67712	6.52%
Threonine	59922	5.77%
Aspartate	59872	5.77%
Arginine	54023	5.20%
Lysine	52557	5.06%
Proline	48440	4.67%
Phenylalanine	41577	4.00%
Asparagine	37627	3.62%
Tyrosine	35842	3.45%
Glutamine	33158	3.19%
Methionine	27287	2.63%
Histidine	22954	2.21%
Cysteine	14307	1.38%
Tryptophan	11004	1.06%

was previously determined to be present at 0.66 % by mol (Patel *et al.* 1986) in the *M. hungatei* sheath. These data suggest that *M. hungatei* has a novel mechanism for His incorporation and this necessary role is likely fulfilled by one of the eight pseudo-tRNAs detected. Additionally, *M. hungatei* must possess a novel mechanism, as yet not described, for fulfilling the role of histidinol phosphate phosphatase.

Peptides derived from a total of 1,417 unique proteins were detected in the proteome of *M. hungatei*. Genes encoding the detected peptides were distributed evenly around the chromosome regardless of the growth condition (Figure 10). I did not

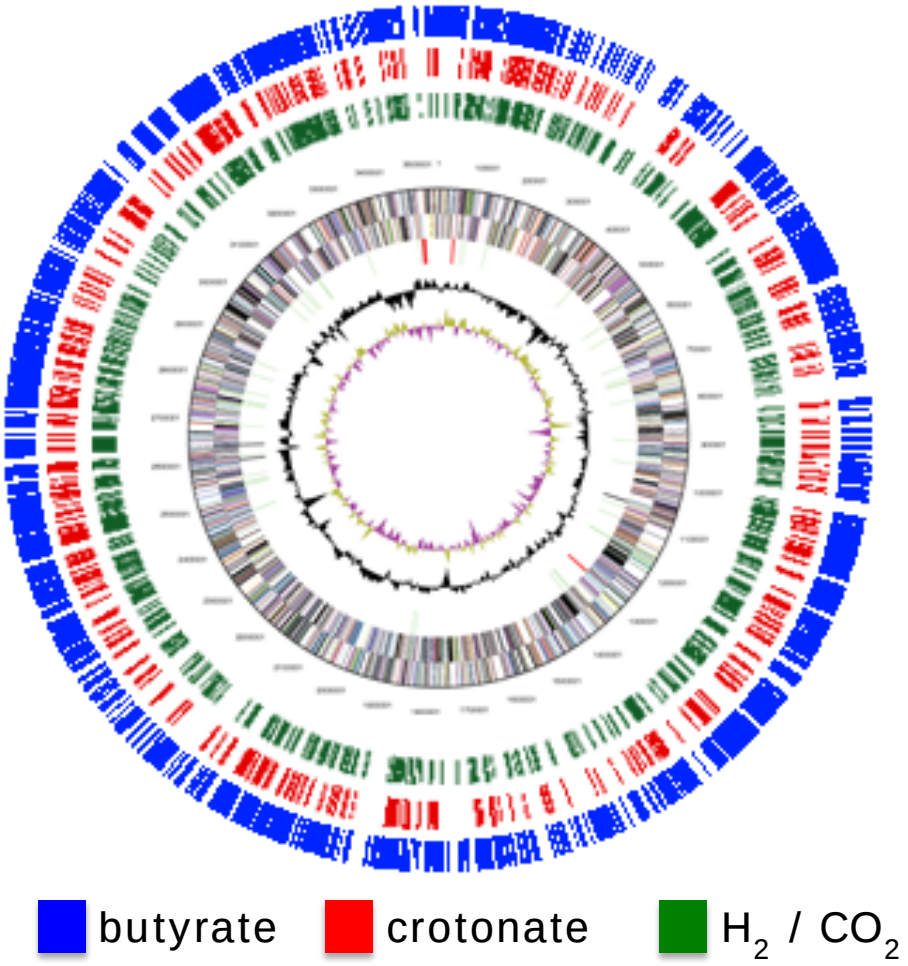

Figure 10: Circular chromosome of *M. hungatei* JF1 with detected peptides shown. A total of 1,417 unique peptides were detected (see text) across the three growth conditions. 843 peptides were detected in JF1 cells from butyrate-oxidizing coculture (blue), 204 were detected in JF1 cells from crotonate-oxidizing coculture (red) and 318 were detected in JF1 cells grown in pure culture on H_2:CO_2 (green).

detect a region of the chromosome where proteins specifically related to syntrophy were expressed. A total of 884 peptides were detected in at least three of the four replicates for a given growth condition. All further analyses are with this class of detected peptides.

Nonmetric multidimensional scaling (NMDS) ordination showed that the *M. hungatei* protein abundance pattern was highly reproducible between the two biological replicates when *M. hungatei* was grown in pure culture and in coculture with *S. wolfei* on butyrate (Figure 11). The protein abundance pattern differed between the two

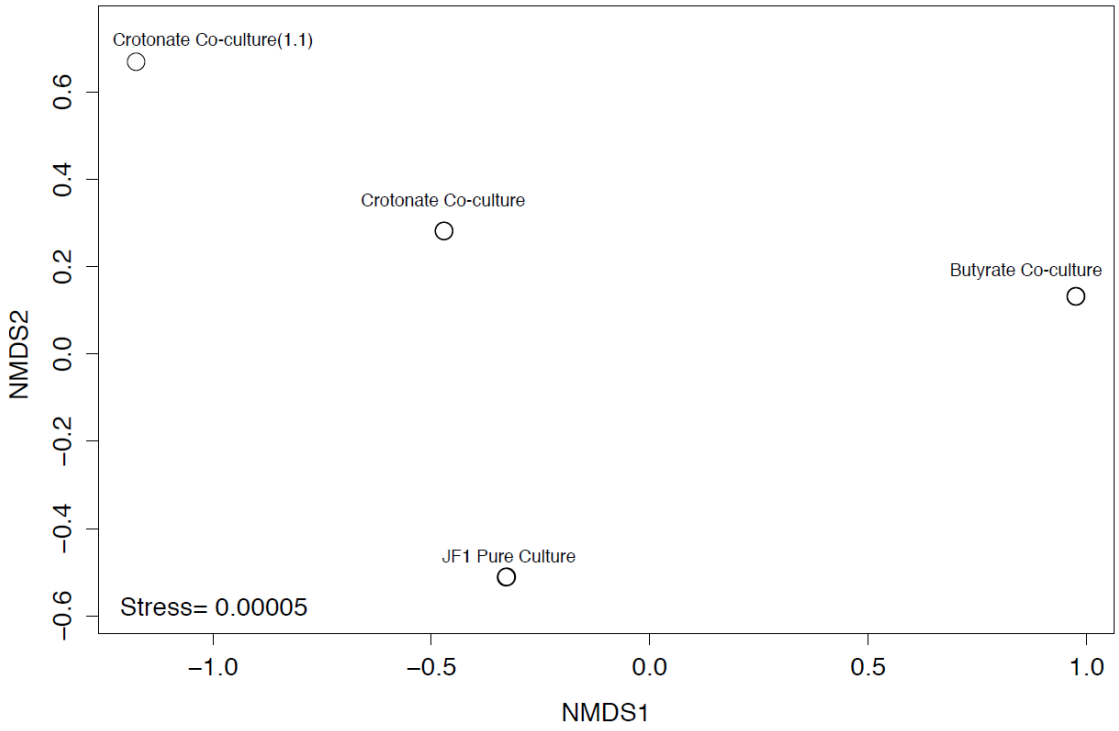

Figure 11: NMDS ordination plot of detected peptides detected in *M. hungatei* JF1 under three growth conditions. Clustering of duplicate samples was extremely tight and nearly overlaps in ordination space.

biological replicates when *M. hungatei* was grown in coculture with *S. wolfei* on crotonate, although each abundance pattern differed from that obtained with the two other growth conditions (Figure 11).

One hundred thirty-two of the detected proteins were shared across all three growth conditions. I detected a total of 316 proteins from cells grown in pure culture on H_2/CO_2 and 40 of these were unique to this growth condition (Figure 12). One peptide

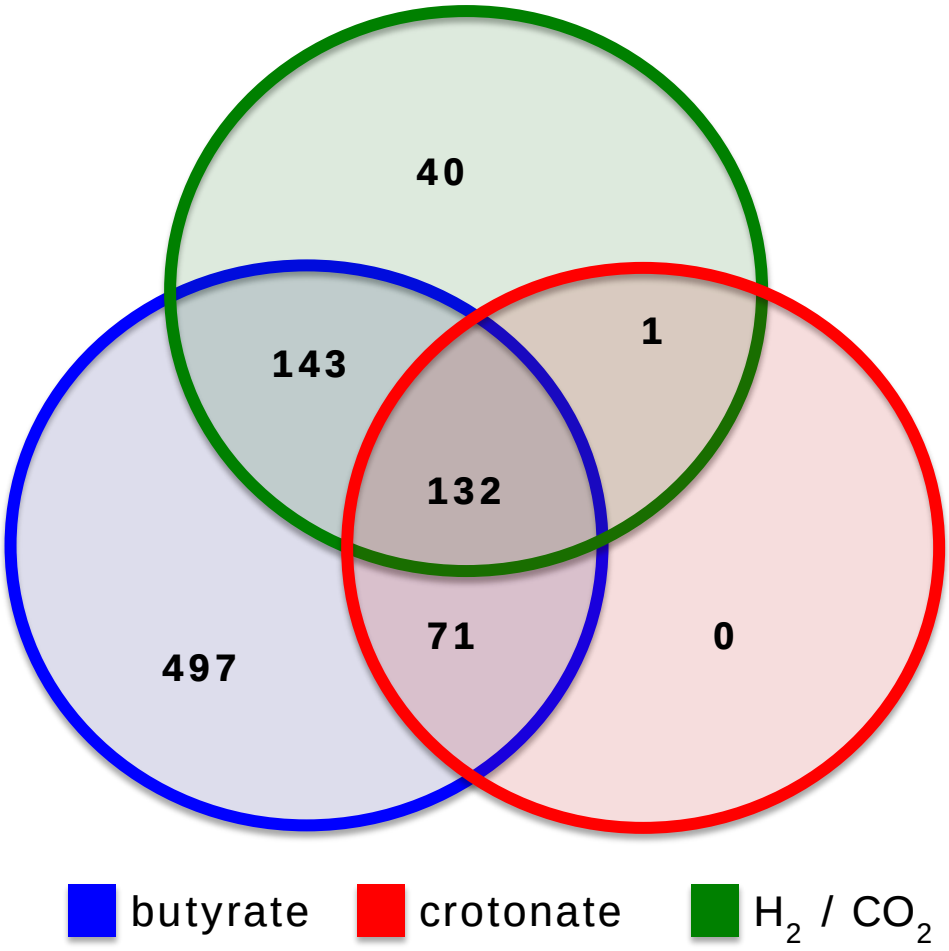

Figure 12: Distribution of proteins detected from *M. hungatei*. Cells were grown in butyrate-oxidizing coculture (blue), crotonate oxidizing coculture (red) and from pure culture growth on H_2:CO_2 (green). A total of 132 peptides were detected in all three conditions while 71 were unique to coculture conditions. 497 peptides were detected only during growth on butyrate – though many more peptides were detected in general from this condition than others.

detected from cells grown in pure culture was also detected in *M. hungatei* cells obtained from the crotonate coculture; 143 peptides detected from cells grown in pure culture were likewise detected in *M. hungatei* cells obtained from the butyrate coculture. A total of 204 peptides were detected in *M. hungatei* cells obtained from the crotonate coculture and none of these were unique to this growth condition (Figure 12). Seventy-one of the peptides detected in cells obtained from crotonate cocultures were also detected in cells obtained from the butyrate coculture (Figure 12). A total of 843 peptides were detected in *M. hungatei* cells obtained from the butyrate coculture with 497 of these peptides being unique to this condition (Figure 12).

The detected peptides were binned according to cluster of orthologous groups (COGs) and the relative abundance of peptides in each COG category (based on total NSAF signal) for each growth condition was determined (Figure 13 and Table 11). A

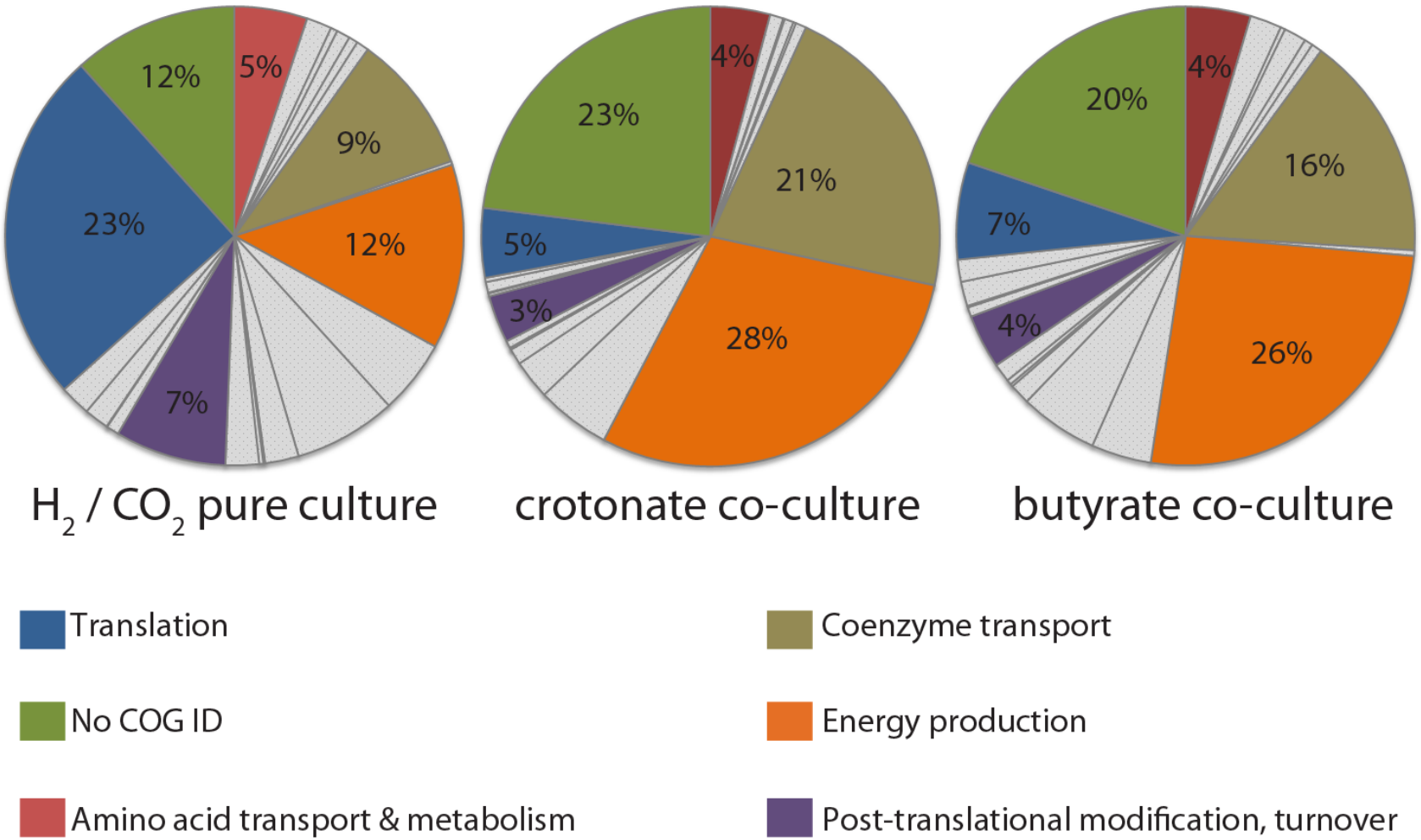
12%
5%
9%
23%
12%
7%
23%
4%
21%
5%
3%
28%
20%
4%
16%
7%
4%
26%
H2 / CO2 pure culture
crotonate co-culture
butyrate co-culture
Translation
Coenzyme transport
No COG ID
Energy production
Amino acid transport & metabolism
Post-translational modification, turnover

Figure 13: COG distribution of peptides detected from *M. hungatei* whole cell proteome. Less signal (and consequently fewer peptides) were associated with translation (blue) during coculture growth relative to pure culture growth. Relative to pure culture, signal intensity increased for peptides associated with coenzyme transport and energy production (tan and orange respectively). Interestingly, 20% of peptide signal or more detected during growth in coculture was from unannotated peptides while only 12% of signal was from unannotated peptides during pure culture growth.

Table 11: Distribution of proteins detected from *M. hungatei* by functional category. Percent values represent the percent of signal attributable to individual COG category for peptides with a COG category assignment. Columns do not add to 100% because some proteins may have more than on COG assignment and some proteins may have no COG assignment.

Cog Category	H_2 / CO_2	Crotonate	Butyrate
Amino Acid Transport & Metabolism	4.80%	4.06%	4.49%
Carbohydrate Transport & Metabolism	1.67%	0.92%	2.19%
Cell Cycle Control, Division	0.45%	0.10%	0.32%
Cell Motility	0.89%	0.63%	1.54%
Cell Wall, Envelope & Membrane Biogenesis	0.60%	0.18%	0.59%
Chromatin Structure & Dynamics	0.83%	0.73%	0.72%
Coenzyme Transport & Metabolism	9.17%	20.92%	15.62%
Defense Mechanisms	0.23%	0.00%	0.39%
Energy Production	12.17%	28.35%	25.51%
Function Unknown	4.87%	5.05%	4.15%
General Function Preduction	6.76%	2.68%	5.40%
Inorganic Ion Transport & Metabolism	2.21%	1.10%	1.42%
Intracellular Trafficking, Secretion & Vesicular Transport	0.12%	0.06%	0.18%
Lipid Transport & Metabolism	0.28%	0.08%	0.34%

Nucleotide Transport & Metabolism	2.19%	0.50%	1.28%
Post-translational modification & Protein Turnover	7.33%	3.24%	3.74%
Replication, Recombination & Repair	0.83%	0.20%	0.66%
Secondary Metabolite Biosynthesis	0.05%	0.06%	0.11%
Signal Transduction	1.62%	0.72%	1.69%
Transcription	2.04%	0.29%	1.52%
Translation	23.32%	4.74%	6.70%

marked difference between the three growth conditions was observed for several COG categories. For example, *M. hungatei* peptides associated with coenzyme transport increased from approximately 9% of the total proteome in pure-culture-grown cells to 21% and 16% in *M. hungatei* cells from crotonate-oxidizing and butyrate-oxidizing coculture conditions, respectively (Figure 13 and Table 11). Similarly, energy production associated peptides increased from 12% in the total proteome in pure-culture-grown cells to approximately 28% and 26% of the total proteome in *M. hungatei* cells from crotonate- and butyrate-oxidizing conditions, respectively (Figure 13 and Table 11). The increase in the percentage of peptides associated with energy production and cofactor synthesis in the proteome of cells grown in partnership with *S. wolfei* may be a consequence of the down-regulation of proteins involved in translation as the percentage of peptides in the total proteome associated with translation decreased in *M. hungatei* cells obtained from cocultures relative to that from pure-culture (Figure 13 and Table 11). This observation is not unexpected given the slow growth rates for *S. wolfei* and *M. hungatei* cocultures (Robinson and Tiedje 1984).

Methane metabolism

Methanogenesis is the only known metabolic pathway by which the methanarchaea generate energy for use in biosynthesis (Thauer *et al.* 2008). In methanogens lacking cytochromes, reduction of the CoM-S-S-CoB heterodisulfide has been shown to be linked with ferredoxin reduction via an electron bifurcating enzyme complex. This enzyme complex is composed of a formyl methanofuran dehydrogenase,

heterodisulfide reductase and either a F_{420} non-reducing hydrogenase or formate dehydrogenase (Costa *et al.* 2010). This is the currently accepted model for the production of reduced ferredoxin in methanarchaea which lack cytochromes. Interestingly, the genetic evidence from *M. hungatei* does not support this model as no genes coding a F_{420} non-reducing hydrogenase were detected in the genome (Anderson *et al.* 2009).

The *M. hungatei* genome encodes the full suite of proteins necessary to carry out hydrogenotrophic methanogenesis and peptides for these enzymes were detected under all growth conditions (Figure 14 and Table 12). Several gene clusters were detected

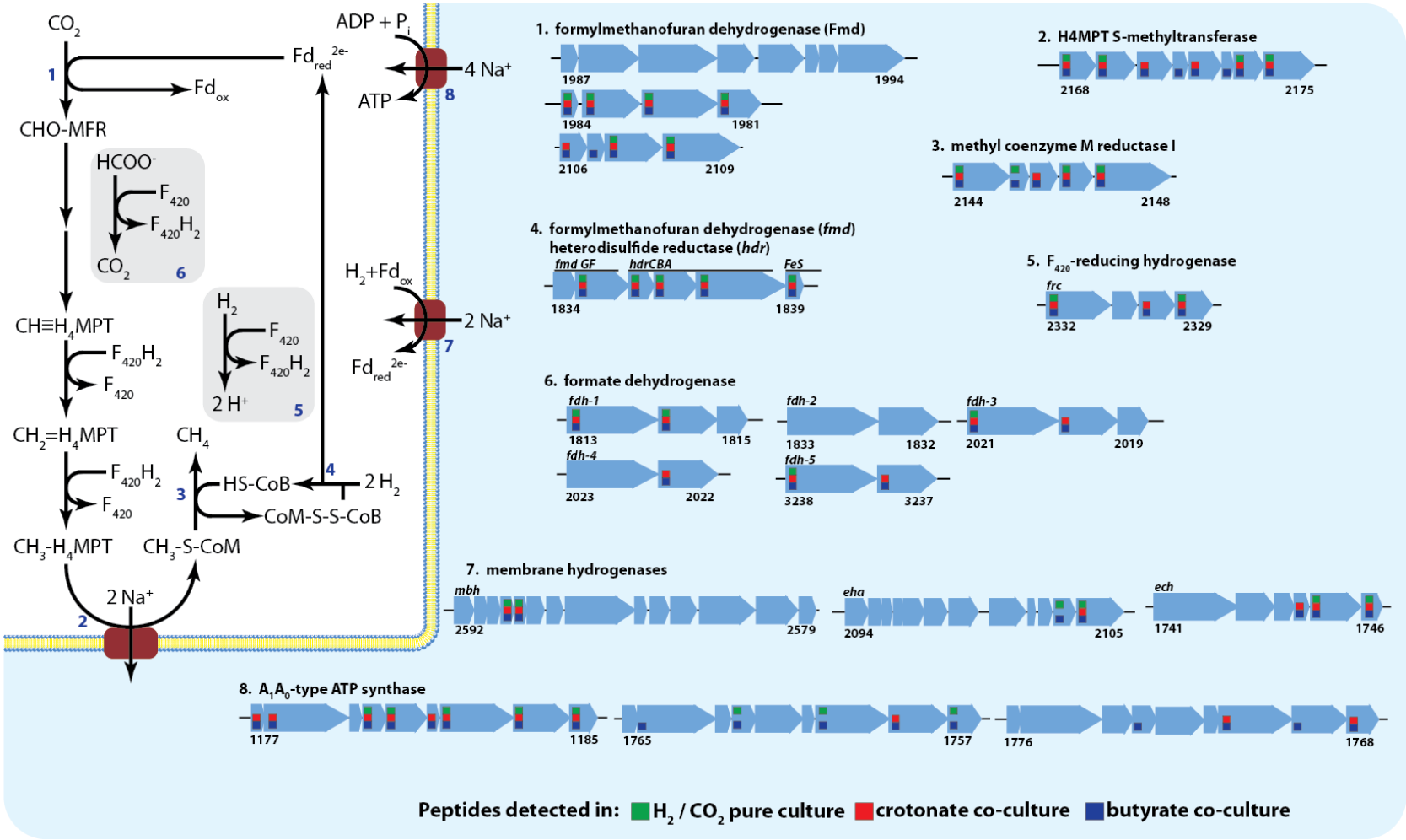
CO2
1
Fdred2e-
Fdox
ADP + Pi
4 Na+
ATP
8
CHO-MFR
HCOO-
F420
F420H2
CO2
6
H2
F420
F420H2
2 H+
5
H2+Fdox
2 Na+
7
Fdred2e-
CH≡H4MPT
F420H2
F420
CH2=H4MPT
CH4
F420H2
F420
3
HS-CoB
4
2 H2
CoM-S-S-CoB
CH3-H4MPT
CH3-S-CoM
2 Na+
2
1. formylmethanofuran dehydrogenase (Fmd)
1987
1994
1984
1981
2106
2109
2. H4MPT S-methyltransferase
2168
2175
3. methyl coenzyme M reductase I
2144
2148
4. formylmethanofuran dehydrogenase (fmd) heterodisulfide reductase (hdr)
fmd GF
hdrCBA
FeS
1834
1839
5. F420-reducing hydrogenase
frc
2332
2329
6. formate dehydrogenase
fdh-1
1813
1815
fdh-2
1833
1832
fdh-3
2021
2019
fdh-4
2023
2022
fdh-5
3238
3237
7. membrane hydrogenases
mbh
2592
2579
eha
2094
2105
ech
1741
1746
8. A1A0-type ATP synthase
1177
1185
1765
1757
1776
1768
Peptides detected in: H2 / CO2 pure culture
crotonate co-culture
butyrate co-culture

Figure 14: Pathway for hydrogenotrophic methanogenesis and genes detected in *M. hungatei* JF1 genome. *M. hungatei* JF1 lacks cytochromes and, unlike other non-cytochrome-containing methanogens, lacks a catalytic F_{420}-nonreducing hydrogenase subunit. Peptides detected in pure culture (green), crotonate grown coculture (red) and butyrate grown coculture (blue) are indicated. Detection indicates peptides were detected in at least three of four replicates from that particular condition.

Table 12: Core methanogenesis proteins detected from *M. hungatei*. Percent values represent percent of total normalized spectral abundance factors (NSAF) values prior to eliminating peptides detected in less than three replicates.

			Corrected NSAF values (expressed in %)					
			H_2/CO_2		Crotonate		Butyrate	
Gene ID	**Locus**	**Gene Product Name**	**Avg**	**SD**	**Avg**	**SD**	**Avg**	**St. Dev**
637897454	Mhun_1835	formylmethanofuran dehydrogenase, subunit F	0.45%	0.16%	0.88%	0.19%	0.65%	0.08%
637897455	Mhun_1836	CoB--CoM heterodisulfide reductase subunit C	1.93%	1.17%	0.56%	0.42%	0.51%	0.03%
637897456	Mhun_1837	CoB--CoM heterodisulfide reductase subunit B	0.19%	0.05%	0.68%	0.19%	0.62%	0.05%
637897457	Mhun_1838	CoB--CoM heterodisulfide reductase subunit A	0.66%	0.18%	1.08%	0.11%	0.90%	0.14%
637897458	Mhun_1839	F420-non-reducing hydrogenase subunit D	0.21%	0.16%	0.15%	0.14%	0.40%	0.08%
637897590	Mhun_1981	formylmethanofuran dehydrogenase, subunit C	0.23%	0.04%	0.42%	0.10%	0.53%	0.05%
637897591	Mhun_1982	formylmethanofuran dehydrogenase, subunit A	0.26%	0.05%	0.30%	0.10%	0.34%	0.06%
637897592	Mhun_1983	formylmethanofuran dehydrogenase, subunit B	0.12%	0.05%	0.22%	0.08%	0.36%	0.04%
637897593	Mhun_1984	formylmethanofuran dehydrogenase, subunit D	0.19%	0.08%	0.29%	0.20%	0.39%	0.12%
637897712	Mhun_2106	formylmethanofuran dehydrogenase, subunit G	ND	--	0.02%	0.03%	0.04%	0.03%
637897713	Mhun_2107	formylmethanofuran dehydrogenase, subunit D	ND	--	ND	--	0.06%	0.02%
637897714	Mhun_2108	formylmethanofuran dehydrogenase, subunit B	0.03%	0.03%	0.08%	0.02%	0.07%	0.01%
637897715	Mhun_2109	formylmethanofuran dehydrogenase, subunit A	0.02%	0.02%	0.02%	0.03%	0.06%	0.01%
637897749	Mhun_2144	methyl-coenzyme M reductase, beta subunit	0.55%	0.16%	6.49%	2.56%	3.10%	0.17%
637897750	Mhun_2145	Methyl-coenzyme M reductase, protein D	0.08%	0.09%	ND	--	0.16%	0.04%
637897751	Mhun_2146	Methyl-coenzyme M reductase operon protein C	ND	--	0.02%	0.03%	0.03%	0.02%

637897752	Mhun_2147	methyl-coenzyme M reductase, gamma subunit	3.24%	1.37%	5.99%	0.75%	2.55%	0.24%
637897753	Mhun_2148	methyl-coenzyme M reductase, alpha subunit	1.43%	0.20%	3.11%	0.63%	1.67%	0.19%
637897772	Mhun_2168	tetrahydromethanopterin S-methyltransferase, subunit E	0.01%	0.02%	0.13%	0.12%	0.11%	0.04%
637897773	Mhun_2169	tetrahydromethanopterin S-methyltransferase, subunit D	0.10%	0.08%	0.11%	0.15%	0.04%	0.03%
637897774	Mhun_2170	tetrahydromethanopterin S-methyltransferase, subunit C	ND	--	0.16%	0.18%	0.20%	0.02%
637897775	Mhun_2171	tetrahydromethanopterin S-methyltransferase, subunit B	ND	--	ND	--	0.55%	0.23%
637897776	Mhun_2172	tetrahydromethanopterin S-methyltransferase, subunit A	ND	--	1.13%	0.43%	0.86%	0.48%
637897777	Mhun_2173	tetrahydromethanopterin S-methyltransferase, subunit F	ND	--	ND	--	0.26%	0.05%
637897779	Mhun_2175	tetrahydromethanopterin S-methyltransferase, subunit H	0.34%	0.11%	2.13%	0.22%	1.67%	0.19%

which encode putative subunits of formyl-methanofuran (MFR) dehydrogenase (Fmd). Fmd is a six-subunit molybdopterin-containing complex, which catalyzes the endergonic reduction of CO_2 to formyl-MFR (Thauer *et al.* 2008). Genes coding for several duplicate Fmd subunits were detected between locus tag Mhun_1981 and Mhun_1994 including two *fmdA* genes (Mhun_1982, 1989), three *fmdB* genes (Mhun_1983, 1988, 1994), two *fmdC* genes (Mhun_1981, 1990), three *fmdD* genes (Mhun_1984, 1987, 1993), and one *fmdE* gene (Mhun_1985). No Fmd-F or Fmd-G subunits were detected within this region. Another apparent *fmd* operon, containing *fmd*GDBAC genes, was also detected (Mhun_2106-2109, 2112). Several *fmd* genes were detected elsewhere on the chromosome, including *fmdE* (Mhun_250, 1329, 2004, 2082), *fmdG* (Mhun_1834, 1972, and *fmdF* (Mhun_1835).

The next step in the pathway is catalyzed by formyl-MFR:tetrahydromethanopterin (H_4MPT) formyl transferase (Ftr) encoded by Mhun_1808. The *M. hungatei* genome has three genes encoding methenyl-H_4MPT cyclohydrolase (Mhun_2384, 0444, 0022), one gene encoding methylene-H_4MPT dehydrogenase (Mhun_2255), and one gene encoding methylene-H_4MPT reductase (Mhun_2257). One operon encoding genes for H_4MPT S-methyltransferase (Mtr) was detected, which contains two genes for *mtrA* (Mhun_2172, 2174) and one gene each for the remaining *mtr* genes, *mtrBCDEFH* (Mhun_2171, 2170, 2169, 2168, 2173, 2175 respectively). The *M. hungatei* genome contains genes for methyl-CoM reductase (Mcr) type I (*mcr*BDCGA encoded by Mhun_2144-2148, respectively) isozyme. A second Mcr isozyme, McrII, has been identified, and in methanogens that contain both Mcr isozymes, type McrI is the one detected when the methanogen grows syntrophically

(Enoki *et al.* 2011). The presence of only the type I Mcr in *M. hungatei* is consistent with its function as a syntrophic specialist.

Proteomic analysis detected peptides corresponding to various subunits of methane production enzymes under all three growth conditions (Table 12). Fmd peptides (FmdCABD), encoded by Mhun_1981-1984, respectively, were abundant and detected under all growth conditions (Table 12). FmdG (Mhun_2106 gene product) was detected only in cells obtained from crotonate- and butyrate-grown cocultures (Table 13). Ftr (Mhun_1808 gene product), MtrH (Mhun_2175 gene product), McrB (Mhun_2144 gene product) and the methylene-H_4MPT dehydrogenase (Mhun_2255 gene product) had 4-fold or greater increases in relative abundance (higher NSAF signal) in cells from butyrate-grown cocultures compared to pure culture-grown cells (Table 14). In addition, MtrB and MtrF were only detected in cells obtained from butyrate-grown cocultures (Table 13). Other investigators have observed increases in various enzymes in the methane production pathway during syntrophic growth (Walker *et al.* 2012). This phenomenon is consistent with the need to maximize energy production under thermodynamically limited energy conditions involved in syntrophic growth.

Table 13: Core methanogenesis proteins detected from *M. hungatei* only during growth butyrate-oxidizing coculture. Percent values represent percent of total normalized spectral abundance factors (NSAF) values prior to eliminating peptides detected in less than three replicates.

			Corrected NSAF values (expressed in %)					
			H_2 / CO_2		Crotonate		Butyrate	
Gene ID	**Locus**	**Gene Product Name**	**Avg**	**SD**	**Avg**	**SD**	**Avg**	**St. Dev**
637897713	Mhun_2107	formylmethanofuran dehydrogenase, subunit D	ND	--	ND	--	0.06%	0.02%
637897775	Mhun_2171	tetrahydromethanopterin S-methyltransferase, subunit B	ND	--	ND	--	0.55%	0.23%
637897777	Mhun_2173	tetrahydromethanopterin S-methyltransferase, subunit F	ND	--	ND	--	0.26%	0.05%

Table 14: Peptides detected from *M. hungatei* showing a greater than a Log_2 change of 2 increase in relative abundance in cultures from butyrate-oxidizing conditions. Values calculated using percent values of NSAF attributable to *M. hungatei* prior to eliminating peptides detected in less than three replicates.

Gene ID	Locus	Gene Product Name	Log_2 Bt/Cro	Log_2 Bt/Pure	Log_2 Cro/Pure
637898161	Mhun_2549	thermosome subunit	0.00	3.02	3.02
637897433	Mhun_1814	formate dehydrogenase, beta subunit	0.21	2.92	2.72
637896064	Mhun_0423	PKD	1.00	2.90	1.91
637897861	Mhun_2255	methylenetetrahydromethanopterin dehydrogenase	-1.00	2.52	3.52
637897749	Mhun_2144	methyl-coenzyme M reductase, beta subunit	-1.07	2.41	3.48
637897427	Mhun_1808	formylmethanofuran-tetrahydromethanopterin formyltransferase	0.05	2.27	2.22
637895806	Mhun_0154	heat shock protein Hsp20	-0.54	2.24	2.78
637897779	Mhun_2175	tetrahydromethanopterin S-methyltransferase, subunit H	-0.35	2.21	2.56
637896235	Mhun_0597	PKD	0.33	2.04	1.71
637896587	Mhun_0951	methyl-accepting chemotaxis sensory transducer	0.67	2.02	1.35

Hydrogenase and formate dehydrogenase

Genes for four hydrogenases were detected in the *M. hungatei* chromosome (Figure 14), including three membrane-bound hydrogenases, *ech* (energy-conserving hydrogenase), *eha* (energy-conserving hydrogenase A) and *mbh* (membrane-bound hydrogenase), and a cytosolic, F_{420}-reducing hydrogenase (*frc*). *M. hungatei* lacks a F_{420}-nonreducing hydrogenase (*vhu* or *vhc*), making it unlikely that electron bifurcation between CoM-S-S-CoB heterodisulfide and H_2 drives synthesis of reduced ferredoxin from H_2 (Anderson *et al.* 2009; Costa *et al.* 2010; Thauer *et al.* 2008; Worm *et al.* 2011). Anderson et al (Anderson *et al.* 2009) proposed that Methanomicrobiales may use the energy of ion gradients to drive the unfavorable reduction of ferredoxin by H_2 because the genes for *eha* are adjacent to those for formylmethanofuran dehydrogenase (*fmd*) (Anderson *et al.* 2009). Alternatively, Ech, which serves this function in *Methanosarcina barkeri* (Meuer *et al.* 2002), or Mbh could serve this role in *M. hungatei*.

Table 15: Hydrogenase proteins detected from *M. hungatei*. Percent values represent percent of total normalized spectral abundance factors (NSAF) values prior to eliminating peptides detected in less than three replicates.

			Corrected NSAF values (expressed in %)					
			H_2 / CO_2		Crotonate		Butyrate	
Gene ID	**Locus**	**Gene Product Name**	**Avg**	**SD**	**Avg**	**SD**	**Avg**	**St. Dev**
637897365	Mhun_1744	ech hydrogenase subunit D	ND	--	0.06%	0.07%	0.11%	0.06%
637897366	Mhun_1745	ech hydrogenase subunit E	0.24%	0.14%	0.04%	0.05%	0.16%	0.05%
637897367	Mhun_1746	ech hydrogenase subunit F	0.02%	0.05%	0.04%	0.07%	0.23%	0.09%
637897710	Mhun_2104	membrane-bound hydrogenase subunit ehaN	0.17%	0.18%	ND	--	0.07%	0.03%
637897711	Mhun_2105	membrane-bound hydrogenase subunit ehaO	0.09%	0.05%	0.02%	0.03%	0.04%	0.02%
637898199	Mhun_2588	Membrane bound hydrogenase subunit mbhJ	0.02%	0.04%	0.02%	0.05%	0.05%	0.02%
637898200	Mhun_2589	Membrane bound hydrogenase subunit mbhK	0.25%	0.03%	0.01%	0.03%	0.05%	0.01%
637897938	Mhun_2329	coenzyme F420-reducing hydrogenase, beta subunit	0.16%	0.08%	0.61%	0.56%	0.44%	0.10%
637897939	Mhun_2330	coenzyme F420-reducing hydrogenase, gamma subunit	ND	--	3.40%	1.21%	2.78%	0.42%
637897941	Mhun_2332	coenzyme F420-reducing hydrogenase, alpha subunit	0.28%	0.10%	0.97%	0.29%	0.88%	0.09%

Peptides were detected from subunits of all three membrane bound hydrogenases (Ech, Eha and Mbh) under all three growth conditions. (Figure 14; Table 15). EchD and EchF (Mhun_1744 and 1746 gene products) were detected in cells obtained from crotonate- and butyrate-grown cocultures (Table 15). MbhK was more abundant in pure culture growth relative to growth in coculture (Table 15) though this difference was not significant (p=0.23). *ech* and *mbh* transcripts were previously detected during growth on either hydrogen or formate, or when *M. hungatei* was grown in propionate-oxidizing coculture with *Syntrophobacter fumaroxidans;* however, no statistically significant differences in the expression of any of the membrane-bound hydrogenase genes was detected among the different growth conditions (Worm *et al.* 2011).

Peptides corresponding to various subunits of Frc were detected under all three growth conditions (Figure 14; Table 15). The relative abundance of FrcA was 3-fold higher (p=0.0002) in cells obtained from butyrate-oxidizing cocultures and was 3.3-fold higher (p=0.0117) in cells obtained from crotonate-oxidizing cocultures relative to that detected in cells grown in pure culture (Table 14). Additionally, FrcB was 4.7-fold more abundant in cells obtained from crotonate-oxidizing cocultures relative to cells grown in pure culture on H_2 / CO_2, although this difference was not statistically significant. FrcB was 2.6-fold more abundant in cells obtained from butyrate-oxidizing cocultures relative to pure culture-grown cells, which was statistically significant (p=0.0055) (Table 14). Transcripts of *frc* have been reported as having 3-fold to 430-fold higher abundance than those of *mbh* or *ech* (Worm *et al.* 2011). An increase in abundance of FrcA and FrcB was observed when *Methanococcus maripaludis* was

grown in coculture with *Desulfovibrio vulgaris* (Walker *et al.* 2012). Our data suggests that Frc plays an important role during hydrogen-limited, syntrophic growth.

Five genes predicted to encode formate dehydrogenases (Fdh) were detected in the *M. hungatei* genome (Figure 14). All *M. hungatei* Fdh enzymes are predicted to be F_{420}-reducing (Worm *et al.* 2011). Peptides for four of the five Fdhs were detected in the proteome (Figure 14; Table 16). Subunits of Fdh-1, Fdh-3 and Fdh-5 were detected under all growth conditions while those of Fdh-2 were not detected under any growth condition. FdhA-1 peptides had similar abundances under all growth conditions but, the relative abundance of FdhB-1 peptides (Mhun_1814 gene product) increased 6.5-fold in cells obtained form crotonate-oxidizing cocultures relative to pure culture-grown cells ($p=0.009$) and increased 7.5-fold in cells obtained from butyrate-oxidizing cocultures relative to pure culture-grown cells ($p=0.0003$). The relative abundance of FdhA-5 (Mhun_3238 gene product) increased over 2-fold in cells obtained from crotonate- and butyrate-oxidizing cocultures compared to pure culture-grown cells ($p=0.0009$ and $p=0.0001$, respectively) (Table 14). Transcripts of all five *fdh* genes were detected in *M. hungatei* cells grown in pure culture on either hydrogen or formate, and in cells grown in coculture with *S. fumaroxidans* on propionate (Worm *et al.* 2011).

Table 16: Formate dehydrogenase proteins detected from *M. hungatei*. Percent values represent percent of total normalized spectral abundance factors (NSAF) values prior to eliminating peptides detected in less than three replicates.

			Corrected NSAF values (expressed in %)					
			H_2 / CO_2		Crotonate		Butyrate	
Gene ID	**Locus**	**Gene Product Name**	**Avg**	**SD**	**Avg**	**SD**	**Avg**	**St. Dev**
637897432	Mhun_1813	formate dehydrogenase, alpha subunit	0.52%	0.10%	0.84%	0.19%	0.63%	0.05%
637897433	Mhun_1814	formate dehydrogenase, beta subunit	0.14%	0.04%	0.99%	0.28%	1.13%	0.14%
637897628	Mhun_2020	formate dehydrogenase, beta subunit	ND	--	0.01%	0.01%	0.01%	0.00%
637897629	Mhun_2021	formate dehydrogenase, alpha subunit	0.02%	0.02%	0.00%	0.01%	0.01%	0.01%
637897630	Mhun_2022	formate dehydrogenase, beta subunit	ND	--	0.00%	0.00%	0.01%	0.00%
637898852	Mhun_3237	formate dehydrogenase, beta subunit	ND	--	0.01%	0.02%	0.03%	0.02%
637898853	Mhun_3238	formate dehydrogenase, alpha subunit	0.04%	0.02%	0.01%	0.01%	0.04%	0.01%

Bioenergetics

Unlike cytochrome-containing methanogens, which create both H^+ and Na^+ gradients during methanogenesis (Thauer *et al.* 2008), cytochrome-lacking methanogens like *M. hungatei* are only known to generate Na^+ gradients. In methanogens that lack cytochromes, there is only one step in the methanogenic pathway which is linked to Na^+ efflux – the reaction of H_4MPT S-methyltransferase (Mtr), which couples the transfer of the methyl group from methyl-H_4MPT to reduced coenzyme M (CoM) to the efflux of two Na^+ ions (Saum *et al.* 2009; Schlegel *et al.* 2012). Four Na^+ ions are, in general, required for ATP synthesis (Saum *et al.* 2009; Schlegel *et al.* 2012) and, therefore, 0.5 mol ATP per mol of methane can potentially be made assuming that the sodium gradient is not needed for other purposes such as creating reduced ferredoxin needed to reduce CO_2 to formyl-MFR. Peptides were detected across all growth conditions for methyltransferase subunits and peptides for three subunits were substantially more abundant in cells obtained from butyrate-grown cocultures (Table 12).

Three A_1A_0 –type (archaeal-type) ATP synthases were identified on the *M. hungatei* genome (Mhun_1177-85, Mhun_1757-64, Mhun_1768-75) (Table 17; Figure 14), which would use the sodium gradient to make ATP. Each cluster contains multiple genes for the c-subunit with putative Na^+-binding motifs (Glu^n, Ser^{n+1}) (Müller and Grüber 2003). Peptides encoded by Mhun_1177-85 were detected in cells from at least three of four replicates grown in pure culture and in coculture on crotonate (Table 17).

Table 17: ATP synthase proteins detected from *M. hungatei*. Percent values represent percent of total normalized spectral abundance factors (NSAF) values prior to eliminating peptides detected in less than three replicates.

			Corrected NSAF values (expressed in %)					
			H_2 / CO_2		Crotonate		Butyrate	
Gene ID	**Locus**	**Gene Product Name**	**Avg**	**SD**	**Avg**	**SD**	**Avg**	**St. Dev**
637896819	Mhun_1177	V-type H+-transporting ATPase subunit E	ND	--	0.02%	0.04%	0.12%	0.05%
637896820	Mhun_1178	V-type ATPase, 116 kDa subunit	ND	--	0.04%	0.03%	0.05%	0.01%
637896822	Mhun_1180	H+-transporting two-sector ATPase, E subunit	0.15%	0.12%	0.17%	0.14%	0.24%	0.03%
637896823	Mhun_1181	H+-transporting two-sector ATPase, C (AC39) subunit	0.09%	0.07%	0.12%	0.05%	0.11%	0.03%
637896824	Mhun_1182	Vacuolar H+-transporting two-sector ATPase, F subunit	ND	--	0.07%	0.09%	0.15%	0.03%
637896825	Mhun_1183	Sodium-transporting two-sector ATPase	0.13%	0.05%	0.16%	0.06%	0.27%	0.04%
637896826	Mhun_1184	Sodium-transporting two-sector ATPase	0.58%	0.13%	0.21%	0.05%	0.41%	0.01%
637896827	Mhun_1185	V-type ATPase, D subunit	0.59%	0.13%	0.01%	0.02%	0.07%	0.02%
637897377	Mhun_1757	V-type ATPase, D subunit	0.06%	0.08%	ND	--	0.02%	0.01%
637897378	Mhun_1758	Sodium-transporting two-sector ATPase	ND	--	0.01%	0.02%	0.06%	0.01%
637897379	Mhun_1759	Sodium-transporting two-sector ATPase	0.01%	0.01%	ND	--	0.02%	0.01%
637897382	Mhun_1762	H+-transporting two-sector ATPase, E subunit	0.01%	0.02%	ND	--	0.07%	0.02%
637897384	Mhun_1764	V-type ATPase, 116 kDa subunit	ND	--	ND	--	0.01%	0.00%
637897388	Mhun_1768	V-type ATPase, D subunit	ND	--	0.01%	0.03%	0.02%	0.01%

637897389	Mhun_1769	Sodium-transporting two-sector ATPase	ND	--	ND	--	0.02%	0.01%
637897390	Mhun_1770	Sodium-transporting two-sector ATPase	ND	--	0.00%	0.00%	0.03%	0.01%
637897393	Mhun_1773	H+-transporting two-sector ATPase, E subunit	ND	--	ND	--	0.03%	0.01%

Peptides from all three ATP synthase gene clusters were detected in cells obtained from butyrate-grown cocultures (Figure 14 and Table 17).

The remaining bioenergetics enigma is how reduced ferredoxin, needed for the reduction of CO_2 to formyl-MFR, is made. In *M. maripaludis* it is believed that an electron bifurcating complex composed of heterodisulfide reductase (Hdr), formyl-methanofuran dehydrogenase (Fmd), F_{420}-nonreducing hydrogenase (Vhu) and formate dehydrogenase (Fdh) (Fmd/Hdr/Vhu/Fdh) complex is formed. This complex couples the oxidation of hydrogen and formate ($E^{0'}$ = -414 mV, -432 mV, respectively) to the exergonic reduction of the coenzyme B:coenzyme M heterodisulfide (CoM-S-S-CoB) ($E^{0'}$ = -140 mV)(discussed later). Energy conserved from this reaction is used to drive the endergonic reduction of ferredoxin ($E^{0'}$ = -500 mV) (Costa *et al.* 2010; Hendrickson and Leigh 2008). In the *M. hungatei* genome, two genes encoding *fmdGF* (Mhun_1834-35) are adjacent to three genes for heterodisulfide reductase (*hdrABC*, Mhun_1836-38) and a gene encoding methyl viologen-reducing hydrogenase subunit D (*hydD*) (Mhun_1839), which is the electron-transferring subunit. While genes for F_{420}-nonreducing hydrogenase (*vhu* or *vhc*) were not detected in the *M. hungatei* genome, it is possible that Fdh or another hydrogenase could form an electron bifurcating complex with FmdGF, HdrABC and HydD to drive the synthesis of formyl-MFR without the need to use the sodium gradient. Peptides of FmdF and HdrABC were consistently detected under all three growth conditions (Table 12).

Intermediary metabolism

M. hungatei is unique among the methanogens in that isolates require acetate supplementation (Ekiel *et al.* 1983) and no spontaneous mutants are known of either strain JF1 or GP1 which grow in an acetate-free medium (Sprott and Jarrell 1981). Studies with *M. hungatei* strain GP1 grown in the presence of ^{13}C-acetate show that the carbon atom of the methane is not isotopically labeled and thus is not derived from acetoclastic methanogenesis. Moreover, no evidence was obtained for condensation of CO_2 to form acetate and instead label from $^{13}CO_2$ was only detected in carboxyl groups of amino acids (Ekiel *et al.* 1983).

It is interesting, then, that the genome of *M. hungatei* encodes enzymes necessary for generating acetyl-CoA from CO_2 (Table 18). A gene cluster, predicted

Table 18: Carbon fixation proteins detected from *M. hungatei*. Percent values represent percent of total normalized spectral abundance factors (NSAF) values prior to eliminating peptides detected in less than three replicates.

			Corrected NSAF values (expressed in %)					
			H_2 / CO_2		Crotonate		Butyrate	
Gene ID	**Locus**	**Gene Product Name**	**Avg**	**SD**	**Avg**	**SD**	**Avg**	**St. Dev**
637895998	Mhun_0352	acetyl-coenzyme A synthetase	0.03%	0.02%	ND	--	ND	--
637896206	Mhun_0567	acetyl-coenzyme A synthetase	0.01%	0.02%	ND	--	0.02%	0.00%
637896323	Mhun_0686	acetyl-CoA decarbonylase/synthase gamma subunit	ND	--	ND	--	0.01%	0.01%
637896327	Mhun_0690	acetyl-CoA decarbonylase/synthase alpha subunit	0.04%	0.02%	ND	--	0.01%	0.01%

to encode a complete Acs/CODH complex (Mhun_0686-0690) and three acetyl-CoA synthetase genes (Mhun_0352, _0567, _1721), was detected in the *M. hungatei* genome. Peptides were detected for subunits of both the Acs/CODH complex as well as for the acetyl-CoA synthetases in cells grown in pure culture and in coculture on butyrate. Peptides were not detected for any subunits of Acs/CODH or for any of the acetyl-CoA synthetases in cells obtained from crotonate-grown cocultures (Table 18). It is tempting to speculate, therefore, that the acetate requirement may be fulfilled during growth on crotonate through acetate production by *S. wolfei*.

Oxaloacetate is a precursor for many biosynthetic reactions in the cell and, therefore, the conversion of pyruvate to oxaloacetate is an essential physiological requirement for an organism dependent on acetyl-CoA and CO_2 as the main biosynthetic starting points (Simpson 1993). Two mechanisms of oxaloacetate synthesis have been described for methanarchaea. In *Methanosarcini barkeri*, a hetero-octameric pyruvate carboxylase catalyzes the ATP dependent carboxylation of pyruvate to form oxaloacetate (Mukhopadhyay *et al.* 2001). In other methanogens, for example *Methanococcus jannaschii* (Mukhopadhyay *et al.* 2000) and *Methanococcus maripaludis* (Shieh and Whitman 1987), phosphoenolpyruvate is used to generate oxaloacetate via phosphoenolpyruvate carboxylation.

The genome of *M. hungatei* encodes a phosphoenolpyruvate carboxylase and both pyruvate carboxylase subunits; either enzyme could serve to synthesize oxaloacetate. Peptides derived from phosphoenolpyruvate carboxylase and pyruvate

carboxylase enzymes were detected from cells obtained from all growth conditions (Table 19).

Amino acid synthesis

Figure 15 shows the amino acid biosynthesis pathways detected in the *M. hungatei* genome. Complete biosynthetic pathways were detected for all amino acids except histidine. As mentioned above, no gene encoding his-tRNA was detected nor was a gene encoding histidinolphosphate phosphatase detected (Figure 15; Table 20).

Table 19: Phosphoenolpyruvate carboxylase/pyruvate carboxylase proteins detected from *M. hungatei*. Percent values represent percent of total normalized spectral abundance factors (NSAF) values prior to eliminating peptides detected in less than three replicates.

			Corrected NSAF values (expressed in %)					
			H_2 / CO_2		Crotonate		Butyrate	
Gene ID	**Locus**	**Gene Product Name**	**Avg**	**SD**	**Avg**	**SD**	**Avg**	**St. Dev**
637895825	Mhun_0174	Phosphoenolpyruvate carboxylase	0.06%	0.03%	0.01%	0.01%	0.02%	0.01%
637898794	Mhun_3189	pyruvate carboxylase subunit B	0.13%	0.04%	0.01%	0.01%	0.01%	0.01%
637898795	Mhun_3190	pyruvate carboxylase subunit A	ND	--	ND	--	0.02%	0.01%

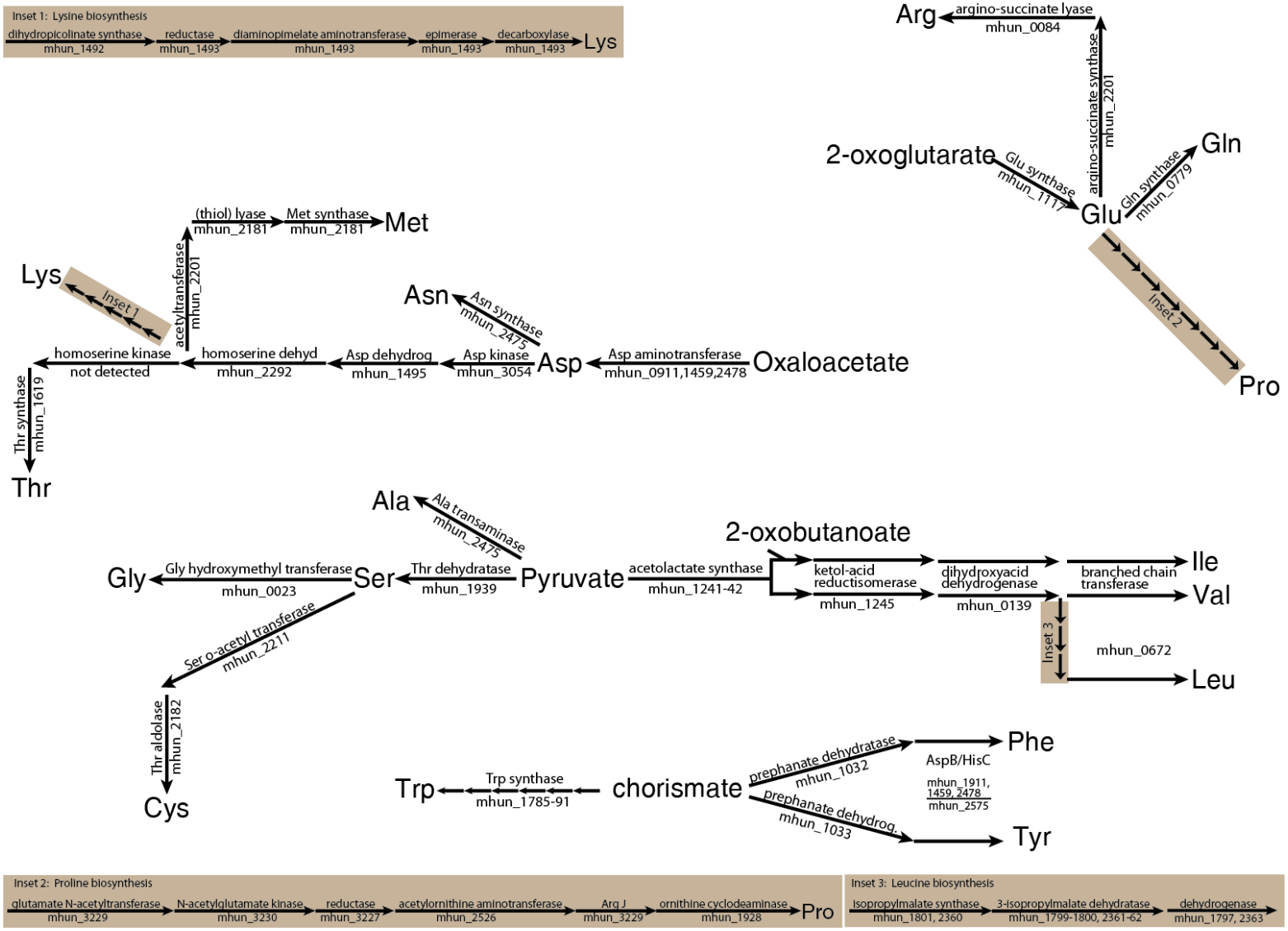
Inset 1: Lysine biosynthesis
dihydropicolinate synthase
mhun_1492
reductase
mhun_1493
diaminopimelate aminotransferase
mhun_1493
epimerase
mhun_1493
decarboxylase
mhun_1493
Lys
Arg
argino-succinate lyase
mhun_0084
argino-succinate synthase
mhun_2201
2-oxoglutarate
Glu synthase
mhun_1117
Glu
Gln synthase
mhun_0779
Gln
Inset 2
Pro
(thiol) lyase
mhun_2181
Met synthase
mhun_2181
Met
Lys
Inset 1
acetyltransferase
mhun_2201
Asn
Asn synthase
mhun_2475
homoserine kinase
not detected
homoserine dehyd
mhun_2292
Asp dehydrog
mhun_1495
Asp kinase
mhun_3054
Asp
Asp aminotransferase
mhun_0911,1459,2478
Oxaloacetate
Thr synthase
mhun_1619
Thr
Ala
Ala transaminase
mhun_2475
2-oxobutanoate
Gly
Gly hydroxymethyl transferase
mhun_0023
Ser
Thr dehydratase
mhun_1939
Pyruvate
acetolactate synthase
mhun_1241-42
ketol-acid
reductisomerase
mhun_1245
dihydroxyacid
dehydrogenase
mhun_0139
branched chain
transferase
Ile
Val
Inset 3
mhun_0672
Leu
Ser o-acetyl transferase
mhun_2211
Thr aldolase
mhun_2182
Cys
Trp
Trp synthase
mhun_1785-91
chorismate
prephanate dehydratase
mhun_1032
AspB/HisC
mhun_1911,
1459, 2478
mhun_2575
Phe
prephanate dehydrog.
mhun_1033
Tyr
Inset 2: Proline biosynthesis
glutamate N-acetyltransferase
mhun_3229
N-acetylglutamate kinase
mhun_3230
reductase
mhun_3227
acetylornithine aminotransferase
mhun_2526
Arg J
mhun_3229
ornithine cyclodeaminase
mhun_1928
Pro
Inset 3: Leucine biosynthesis
isopropylmalate synthase
mhun_1801, 2360
3-isopropylmalate dehydratase
mhun_1799-1800, 2361-62
dehydrogenase
mhun_1797, 2363

Figure 15: Amino acid biosynthesis pathway reconstruction in *M. hungatei* strain JF1. Genes encoding the gene products necessary for all amino acid biosynthetic pathways were detected except for the synthesis of histidine.

Table 20: Amino acid synthesis genes and gene products detected in *M. hungatei*. Percent values represent percent of total normalized spectral abundance factors (NSAF) values prior to eliminating peptides detected in less than three replicates.

			Corrected NSAF values (expressed in %)					
			H_2 / CO_2		Crotonate		Butyrate	
Gene ID	**Locus**	**Gene Product Name**	**Avg**	**SD**	**Avg**	**SD**	**Avg**	**St. Dev**
637895669	Mhun_0023	serine hydroxymethyltransferase	0.03%	0.03%	0.02%	0.04%	0.07%	0.01%
637895737	Mhun_0084	argininosuccinate lyase	0.02%	0.03%	ND	--	0.01%	0.00%
637895742	Mhun_0089	fumarase alpha subunit	0.09%	0.04%	ND	--	0.01%	0.01%
637895743	Mhun_0090	fumarase beta subunit	ND	--	ND	--	0.04%	0.00%
637895748	Mhun_0095	succinyl-CoA synthetase (ADP-forming) beta subunit	0.06%	0.02%	0.01%	0.02%	0.03%	0.01%
637895749	Mhun_0096	succinyl-CoA synthetase (ADP-forming) alpha subunit	ND	--	0.03%	0.03%	0.06%	0.02%
637895791	Mhun_0139	dihydroxyacid dehydratase	0.02%	0.02%	0.07%	0.07%	0.10%	0.01%
637896311	Mhun_0672	branched chain amino acid aminotransferase apoenzyme	0.42%	0.15%	0.02%	0.03%	0.09%	0.02%
637896416	Mhun_0779	L-glutamine synthetase	0.11%	0.01%	0.13%	0.01%	0.19%	0.03%
637896547	Mhun_0911	aminotransferase, class I and II	ND	--	0.02%	0.02%	0.03%	0.01%
637896556	Mhun_0920	imidazoleglycerol-phosphate dehydratase	ND	--	ND	--	0.02%	0.01%
637896579	Mhun_0943	putative phosphoserine phosphatase	0.30%	0.04%	0.10%	0.12%	0.12%	0.04%
637896670	Mhun_1032	prephenate dehydratase	0.09%	0.03%	ND	--	0.01%	0.01%

637896740	Mhun_1101	Enolase	0.06%	0.04%	0.02%	0.02%	0.08%	0.01%
637896756	Mhun_1117	sulfide dehydrogenase (flavoprotein) subunit SudA	ND	--	0.01%	0.02%	0.02%	0.01%
637896780	Mhun_1141	pyruvate phosphate dikinase	0.01%	0.01%	0.01%	0.01%	0.07%	0.01%
637896883	Mhun_1241	acetolactate synthase, small subunit	ND	--	0.15%	0.14%	0.24%	0.04%
637896884	Mhun_1242	acetolactate synthase, large subunit	0.08%	0.04%	0.10%	0.04%	0.14%	0.02%
637896887	Mhun_1245	ketol-acid reductoisomerase	1.49%	0.19%	0.97%	0.27%	0.77%	0.11%
637897090	Mhun_1459	aminotransferase, class I and II	0.04%	0.04%	0.02%	0.02%	0.07%	0.01%
637897123	Mhun_1492	dihydrodipicolinate synthase	0.02%	0.04%	0.13%	0.04%	0.15%	0.02%
637897124	Mhun_1493	dihydrodipicolinate reductase	0.05%	0.08%	0.13%	0.10%	0.16%	0.04%
637897248	Mhun_1619	L-threonine synthase	0.12%	0.03%	0.07%	0.06%	0.09%	0.01%
637897409	Mhun_1789	phosphoribosylanthranilate isomerase	ND	--	ND	--	0.03%	0.02%
637897410	Mhun_1790	tryptophan synthase, beta chain	ND	--	ND	--	0.01%	0.00%
637897417	Mhun_1797	3-isopropylmalate dehydrogenase	ND	--	0.01%	0.01%	0.03%	0.01%
637897421	Mhun_1801	2-isopropylmalate synthase	ND	--	ND	--	0.02%	0.01%
637897657	Mhun_2050	ATP phosphoribosyltransferase (homohexameric)	ND	--	ND	--	0.04%	0.02%
637897658	Mhun_2051	phosphoribosyl-AMP cyclohydrolase	0.10%	0.08%	ND	--	ND	--

637897732	Mhun_2126	DegT/DnrJ/EryC1/StrS aminotransferase	0.03%	0.03%	ND	--	0.03%	0.01%
637897787	Mhun_2181	O-acetylhomoserine sulfhydrolase	0.04%	0.03%	0.12%	0.06%	0.13%	0.02%
637897788	Mhun_2182	cysteine synthase	0.11%	0.08%	ND	--	0.08%	0.02%
637897807	Mhun_2201	homoserine O-acetyltransferase	ND	--	0.05%	0.04%	0.11%	0.02%
637897815	Mhun_2209	aminotransferase, class V	0.03%	0.04%	0.01%	0.02%	0.02%	0.01%
637897817	Mhun_2211	serine O-acetyltransferase	ND	--	ND	--	0.01%	0.01%
637897819	Mhun_2213	aminotransferase, class V	ND	--	ND	--	0.01%	0.01%
637897902	Mhun_2292	homoserine dehydrogenase	ND	--	ND	--	0.04%	0.02%
637897934	Mhun_2324	phosphoglycerate mutase	0.19%	0.10%	ND	--	0.05%	0.02%
637897954	Mhun_2343	malate dehydrogenase (NADP) / malate dehydrogenase (NAD)	ND	--	0.01%	0.01%	0.02%	0.01%
637897973	Mhun_2361	3-isopropylmalate dehydratase, large subunit	ND	--	0.09%	0.05%	0.08%	0.02%
637897974	Mhun_2362	3-isopropylmalate dehydratase, small subunit	0.13%	0.09%	0.10%	0.07%	0.14%	0.03%
637897975	Mhun_2363	3-isopropylmalate dehydrogenase	0.03%	0.02%	0.02%	0.03%	0.04%	0.02%
637898084	Mhun_2475	phosphoserine aminotransferase apoenzyme / L-aspartate aminotransferase apoenzyme	0.32%	0.09%	0.15%	0.05%	0.17%	0.02%

637898127	Mhun_2514	aromatic amino acid aminotransferase apoenzyme	ND	--	ND	--	0.02%	0.00%
637898138	Mhun_2525	histidinol phosphate aminotransferase apoenzyme	0.03%	0.03%	ND	--	0.02%	0.01%
637898139	Mhun_2526	acetylornithine aminotransferase apoenzyme	0.02%	0.03%	0.03%	0.05%	0.09%	0.02%
637898144	Mhun_2531	histidinol dehydrogenase	ND	--	0.02%	0.02%	0.03%	0.01%
637898223	Mhun_2610	phosphoenolpyruvate synthase	0.22%	0.17%	0.09%	0.03%	0.09%	0.01%
637898505	Mhun_2893	enolase	0.02%	0.02%	ND	--	0.02%	0.01%
637898557	Mhun_2943	LL-diaminopimelate aminotransferase apoenzyme	0.03%	0.04%	ND	--	0.02%	0.00%
637898661	Mhun_3052	thiol-driven fumarate reductase, iron-sulfur protein	ND	--	ND	--	0.04%	0.01%
637898662	Mhun_3053	thiol-driven fumarate reductase, flavoprotein subunit	ND	--	ND	--	0.04%	0.01%
637898663	Mhun_3054	aspartate kinase	0.02%	0.02%	0.00%	0.01%	0.04%	0.02%
637898672	Mhun_3063	D-3-phosphoglycerate dehydrogenase	0.06%	0.01%	ND	--	0.16%	0.01%
637898842	Mhun_3227	N-acetyl-gamma-glutamyl-phosphate reductase	ND	--	ND	--	0.09%	0.02%
637898844	Mhun_3229	N-acetylglutamate synthase / glutamate N-acetyltransferase	ND	--	0.09%	0.05%	0.02%	0.01%
637898845	Mhun_3230	N-acetylglutamate kinase	ND	--	0.07%	0.03%	0.03%	0.01%

Alanine. ^{13}C labeling analysis of *M. hungatei* GP1 (GP1) revealed an alanine biosynthetic pathway which was consistent with reductive carboxylation of acetyl-CoA to pyruvate and subsequent conversion of pyruvate to alanine (Ekiel *et al.* 1983). The *M. hungatei* genome contains many gene sequences which encode aminotransferase enzymes (Figure 15; Table 20) and gene products necessary for the conversion of acetate to pyruvate, e.g. phosphoenolpyruvate carboxylase and pyruvate carboxylase subunits. Genomic analysis is consistent with the model established in GP1 (Ekiel *et al.* 1983) although it is difficult to predict which aminotransferase is involved based on sequence analysis alone (Kameya *et al.* 2010).

Serine and glycine. The biosynthetic pathway for serine and glycine in GP1 channels through phosphoenolpyruvate and involves the formation of 3-phosphoglycerate. Essential for this mechanism is the conversion of 3-phosphohydroxypyruvate to phosphoserine via a phosphoserine transaminase and subsequent dephosphorylation of phosphoserine by 3-phosphoserine phosphatase. Glycine, then, is produced from serine via the serine hydroxymethyltransferase. The *M. hungatei* genome contains all the genes necessary for production of serine and glycine (Figure 15; Table 20) consistent with the mechanisms established in GP1.

Aspartic acid, asparagine, methionine, lysine and threonine. Biosynthesis of aspartate was shown in GP1 to proceed from the conversion of pyruvate to oxaloacetate and subsequent conversion to aspartic acid via a transamination reaction. As previously discussed (see above), *M. hungatei* contains gene loci which are predicted to encode the necessary machinery for conversion of pyruvate to oxaloacetate (Figure 15; Table 20).

These data are consistent with the model for aspartate synthesis established in GP1 (Ekiel *et al.* 1983). ^{13}C labeled asparagine was not detected in GP1, however the *M. hungatei* genome contains a gene locus for asparagine synthetase - the enzyme responsible for the conversion of aspartate to asparagine with concomitant conversion of glutamine to glutamate (Mhun_2475).

^{13}C labeling showed that biosynthesis of threonine, methionine and a portion of lysine proceeded from aspartate in GP1 (Ekiel *et al.* 1983). Aspartate is first converted to homoserine and from there the pathways diverge, forming threonine, methionine or lysine. The *M. hungatei* genome contains loci to encode the machinery necessary for the conversion of homoserine to lysine (or methionine (Crucial, however, for the conversion of homoserine to threonine is the formation of phosphoserine through the action of homoserine kinase. Genes encoding homoserine kinase were not detected in the *M. hungatei* genome); however, homoserine kinase belongs to the GHMP kinase family (Bork *et al.* 1993; Daugherty *et al.* 2001), and a gene loci which is annotated as a GHMP kinase encoding gene was detected (Mhun_0932). This peptide is predicted to have 43% identity over 40% of the peptides to a homoserine kinase identified in *Methanococcus jannaschii* (blast.ncbi.nlm.nih.gov).

Glutamic acid, glutamine, arginine and proline. ^{13}C labeling analysis in GP1 revealed that glutamic acid was derived from 2-oxoglutarate in the cell (Ekiel *et al.* 1983). Gene loci predicted to encode enzymes necessary for the conversion of oxaloacetate to 2-oxoglutarate were detected in the *M. hungatei* genome (Figure 15; Table 20). Genes detected include those that code for glutamate synthase (Mhun_1117), which is essential for the conversion of 2-oxoglutratate to glutamate, and glutamine synthase

(Mhun_0779), which is essential for the conversion of glutamate to glutamine (Figure 15; Table 20). ^{13}C labeling in GP1 showed that both arginine and proline had similar labeling patterns to glutamate; demonstrating that these amino acids were derived from glutamate as precursor (Ekiel *et al.* 1983). The *M. hungatei* genome contains genes predicted to encode argino-succinate synthase and argino-succinate lyase (Mhun_2201 and Mhun_0084 respectively) and the genes necessary for conversion of glutamate to proline (Figure 15; Table 20).

Leucine, valine, and isoleucine. ^{13}C labeling studies showed that leucine and valine were synthesized from pyruvate via acetolactate in GP1 (Ekiel *et al.* 1983). Isoleucine was shown to be synthesized from conversion of pyruvate to 2-oxobutanoate via citramalate rather than 2-oxobutanoate synthesis from threonine via threonine dehydratase in GP1 (Ekiel *et al.* 1983). Genes predicted to code for the enzymes necessary for synthesis of leucine, valine and isoleucine (Figure 15; Table 20)were detected in the *M. hungatei* genome. Of particular note is the genetic potential for conversion of threonine to 2-oxobutanoate via threonine dehydratase (Mhun_1939) providing genetic potential for two routes for the biosynthesis of isoleucine.

Tryptophan, phenylalanine and tyrosine. Phenylalanine and tyrosine were shown to be synthesized from chorismate and shikimate in GP1 while tryptophan was not detected (Ekiel *et al.* 1983). Aromatic acid biosynthesis usually begins with the synthesis of 3-deoxy-7-phosphoheptulonate from phosphoenolpyruvate and D-erythrose-4-phosphate; however, a gene encoding 3-deoxy-7-phosphoheptulonate synthase was not detected in the *M. hungatei* genome. Genes necessary for converting pyruvate to shikimate and subsequently chorismate via the gluconeogenic pathway (not

shown) were detected as were genes necessary for subsequent biosynthesis of tyrosine, phenylalanine, and tryptophan of tyrosine, phenylalanine, and tryptophan (Figure 15; Table 20).

Cysteine. Isotopically labeled cysteine was not detected in ^{13}C-labeling studies in GP1 (Ekiel *et al.* 1983). The genome of *M. hungatei*, however, contains gene loci necessary for the conversion of serine to cysteine (Figure 15; Table 20).

Histidine. Very low levels of isotopically labeled histidine were detected during ^{13}C-labeling experiments in GP1 (Ekiel *et al.* 1983), suggesting that histidine was synthesized via the pentose phosphate pathway forming phosphoribosylpentose phosphate (PRPP), which is converted to histidine, presumably via the commonly used pathway encoded by *hisGDCNBAFIE*. The genome of *M. hungatei* contains loci encoding all enzymes necessary for the conversion of PRPP to histidine except for a gene encoding histidinol-phosphate phosphatase (HisN) (Figure 15); a finding which is not unusual among archaea (Fondi *et al.* 2009).

Genes unique to Methanomicrobiales

There are 62 signature genes of the Methanomicrobiales class of methanogens (Anderson *et al.* 2009). All 62 signature Methanomicrobiales genes were detected in the *M. hungatei* chromosome and corresponding peptides were detected for eleven of these genes, seven of which were unique to syntrophic growth conditions (Table 21). Of note, peptides derived from three of these: an unknown protein (Mhun_0048 gene product), the gamma subunit of pyruvate ferredoxin oxidoreductase (Mhun_2394 gene product),

and a phosphoesterase enzyme (Mhun_2823 gene product) were detected only during growth on butyrate (Table 21).

Table 21: Genes and gene products unique to Methanomicrobiales and their detection in *M. hungatei.* Percent values represent percent of total normalized spectral abundance factors (NSAF) values prior to eliminating peptides detected in less than three replicates.

			Corrected NSAF values (expressed in %)					
			H_2 / CO_2		Crotonate		Butyrate	
Gene ID	**Locus**	**Gene Product Name**	**Avg**	**SD**	**Avg**	**SD**	**Avg**	**St. Dev**
637895670	Mhun_0024	hypothetical protein	0.17%	0.12%	ND	--	0.05%	0.03%
637895699	Mhun_0048	hypothetical protein	ND	--	ND	--	0.01%	0.01%
637896568	Mhun_0932	GHMP kinase	0.05%	0.03%	ND	--	0.02%	0.01%
637896609	Mhun_0972	chaperonin Cpn60/TCP-1	0.07%	0.04%	0.12%	0.10%	0.11%	0.02%
637896660	Mhun_1022	protein of unknown function DUF47	0.08%	0.07%	0.02%	0.04%	0.02%	0.01%
637897116	Mhun_1485	hypothetical protein	0.04%	0.04%	ND	--	0.05%	0.00%
637897443	Mhun_1824	Carbonate dehydratase	0.20%	0.06%	0.08%	0.05%	0.14%	0.01%
637897870	Mhun_2263	hypothetical protein	0.53%	0.26%	2.07%	0.44%	1.79%	0.02%
637898004	Mhun_2394	pyruvate ferredoxin oxidoreductase, gamma subunit	ND	--	ND	--	0.08%	0.04%
637898005	Mhun_2395	pyruvate flavodoxin/ferredoxin oxidoreductase-like	ND	--	0.01%	0.01%	0.06%	0.01%
637898006	Mhun_2396	thiamine pyrophosphate enzyme-like TPP-binding	0.04%	0.05%	0.01%	0.03%	0.03%	0.01%
637898166	Mhun_2554	Uncharacterised conserved protein UCP033563	0.06%	0.05%	0.03%	0.02%	0.02%	0.01%
637898433	Mhun_2823	phosphoesterase, DHHA1	ND	--	ND	--	0.02%	0.01%
637898463	Mhun_2851	hypothetical protein	0.03%	0.03%	ND	--	0.06%	0.02%

Discussion

Methanarchaea play a critical role in maintaining low hydrogen and formate levels in anaerobic ecosystems. Methanogenic activity creates thermodynamically favorable conditions for the oxidation of many organic acids and alcohols, including among these butyrate (McInerney *et al.* 2009; Sieber *et al.* 2012). This interspecies electron transfer is essential for anaerobic communities to flourish in the absence of lower potential acceptors and, in principle, can occur with either hydrogen or formate as the interspecific electron carrier. Theoretical calculations suggest that hydrogen diffusion is insufficient to explain the metabolic flux of freely suspended butyrate oxidizing cocultures (Dong and Stams 1995) and have led to suggestions elsewhere that formate represents the dominant interspecies electron carrier in suspended syntrophic cocultures (Stams and Plugge 2009).

The increase in relative abundance for F_{420}-reducing hydrogenase subunits seen here (Table 15) during growth in crotonate-oxidizing and butyrate-oxidizing cocultures is consistent with a prominent role for hydrogen in the overall energy economy of the organism. These observations are consistent with the observation that transcripts encoding the seleno-cysteine containing F_{420}-reducing hydrogenase (Fru) of *M. maripaludis* demonstrated a nearly ten-fold increase in syntrophic coculture relative to hydrogen limited cultures (Walker *et al.* 2012). The greater relative abundance of Frc during syntrophic growth is consistent with unpublished studies which demonstrate an essential role for hydrogen transfer in butyrate-oxidizing cocultures of *Syntrophomonas wolfei* and *M. hungatei* JF1 (Sieber *et al.* 2013) and an earlier study demonstrating the production of micromolar amounts of hydrogen from inverted membrane vesicles of *S.*

wolfei (Wallrabenstein and Schink 1994). The observed increase in peptides of Fdh (Mhun_1813-14 gene product) in cells grown in coculture with *S. wolfei* on crotonate and butyrate (Table 16) also implicates the importance of interspecies formate transfer. My observations here suggest that both formate and hydrogen are important interspecies electron carriers.

Increased abundance of transcripts encoding core methanogenic peptides MtrH, McrA and FwdD has been seen for syntrophically grown cells of *M. maripaludis* (Sieber *et al.* 2012). Here, ten peptides were detected in *M. hungatei* at greater than four-fold induction from cells obtained from butyrate-oxidizing cocultures (Table 14) and five of these are core methanogenic peptides. In pure culture, the high abundance of hydrogen presents no physiological limit to energy production by the methanogen and, therefore, the methanogenic machinery represents only a small fraction of the global protein demand in rapidly growing cells. Proteins involved in other physiological necessities, such as DNA replication and repair, amino acid biosynthesis and other biosynthetic proteins are in high demand in rapidly growing cultures. Pure culture growth is in stark contrast to the energetic reality faced by *M. hungatei* growing in crotonate or butyrate-oxidizing cocultures. Under these conditions, the rate of production of hydrogen, and consequently the free energy available to the methanogen, is low due to the low pool sizes of methanogenic substrates (Jackson and McInerney 2002). It is, therefore, of paramount importance to curtail biosynthesis and maximize energy production.

M. hungatei, like other methanogens that lack cytochromes, relies on sodium gradients to conserve energy. *M. hungatei* contains the genes H_4MPT S-

methyltransferase (Mtr) to create a sodium gradient and three A_1A_0 –type (archaeal-type) ATP synthases to use the sodium gradient to make ATP. Subunits of all three ATP synthases were detected in the proteome of M. hungatei when it was grown syntrophically with *S. wolfei* on butyrate (Figure 14, Table 17). However, it is not clear what system *M. hungatei* uses to create reduced ferredoxin needed for the reduction of carbon dioxide to formyl-MFR. Anderson and colleagues (2009) proposed that Methanomicrobiales use ion-translocating Eha to form reduced ferredoxin. However, use of a sodium gradient to form reduced ferredoxin would diminish the ability of *M. hungatei* to make ATP. Alternatively, *M. hungatei* may use an electron-bifurcating heterodisulfide reductase system (Anderson *et al.* 2009) analogous to that previously described for *M. maripaludis* (Costa *et al.* 2010). *fmdGF* (Mhun_1834-35) are adjacent to three genes for heterodisulfide reductase (*hdrABC*, Mhun_1836-38) and a gene encoding methyl viologen-reducing hydrogenase subunit D (*hydD*) (Mhun_1839). These genes could encode for a portion of the electron-bifurcating heterodisulfide reductase system. Although *M. hungatei* lacks genes for F_{420}-nonreducing hydrogenase, it is possible that one of the formate dehydrogenases could be the source of electrons. Consistent with this model is the fact that peptides of FmdF and HrdABC were detected under all three growth conditions (Table 12).

I see additional evidence here and elsewhere (Walker *et al.* 2012) that methanogens may rely on biosynthetic precursor molecules in the form of acetate, and possibly amino acids, to satisfy biosynthetic requirements. I did detect proteins associated with both anabolic and catabolic amino acid pathways in all three conditions. What is notable, however, was that I did not detect proteins involved in carbon fixation

in cells grown in coculture on crotonate. In *M. maripaludis*, evidence to support interspecies alanine transfer has been obtained to support this emerging facet of syntrophic relationships (Walker *et al.* 2012).

Comparative genomic analysis detected 62 genes, which are unique to members of the Methanomicrobiales class of methanogens (Anderson *et al.* 2009). As Methanomicrobiales species are often involved in syntrophic interactions, the signature Methanomicrobiales genes may have specific syntrophic functions. However, I detected peptides for only fourteen of these genes and only three of these were unique to syntrophic growth conditions (Table 21). These data argue that many Methanomicrobiales signature genes have functions that are not specific to syntrophy.

References

Achtnich, C., F. Bak and R. Conrad. 1995. Competition for electron donors among nitrate reducers, ferric iron reducers, sulfate reducers, and methanogens in anoxic paddy soil. *Biology and Fertility of Soils*. 19(1): 65-72

Ahman, M. 2010. Biomethane in the transport sector--an appraisal of the forgotten option. *Energy Policy*. 38(1): 208-17

Anderson, I., L. E. Ulrich, B. Lupa, D. Susanti, I. Porat, S. D. Hooper, A. Lykidis, M. Sieprawska-Lupa, L. Dharmarajan, E. Goltsman, A. Lapidus, E. Saunders, C. Han, M. Land, S. Lucas, B. Mukhopadhyay, W. B. Whitman, C. Woese, J. Bristow and N. Kyrpides. 2009. Genomic characterization of Methanomicrobiales reveals three classes of methanogens. *PLoS One*. 4(6): e5797

Beaty, P. S., N. Q. Wofford and M. J. McInerney. 1987. Separation of *Syntrophomonas wolfei* from *Methanospirillum hungatii* in syntrophic cocultures by using percoll gradients. *Appl Environ Microbiol*. 53(5): 1183-5

Biegel, E., S. Schmidt, J. M. Gonzalez and V. Müller. 2011. Biochemistry, evolution and physiological function of the Rnf complex, a novel ion-motive electron transport complex in prokaryotes. *Cell Mol Life Sci*. 68(4): 613-34

Bork, P., C. Sander and A. Valencia. 1993. Convergent evolution of similar enzymatic function on different protein folds: The hexokinase, ribokinase, and galactokinase families of sugar kinases. *Protein Sci*. 2(1): 31-40

Breese, K., M. Boll, J. Alt-Morbe, H. Schägger and G. Fuchs. 1998. Genes coding for the benzoyl-CoA pathway of anaerobic aromatic metabolism in the bacterium *Thauera aromatica*. *Eur J Biochem*. 256(1): 148-54

Brodt, A., M. N. Lurie-Weinberger and U. Gophna. 2011. CRISPR loci reveal networks of gene exchange in archaea. *Biol Direct*. 6(1): 65

Buckel, W. and R. K. Thauer. 2013. Energy conservation via electron bifurcating ferredoxin reduction and proton/Na^+ translocating ferredoxin oxidation. *Biochim Biophys Acta*. 1827(2): 94-113

Costa, K. C., P. M. Wong, T. Wang, T. J. Lie, J. A. Dodsworth, I. Swanson, J. A. Burn, M. Hackett and J. A. Leigh. 2010. Protein complexing in a methanogen suggests electron bifurcation and electron delivery from formate to heterodisulfide reductase. *Proc Natl Acad Sci U S A*. 107(24): 11050-5

Costa, K. C., S. H. Yoon, M. Pan, J. A. Burn, N. S. Baliga and J. A. Leigh. 2013. Effects of H_2 and formate on growth yield and regulation of methanogenesis in *Methanococcus maripaludis*. *J Bacteriol*.

Crable, B. R., C. M. Plugge, M. J. McInerney and A. J. Stams. 2011. Formate formation and formate conversion in biological fuels production. *Enzyme Res*. 2011: 532-536

Daugherty, M., V. Vonstein, R. Overbeek and A. Osterman. 2001. Archaeal shikimate kinase, a new member of the GHMP-kinase family. *J Bacteriol*. 183(1): 292-300

de Bok, F. A. M., C. M. Plugge and A. J. M. Stams. 2004. Interspecies electron transfer in methanogenic propionate degrading consortia. *Water Res*. 38(6): 1368-75

Delcher, A. L., D. Harmon, S. Kasif, O. White and S. L. Salzberg. 1999a. Improved microbial gene identification with GLIMMER. *Nucleic Acids Res*. 27(23): 4636-41

Delcher, A. L., S. Kasif, R. D. Fleischmann, J. Peterson, O. White and S. L. Salzberg. 1999b. Alignment of whole genomes. *Nucleic Acids Res*. 27(11): 2369-76

Deublein, D. and A. Steinhauser. 2008. History and status to date in Europe. *In: Biogas from waste and renewable resources*. Wiley.

Dlugokencky, E. J., E. G. Nisbet, R. Fisher and D. Lowry. 2011. Global atmospheric methane: budget, changes and dangers. *Philos Trans A Math Phys Eng Sci*. 369(1943): 2058-72

Dong, X. and A. J. Stams. 1995. Evidence for H_2 and formate formation during syntrophic butyrate and propionate degradation. *Anaerobe*. 1(1): 35-9

Egland, P. G., D. A. Pelletier, M. Dispensa, J. Gibson and C. S. Harwood. 1997. A cluster of bacterial genes for anaerobic benzene ring biodegradation. *Proc Natl Acad Sci U S A*. 94(12): 6484-9

Ekiel, I., I. C. Smith and G. D. Sprott. 1983. Biosynthetic pathways in *Methanospirillum hungatei* as determined by 13C nuclear magnetic resonance. *J Bacteriol*. 156(1): 316-26

Elias, D. A., F. Yang, H. M. Mottaz, A. S. Beliaev and M. S. Lipton. 2007. Enrichment of functional redox reactive proteins and identification by mass spectrometry results in several terminal Fe(III)-reducing candidate proteins in *Shewanella oneidensis* MR-1. *J Microbiol Methods*. 68(2): 367-75

Elshahed, M. S., V. K. Bhupathiraju, N. Q. Wofford, M. A. Nanny and M. J. McInerney. 2001. Metabolism of benzoate, cyclohex-1-ene carboxylate, and cyclohexane carboxylate by *Syntrophus aciditrophicus* strain SB in syntrophic association with H_2-using microorganisms. *Appl Environ Microbiol*. 67(4): 1728-38

Elshahed, M. S. and M. J. McInerney. 2001. Benzoate fermentation by the anaerobic bacterium *Syntrophus aciditrophicus* in the absence of hydrogen-using microorganisms. *Appl Environ Microbiol*. 67(12): 5520-5

Eng, J., A. McCormack and J. Yates. 1994a. An approach to correlate tandem mass spectral data of peptides with amino acid sequences in a protein database. *J Am Soc Mass Spectrom*. 5(11): 976-89

Enoki, M., N. Shinzato, H. Sato, K. Nakamura and Y. Kamagata. 2011a. Comparative proteomic analysis of *Methanothermobacter themautotrophicus* δH in pure culture and in co-culture with a butyrate-oxidizing bacterium. *PLoS One*. 6(8): e24309

Evans, W. C. and G. Fuchs. 1988. Anaerobic degradation of aromatic compounds. *Annu Rev Microbiol*. 42: 289-317

Ewing, B. and P. Green. 1998. Base-calling of automated sequencer traces using PHRED. II. Error probabilities. *Genome Res*. 8(3): 186-94

Ewing, B., L. Hillier, M. C. Wendl and P. Green. 1998. Base-calling of automated sequencer traces using PHRED. I. Accuracy assessment. *Genome Res*. 8(3): 175-85

Fondi, M., G. Emiliani, P. Lio, S. Gribaldo and R. Fani. 2009. The evolution of histidine biosynthesis in archaea: insights into the His genes structure and organization in luca. *J Mol Evol*. 69(5): 512-26

Friedrich, M. and B. Schink. 1993. Hydrogen formation from glycolate driven by reversed electron transport in membrane vesicles of a syntrophic glycolate-oxidizing bacterium. *Eur J Biochem*. 217(1): 233-40

Giannone, R. J., H. Huber, T. Karpinets, T. Heimerl, U. Kuper, R. Rachel, M. Keller, R. L. Hettich and M. Podar. 2011. Proteomic characterization of cellular and molecular processes that enable the *Nanoarchaeum equitans*--*Ignicoccus hospitalis* relationship. *PLoS One*. 6(8): e22942

Gloag, E. S., L. Turnbull, A. Huang, P. Vallotton, H. Wang, L. M. Nolan, L. Mililli, C. Hunt, J. Lu, S. R. Osvath, L. G. Monahan, R. Cavaliere, I. G. Charles, M. P. Wand, M. L. Gee, R. Prabhakar and C. B. Whitchurch. 2013. Self-organization of bacterial biofilms is facilitated by extracellular DNA. *Proc Natl Acad Sci U S A*. 110(28): 11541-6

Gordon, D., C. Abajian and P. Green. 1998. Consed: A graphical tool for sequence finishing. *Genome Res*. 8(3): 195-202

Hendrickson, E. L. and J. A. Leigh. 2008. Roles of coenzyme F_{420}-reducing hydrogenases and hydrogen- and F_{420}-dependent

methylenetetrahydromethanopterin dehydrogenases in reduction of F_{420} and production of hydrogen during methanogenesis. *J Bacteriol*. 190(14): 4818-21

Hendrickson, E. L., Y. Liu, G. Rosas-Sandoval, I. Porat, D. Soll, W. B. Whitman and J. A. Leigh. 2008. Global responses of *Methanococcus maripaludis* to specific nutrient limitations and growth rate. *J Bacteriol*. 190(6): 2198-205

Herrmann, G., E. Jayamani, G. Mai and W. Buckel. 2008. Energy conservation via electron-transferring flavoprotein in anaerobic bacteria. *J Bacteriol*. 190(3): 784-91

Hervey, W. J. t., M. B. Strader and G. B. Hurst. 2007. Comparison of digestion protocols for microgram quantities of enriched protein samples. *J Proteome Res*. 6(8): 3054-61

Jackson, B. E., V. K. Bhupathiraju, R. S. Tanner, C. R. Woese and M. J. McInerney. 1999. *Syntrophus aciditrophicus* sp. nov., a new anaerobic bacterium that degrades fatty acids and benzoate in syntrophic association with hydrogen-using microorganisms. *Arch Microbiol*. 171(2): 107-14

Jackson, B. E. and M. J. McInerney. 2002. Anaerobic microbial metabolism can proceed close to thermodynamic limits. *Nature*. 415(6870): 454-6

James, K. Unpublished data.

Kameya, M., H. Arai, M. Ishii and Y. Igarashi. 2010. Purification of three aminotransferases from *Hydrogenobacter thermophilus* tk-6--novel types of alanine or glycine aminotransferase: enzymes and catalysis. *FEBS J*. 277(8): 1876-85

Kung, J. W. Unpublished data.

Kung, J. W., C. Loffler, K. Dorner, D. Heintz, S. Gallien, A. Van Dorsselaer, T. Friedrich and M. Boll. 2009. Identification and characterization of the tungsten-containing class of benzoyl-coenzyme A reductases. *Proc Natl Acad Sci U S A*. 106(42): 17687-92

Kung, J. W., J. Seifert, M. von Bergen and M. Boll. 2013. Cyclohexanecarboxyl-coenzyme A (CoA) and cyclohex-1-ene-1-carboxyl-coa dehydrogenases, two enzymes involved in the fermentation of benzoate and crotonate in *Syntrophus aciditrophicus*. *J Bacteriol*. 195(14): 3193-200

Kuntze, K., Y. Shinoda, H. Moutakki, M. J. McInerney, C. Vogt, H. H. Richnow and M. Boll. 2008. 6-oxocyclohex-1-ene-1-carbonyl-coenzyme A hydrolases from obligately anaerobic bacteria: Characterization and identification of its gene as a functional marker for aromatic compounds degrading anaerobes. *Environ Microbiol*. 10(6): 1547-56

Laempe, D., W. Eisenreich, A. Bacher and G. Fuchs. 1998. Cyclohexa-1,5-diene-1-carbonyl-coa hydratase [corrected], an enzyme involved in anaerobic metabolism of benzoyl-CoA in the denitrifying bacterium *Thauera aromatica*. *Eur J Biochem*. 255(3): 618-27

Laempe, D., M. Jahn and G. Fuchs. 1999. 6-hydroxycyclohex-1-ene-1-carbonyl-coa dehydrogenase and 6-oxocyclohex-1-ene-1-carbonyl-coa hydrolase, enzymes of the benzoyl-coa pathway of anaerobic aromatic metabolism in the denitrifying bacterium *Thauera aromatica*. *Eur J Biochem*. 263(2): 420-9

Li, F., J. Hinderberger, H. Seedorf, J. Zhang, W. Buckel and R. K. Thauer. 2008. Coupled ferredoxin and crotonyl coenzyme A (CoA) reduction with NADH

catalyzed by the butyryl-CoA dehydrogenase/Etf complex from *Clostridium kluyveri*. *J Bacteriol*. 190(3): 843-50

Li, X., M. J. McInerney, D. A. Stahl and L. R. Krumholz. 2011. Metabolism of H_2 by *Desulfovibrio alaskensis* G20 during syntrophic growth on lactate. *Microbiology*. 157(Pt 10): 2912-21

Loffler, C., K. Kuntze, J. R. Vazquez, A. Rugor, J. W. Kung, A. Bottcher and M. Boll. 2011. Occurrence, genes and expression of the W/Se-containing Class II benzoyl-coenzyme A reductases in anaerobic bacteria. *Environ Microbiol*. 13(3): 696-709

Luo, H. W., H. Zhang, T. Suzuki, S. Hattori and Y. Kamagata. 2002. Differential expression of methanogenesis genes of *Methanothermobacter thermoautotrophicus* (formerly *Methanobacterium thermoautotrophicum*) in pure culture and in cocultures with fatty acid-oxidizing syntrophs. *Appl Environ Microbiol*. 68(3): 1173-9

Lupa, B., E. L. Hendrickson, J. A. Leigh and W. B. Whitman. 2008. Formate-dependent H_2 production by the mesophilic methanogen *Methanococcus maripaludis*. *Appl Environ Microbiol*. 74(21): 6584-90

Maymó-Gatell, X., Y.-t. Chien, J. M. Gossett and S. H. Zinder. 1997. Isolation of a bacterium that reductively dechlorinates tetrachloroethene to ethene. *Science*. 276(5318): 1568-71

McInerney, M., M. Bryant and N. Pfennig. 1979. Anaerobic bacterium that degrades fatty acids in syntrophic association with methanogens. *Arch Microbiol*. 122(2): 129-35

McInerney, M. J., M. P. Bryant, R. B. Hespell and J. W. Costerton. 1981a. *Syntrophomonas wolfei* gen. nov. sp. nov., an anaerobic, syntrophic, fatty acid-oxidizing bacterium. *Appl Environ Microbiol*. 41(4): 1029-39

McInerney, M. J., R. I. Mackie and M. P. Bryant. 1981b. Syntrophic association of a butyrate-degrading bacterium and Methanosarcina enriched from bovine rumen fluid. *Appl Environ Microbiol*. 41(3): 826-8

McInerney, M. J., L. Rohlin, H. Mouttaki, U. Kim, R. S. Krupp, L. Rios-Hernandez, J. Sieber, C. G. Struchtemeyer, A. Bhattacharyya, J. W. Campbell and R. P. Gunsalus. 2007. The genome of *Syntrophus aciditrophicus*: life at the thermodynamic limit of microbial growth. *Proc Natl Acad Sci U S A*. 104(18): 7600-5

McInerney, M. J., J. R. Sieber and R. P. Gunsalus. 2009. Syntrophy in anaerobic global carbon cycles. *Curr Opin Biotechnol*. 20(6): 623-32

McInerney, M. J., C. G. Struchtemeyer, J. Sieber, H. Mouttaki, A. J. Stams, B. Schink, L. Rohlin and R. P. Gunsalus. 2008. Physiology, ecology, phylogeny, and genomics of microorganisms capable of syntrophic metabolism. *Ann N Y Acad Sci*. 1125: 58-72

Meuer, J., H. C. Kuettner, J. K. Zhang, R. Hedderich and W. W. Metcalf. 2002. Genetic analysis of the archaeon *Methanosarcina barkeri* Fusaro reveals a central role for Ech hydrogenase and ferredoxin in methanogenesis and carbon fixation. *Proc Natl Acad Sci U S A*. 99(8): 5632-7

Michaelis, L. and E. S. Hill. 1933. The viologen indicators. *J Gen Physiol*. 16(6): 859-73

Moore, R. E., M. K. Young and T. D. Lee. 2002. Qscore: An algorithm for evaluating sequest database search results. *J Am Soc Mass Spectrom*. 13(4): 378-86

Mouttaki, H., M. A. Nanny and M. J. McInerney. 2008. Use of benzoate as an electron acceptor by *Syntrophus aciditrophicus* grown in pure culture with crotonate. *Environ Microbiol*. 10(12): 3265-74

Mukhopadhyay, B., V. J. Patel and R. S. Wolfe. 2000. A stable archaeal pyruvate carboxylase from the hyperthermophile *Methanococcus jannaschii*. *Arch Microbiol*. 174(6): 406-14

Mukhopadhyay, B., E. Purwantini, C. L. Kreder and R. S. Wolfe. 2001. Oxaloacetate synthesis in the methanarchaeon *Methanosarcina barkeri*: pyruvate carboxylase genes and a putative *Escherichia coli*-type bifunctional biotin protein ligase gene (*bpl/bira*) exhibit a unique organization. *J Bacteriol*. 183(12): 3804-10

Müller, N., D. Schleheck and B. Schink. 2009. Involvement of NADH:acceptor oxidoreductase and butyryl coenzyme a dehydrogenase in reversed electron transport during syntrophic butyrate oxidation by *Syntrophomonas wolfei*. *J Bacteriol*. 191(19): 6167-77

Müller, N., P. Worm, B. Schink, A. J. Stams and C. M. Plugge. 2010. Syntrophic butyrate and propionate oxidation processes: from genomes to reaction mechanisms. *Environ Microbiol Rep*. 2(4): 489-99

Müller, V. and G. Grüber. 2003. ATP synthases: structure, function and evolution of unique energy converters. *Cellular and Molecular Life Sciences CMLS*. 60(3): 474-94

Müller, V., F. Imkamp, E. Biegel, S. Schmidt and S. Dilling. 2008. Discovery of a ferredoxin:NAD^+-oxidoreductase (Rnf) in *Acetobacterium woodii*: a novel potential coupling site in acetogens. *Ann N Y Acad Sci*. 1125: 137-46

Oksanen, J., R. Kindt, P. Legendre, B. O'Hara, M. H. H. Stevens, M. J. Oksanen and M. Suggests. 2007. The vegan package. *Community ecology package. Disponível. Acesso em*. 10(01): 2008

Patel, G. B., G. D. Sprott, R. W. Humphrey and T. J. Beveridge. 1986. Comparative analyses of the sheath structures of *Methanothrix concilii* gp6 and methanospirillum hungatei strains gp1 and jf1. *Canadian Journal of Microbiology*. 32(8): 623-31

Pelletier, D. A. and C. S. Harwood. 2000. 2-hydroxycyclohexanecarboxyl coenzyme A dehydrogenase, an enzyme characteristic of the anaerobic benzoate degradation pathway used by *Rhodopseudomonas palustris*. *J Bacteriol*. 182(10): 2753-60

Peters, F., Y. Shinoda, M. J. McInerney and M. Boll. 2007. Cyclohexa-1,5-diene-1-carbonyl-coenzyme A (CoA) hydratases of *Geobacter metallireducens* and *Syntrophus aciditrophicus*: Evidence for a common benzoyl-CoA degradation pathway in facultative and strict anaerobes. *J Bacteriol*. 189(3): 1055-60

Pison, I., B. Ringeval, P. Bousquet, C. Prigent and F. Papa. 2013. Stable atmospheric methane in the 2000s: key-role of emissions from natural wetlands. *Atmos. Chem. Phys. Discuss.* 13(4): 9017-49

Plugge, C. M., A. M. Henstra, P. Worm, D. C. Swarts, A. H. Paulitsch-Fuchs, J. C. Scholten, A. Lykidis, A. L. Lapidus, E. Goltsman, E. Kim, E. McDonald, L.

Rohlin, B. R. Crable, R. P. Gunsalus, A. J. Stams and M. J. McInerney. 2012. Complete genome sequence of *Syntrophobacter fumaroxidans* strain MPOB^{T}. *Stand Genomic Sci*. 7(1): 91-106

Robinson, J. A. and J. M. Tiedje. 1984. Competition between sulfate-reducing and methanogenic bacteria for H_2 under resting and growing conditions. *Arch Microbiol*. 137(1): 26-32

Roy, A., A. Kucukural and Y. Zhang. 2010. I-TASSER: a unified platform for automated protein structure and function prediction. *Nat Protoc*. 5(4): 725-38

Sato, K., Y. Nishina, C. Setoyama, R. Miura and K. Shiga. 1999. Unusually high standard redox potential of acrylyl-CoA/propionyl-CoA couple among enoyl-CoA/acyl-CoA couples: A reason for the distinct metabolic pathway of propionyl-CoA from longer acyl-CoAs. *J Biochem*. 126(4): 668-75

Saum, R., K. Schlegel, B. Meyer and V. Müller. 2009. The F_1F_0 atp synthase genes in methanosarcina acetivorans are dispensable for growth and atp synthesis. *FEMS Microbiol Lett*. 300(2): 230-6

Schägger, H. and G. von Jagow. 1991. Blue native electrophoresis for isolation of membrane protein complexes in enzymatically active form. *Anal Biochem*. 199(2): 223-31

Schink, B. 1997. Energetics of syntrophic cooperation in methanogenic degradation. *Microbiol Mol Biol Rev*. 61(2): 262-80

Schlegel, K., V. Leone, J. D. Faraldo-Gomez and V. Müller. 2012. Promiscuous archaeal ATP synthase concurrently coupled to Na^+ and H^+ translocation. *Proc Natl Acad Sci U S A*. 109(3): 947-52

Schmidt, A., N. Müller, B. Schink and D. Schleheck. 2013b. A proteomic view at the biochemistry of syntrophic butyrate oxidation in *Syntrophomonas wolfei*. *PLoS One*. 8(2):

Schöcke, L. and B. Schink. 1997. Energetics of methanogenic benzoate degradation by *Syntrophus gentianae* in syntrophic coculture. *Microbiology*. 143(7): 2345-51

Scholten, J. C. and R. Conrad. 2000. Energetics of syntrophic propionate oxidation in defined batch and chemostat cocultures. *Appl Environ Microbiol*. 66(7): 2934-42

Schut, G. J. and M. W. Adams. 2009. The iron-hydrogenase of *Thermotoga maritima* utilizes ferredoxin and NADH synergistically: a new perspective on anaerobic hydrogen production. *J Bacteriol*. 191(13): 4451-7

Shieh, J. S. and W. B. Whitman. 1987. Pathway of acetate assimilation in autotrophic and heterotrophic methanococci. *J Bacteriol*. 169(11): 5327-9

Sieber, J. R. 2011. Investigations of interspecies electron transfer mechanisms important to syntrophic metabolism. University of Oklahoma, Norman, OK

Sieber, J. R., H. M. Le and M. J. McInerney. 2013. The importance of hydrogen and formate transfer for syntrophic fatty, aromatic and alicyclic metabolism. *Environ Microbiol*.

Sieber, J. R., M. J. McInerney and R. P. Gunsalus. 2012. Genomic insights into syntrophy: The paradigm for anaerobic metabolic cooperation. *Annu Rev Microbiol*. 66: 429-52

Sieber, J. R., D. R. Sims, C. Han, E. Kim, A. Lykidis, A. L. Lapidus, E. McDonnald, L. Rohlin, D. E. Culley, R. Gunsalus and M. J. McInerney.

2010. The genome of *Syntrophomonas wolfei*: new insights into syntrophic metabolism and biohydrogen production. *Environ Microbiol*. 12(8): 2289-301

Simpson, P. G. a. W. B. W. 1993. Anabolic pathways in methanogens. *In:* Methanogenesis: ecology, physiology, biochemistry & genetics. Ed: J. G. Ferry.

Sprott, G. D. and K. F. Jarrell. 1981. K^+, Na^+, and Mg^{2+} content and permeability of *Methanospirillum hungatei* and *Methanobacterium thermoautotrophicum*. *Can J Microbiol*. 27(4): 444-51

Stams, A. J. and X. Dong. 1995. Role of formate and hydrogen in the degradation of propionate and butyrate by defined suspended cocultures of acetogenic and methanogenic bacteria. *Antonie Van Leeuwenhoek*. 68(4): 281-4

Stams, A. J. and C. M. Plugge. 2009. Electron transfer in syntrophic communities of anaerobic bacteria and archaea. *Nat Rev Microbiol*. 7(8): 568-77

Struchtemeyer, C. G., K. E. Duncan and M. J. McInerney. 2011. Evidence for syntrophic butyrate metabolism under sulfate-reducing conditions in a hydrocarbon-contaminated aquifer. *FEMS Microbiol Ecol*. 76(2): 289-300

Swamy, M., G. M. Siegers, S. Minguet, B. Wollscheid and W. W. Schamel. 2006. Blue native polyacrylamide gel electrophoresis (BN-PAGE) for the identification and analysis of multiprotein complexes. *Sci STKE*. 2006(345): pl4

Tabb, D. L., W. H. McDonald and J. R. Yates, 3rd. 2002. DTASelect and contrast: tools for assembling and comparing protein identifications from shotgun proteomics. *J Proteome Res*. 1(1): 21-6

Tanner, R. S. 2002. Cultivation of bacteria and fungi. *In* Manual of Environmental Microbiology. 2nd Ed. Editors: C. J. Hurst, R. L. Crawford, G. R. Knudsen. M. J. McInerney, L. D. Stetzenbach. ASM Press.

Thauer, R. K., A. K. Kaster, H. Seedorf, W. Buckel and R. Hedderich. 2008. Methanogenic archaea: ecologically relevant differences in energy conservation. *Nat Rev Microbiol*. 6(8): 579-91

Thompson, M. R., K. Chourey, J. M. Froelich, B. K. Erickson, N. C. VerBerkmoes and R. L. Hettich. 2008. Experimental approach for deep proteome measurements from small-scale microbial biomass samples. *Anal Chem*. 80(24): 9517-25

Walker, C. B., A. M. Redding-Johanson, E. E. Baidoo, L. Rajeev, Z. He, E. L. Hendrickson, M. P. Joachimiak, S. Stolyar, A. P. Arkin, J. A. Leigh, J. Zhou, J. D. Keasling, A. Mukhopadhyay and D. A. Stahl. 2012. Functional responses of methanogenic archaea to syntrophic growth. *ISME J*. 6(11): 2045-55

Wallrabenstein, C. and B. Schink. 1994. Evidence of reversed electron-transport in syntrophic butyrate or benzoate oxidation by *Syntrophomonas wolfei* and *Syntrophus buswellii*. *Arch Microbiol*. 162(1-2): 136-42

Washburn, M. P., D. Wolters and J. R. Yates, 3rd. 2001. Large-scale analysis of the yeast proteome by multidimensional protein identification technology. *Nat Biotechnol*. 19(3): 242-7

Wischgoll, S., M. Taubert, F. Peters, N. Jehmlich, M. von Bergen and M. Boll. 2009. Decarboxylating and nondecarboxylating glutaryl-coenzyme A

dehydrogenases in the aromatic metabolism of obligately anaerobic bacteria. *J Bacteriol*. 191(13): 4401-9

Wofford, N. Q., P. S. Beaty and M. J. McInerney. 1986. Preparation of cell-free extracts and the enzymes involved in fatty acid metabolism in *Syntrophomonas wolfei*. *J Bacteriol*. 167(1): 179-85

Wolters, D. A., M. P. Washburn and J. R. Yates, 3rd. 2001. An automated multidimensional protein identification technology for shotgun proteomics. *Anal Chem*. 73(23): 5683-90

Worm, P., A. J. Stams, X. Cheng and C. M. Plugge. 2011. Growth- and substrate-dependent transcription of formate dehydrogenase and hydrogenase coding genes in *Syntrophobacter fumaroxidans* and *Methanospirillum hungatei*. *Microbiology*. 157(Pt 1): 280-9

Zhang, Y. 2007. Template-based modeling and free modeling by I-TASSER in casp7. *Proteins*. 69 Suppl 8(108-17

Zhang, Y. 2008. I-TASSER server for protein 3d structure prediction. *BMC Bioinformatics*. 9 40

Zhang, Y. 2009. I-TASSER: fully automated protein structure prediction in casp8. *Proteins*. 77 Suppl 9: 100-13

Zhang, Y., Z. Wen, M. P. Washburn and L. Florens. 2010. Refinements to label free proteome quantitation: how to deal with peptides shared by multiple proteins. *Anal Chem*. 82(6): 2272-81

Zybailov, B., A. L. Mosley, M. E. Sardiu, M. K. Coleman, L. Florens and M. P. Washburn. 2006. Statistical analysis of membrane proteome expression changes in *Saccharomyces cerevisiae*. *J Proteome Res*. 5(9): 2339-47